Experimental Modelling of Flavonoid Membrane Interactions

Didem Sanver

Submitted in accordance with the requirements for the degree of
Doctor of Philosophy

The University of Leeds
School of Food Science and Nutrition
School of Chemistry
Faculty of Mathematics and Physical Sciences

March 2017

The candidate confirms that the work submitted is her own, except where work which has formed part of jointly-authored publications has been included. The contribution of the candidate and the other authors to this work has been explicitly indicated below. The candidate confirms that appropriate credit has been given within the thesis where reference has been made to the work of others.

The work in Chapter 3,4 and 5 of the thesis has appeared in the publication as follows:

Sanver, D., Murray, B.S., Sadeghpour, A., Rappolt, M. and Nelson, A.L. Experimental Modeling of Flavonoid–Biomembrane Interactions. *Langmuir*. 2016.

Details of jointly-authored publication is outlined on the next page.

Further details of the jointly-authored publications and submitted manuscripts and to the work are included below:

Didem Sanver: conducted the experimental design and measurements, data analysis, data interpretation, and drafted the manuscript.

Brent S. Murray: provided supervision and feedback, edited the manuscript, and contributed to reviewers' comments.

Initial discussions and planning, experimental design and feedback of manuscript.

Amin Sadeghpour: gave SAXS training, helped in the experimental protocol of SAXS measurements and data analysis and contributed to SAXS discussion.

Michael Rappolt: helped to proofread of the published manuscript (SAXS part) and also helped to collaborate with researchers for mathematical simulation of the SAXS data (this information will take place in the following manuscripts).

Andrew Nelson: provided supervision and feedback, edited the manuscript, and contributed to reviewers' comments.

Acknowledgements

First and foremost I would like to thank my two supervisors, Professor Brent S. Murray and Professor Andrew Nelson, who encouraged me to pursue my PhD in this project. I would like to thank them both for their help, care and support throughout the project. Much of my work would not have been completed without their valuable guidance and continuous support.

My sincere thanks go to Dr Amin Sadeghpour who helped me with my final chapter and provided me with the opportunity to discuss various aspects of my work. I am also grateful to Professor Michael Rappolt for having made the project more enjoyable with his wonderful sense of humour. Just thinking of all those cherished moments is enough to put a smile on my face.

Words cannot express my heartfelt gratitude to my unique friend Maya, who has become a family to me in Leeds throughout my PhD journey. We have learnt so much in this journey together, and her presence and support helped me persevere through the isolation and loneliness and made me thankful for each day I have spent in Leeds.

I would like to express my gratitude to my family, including my aunt who has always supported me throughout my career and helped out in their special way. Words cannot express how grateful I am to my incredible family for their unconditional love and unlimited support.

I'm having difficulty to put my appreciation into words for my partner Dogukan, for his great patience, moral support and encouragement in my stressful and critical times. I am a stronger person with you, and I will always be grateful for this.

Publications

Sanver, D., Murray, B.S., Sadeghpour, A., Rappolt, M. and Nelson, A.L. Experimental Modeling of Flavonoid–Biomembrane Interactions. *Langmuir*. 2016, 32(49), pp.13234-13243.

Rashid, A., Vakurov, A., Mohamadi, S., Sanver, D. and Nelson, A. Substituents modulate biphenyl penetration into lipid membranes. *Biochimica et Biophysica Acta (BBA) - Biomembranes.* 2017, 1859(5), pp.712-721.

Book Chapter: Sadeghpour, A., Sanver, D, Rappolt, M. Chapter Four-Interactions of Flavonoids With Lipidic Mesophases. *Advances in Biomembranes and Lipid Self-Assembly*. 2017, 25, pp.95-123.

Conferences

- Particles at Interfaces conference, Oral presentation Leeds/UK, 09/2016
- ICOMF16 Conference, Oral presentation, Helsinki/Finland, 07/2016
- MIBio 2015, Stability of biopharmaceuticals Poster presentation, Cambridge/ UK 10/2015
- KTN Early Career Researchers Event, Poster presentation, Birmingham/UK, 10/2015
- 15th International Conference on Electroanalysis (ESEAC), Malmo/Sweden, 06/2014

Manuscripts in Preparation

Sanver, D., Rappolt, M., Murray, B.S., Nelson, A.L., and Sadeghpour A. Thickness and fluctuations of dioleoylphosphatidylcholine (DOPC) bilayer with quercetin and rutin: A small angle X-ray scattering and molecular dynamics study.

Sanver, D., Rappolt, M., Murray, B.S., Nelson, A.L., and Sadeghpour A. Structural characterisation of dioleoylphosphatidylcholine (DOPC) bilayer with tiliroside.

Abstract

Flavonoids, a class of polyphenols, are commonly found in fruits, vegetables, nuts and grains. Increasing evidence from epidemiological and clinical studies show a relationship between high flavonoid consumption in diet and reduced risk of several chronic diseases. Several mechanisms, including specific binding of flavonoids to proteins, have been proposed for flavonoids to exert their biological activities. However, it has also been reported that nonspecific interactions of flavonoids with phospholipids can induce structural changes in the membrane's features (e.g., thickness and fluctuations) and indirectly modulate membrane proteins, as well as influence their pharmacological potentials.

This thesis investigates the interactions between flavonoids and model biomembranes through three distinctively different but complementary approaches, with a special emphasis on employing monolayer membrane model in proof of concept experiments using one lipid type; 1,2 dioleoyl-sn-glycero-3-phosphocholine (DOPC). Hence, a well characterised electrochemical sensor system; phospholipid monolayer coated mercury (Hg) film electrode was established by rapid cyclic voltammetry (RCV) to screen structure-dependent interactions of a variety of flavonoids. The data revealed that flavonoids adopting a planar configuration altered the membrane properties more significantly than nonplanar flavonoids. The extent of interactions can be ranked in the order of quercetin > kaempferol > naringenin > hesperetin > catechin for flavonoid aglycones and tiliroside > rutin > naringin for flavonoid glycosides.

Quercetin, rutin, and tiliroside were selected for follow-up experiments with Langmuir monolayers, Brewster angle microscopy (BAM), and small-angle X-ray scattering (SAXS). Relaxation phenomena in DOPC monolayers and visualisation of the surface with BAM revealed a pronounced monolayer stabilisation effect with both quercetin and tiliroside, whereas rutin disrupted the monolayer structure rendering the surface entirely smooth. The following ranking of the interactions: quercetin>tiliroside>rutin, yielded comparable results to those obtained from the previous technique.

SAXS showed a monotonous membrane thinning for all flavonoids studied associated with an increase in the mean fluctuations of the membrane. The extent of interactions was concentration and temperature dependent with an order of quercetin>tiliroside>rutin except for tiliroside where a high concentration of tiliroside (>2 mol%) revealed the most pronounced response.

In addition to the novelty of employing phospholipid monolayers for the systematic characterisation of a variety of flavonoids, this is the first report investigating the effect of tiliroside with biomimetic membrane models. All the flavonoids studied are believed to be localised in the lipid/water interface region. Both this location and the membrane perturbations might have implications for the therapeutic features of flavonoids.

Table of Contents

List of Figures

List of Tables

Abbreviations

BAM	Brewster Angle Microscopy
CLSM	Confocal laser scanning microscope
DLS	Dynamic Light Scattering
DOPC	1,2 dioleoyl-sn-glycero-3-phosphocholine
DPPC	Dipalmitoylphosphatidylcholine
DSC	Differential scanning calorimetry
EDP	Electron density profile
EDP	Electron density profile
EPR	Electron Paramagnetic Resonance
GUV	Giant unilamellar vesicles
Hg	Mercury
LoD	Limit of Detection
LUVs	Large unilamellar vesicles
MFE	Microfabricated Hg film electrode
MLV(s)	Multilamellar Vesicle(s)
PBS	Phosphate buffered saline
PC	Phosphatidylcholine
PE	Phosphatidylethanolamine
POPC	1-palmitoyl-2-oleoyl-sn-glycero-3-phosphocholine
PS	Phosphatidylserine
PTFE	Polytetrafluoroethylene
RCV	Rapid cyclic voltammetry
SAM(s)	Self-assembled monolayer(s)
SAR	Structure-activity relationship
SAXS	Small angle X-ray scattering
SUV	small unilamellar vesicles

Commonly used symbols and physical constants

B	bulk compression modulus
C	capacitance
d	Lamellar repeat distance
d_{HH}	bilayer thickness
DL	double layer
d_W	water layer thickness
E	potential (V)
F(q)	form factor
I	electric current
K_C	bending rigidity modulus
Lα	lamellar phase
M_W	molecular weight
Pt	platinium
Q	electric charge
S(q)	structure factor
t	time
v	scan rate
η	Bending fluctuation
π-A	surface pressure-area

Chapter 1 Introduction

1.1 Flavonoids: General aspects and structure

Flavonoids, a class of polyphenols, with more than 6500 molecules, consist of one of the largest groups of secondary metabolites produced by plants and are present either as free aglycone (non-glycosylated form) or linked to a sugar molecule (glycoside conjugates). They can also occur as methylated derivatives (1, 2). The flavonoid chemical structure is based on a 15-carbon skeleton with a configuration of C6-C3-C6, consisting of two phenyl rings (A and B) linked to a heterocyclic C-ring as seen in **Figure 1.1** (1, 3).

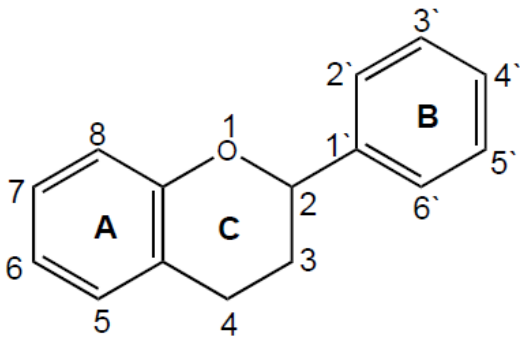

Figure 1.1 General structure and numbering pattern of flavonoids.

Flavonoid activities are structure-dependent. The major flavonoid subclasses can be ranged as; (i) flavonols, (ii) flavanones, (iii) catechins (flavan-3-ols), (iv) flavones, (v) anthocyanidins, (vi) flavanonols (dihydro-flavonols), (vii) isoflavonoids and (viii) chalcones (4). The differences between flavonoid classes arise from their chemical diversity such as the degree of hydroxylation, the presence of a double bond at C-2, oxidation and saturation of C ring, and the presence of sugar group moiety (2).

The *flavonols* constitute the broadest subgroup of flavonoids, with quercetin being the most studied type. Kaempferol and myricetin are the other well-known examples of flavonols. They possess a hydroxyl group at the 3- position, a C2–C3 double bond, and a ketone in position 4 of the C ring (5).

The *flavanones* differ from flavonols with a saturated heterocyclic-C ring. They have no conjugation between the A and B rings. The major examples of this group are naringenin, hesperetin, and their respective glycosides. They are generally glycosylated with a disaccharide at 7- position (6).

Catechins, also known as *flavan-3-ols* are present in large quantities in the diet, and unlike the other flavonoids, they are not present in plants bound to sugars. Similar to *flavonols,* they share a hydroxyl group at 3- position, however, their distinctive features arise from the lack of a keto group, at 4- position and a C2–C3 double bond (7).

Flavones are similar to flavonols; they have a C2–C3 double bond and a keto group at the 4-position. Typical examples of this group are apigenin, luteolin and tangeritin (3).

Anthocyanidins are the only group of flavonoids whose pigments are responsible for the distinctive colour of many fruits and also vegetables, for example, the purple, red, and blue colours of berries. Their colour is pH-dependent. Moreover, methylation or acylation can influence their colour. Anthocyanidins are flavylium cations and most often present as chloride salts. The glycosides of anthocyanidins are referred as anthocyanins (6, 8).

Flavanonols (also known as dihydro-flavonols) share a similar chemical backbone to those of flavanones with the presence of a -OH group at the 3- position. A well-known example of this group is taxifolin (9).

Isoflavonoids; the structural difference of isoflavonoids from flavonoids is the position of the B ring. With isoflavonoids, B-ring is attached to 3- position of the C-ring and the major type of isoflavones are genistein and daidzein (8).

Chalcones with an open structure, share similar synthetic pathways to flavonoids; hence, are considered as a flavonoid subclass (3).

Two-dimensional structures of flavonoids used in the current study are presented in **Figure 1.2**.

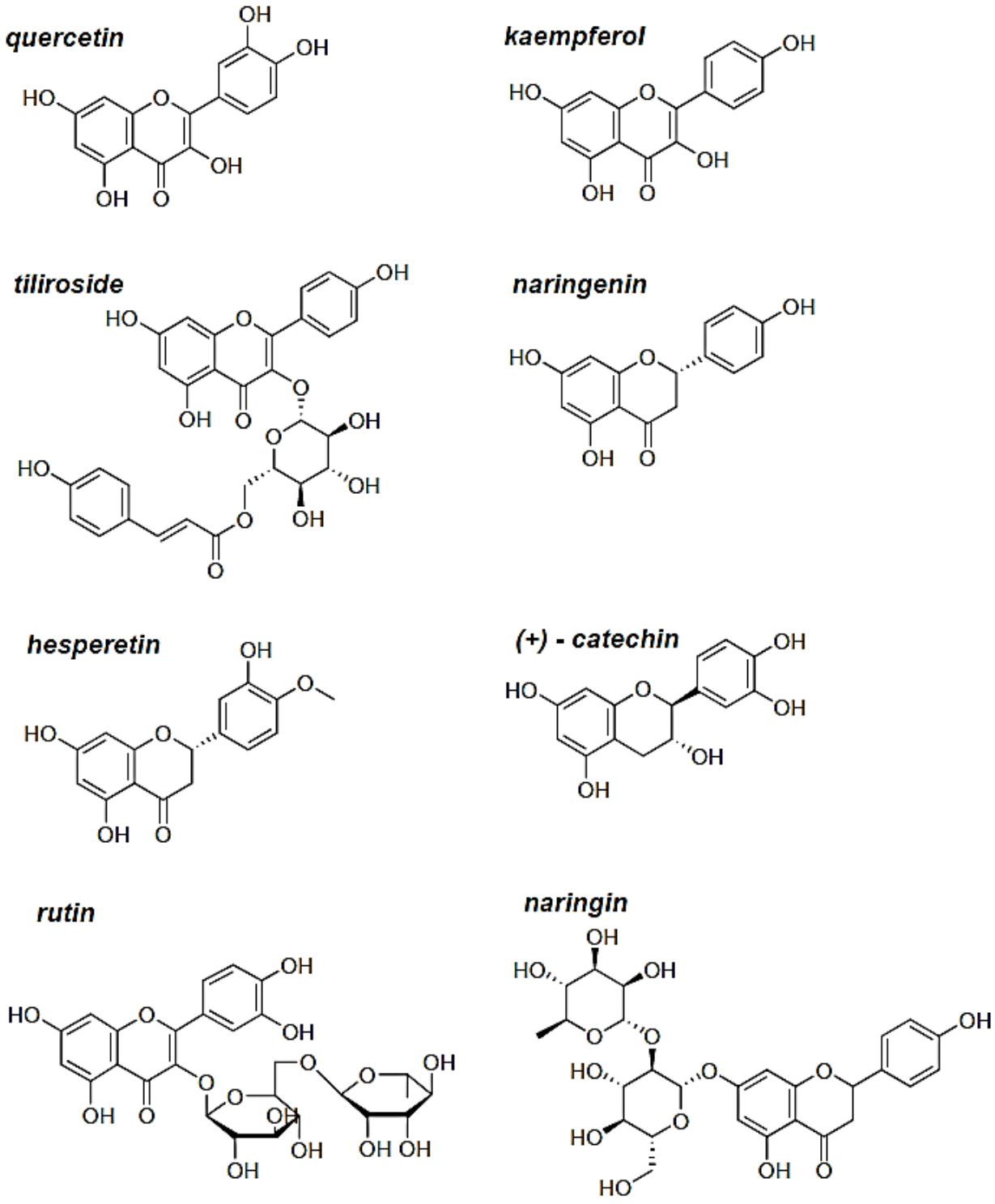

Figure 1.2 Two-dimensional structure of flavonoids used in the current study: quercetin dihydrate, kaempferol, tiliroside, naringenin, hesperetin, (+)-catechin, rutin trihydrate, and naringin**.**

1.2 Medical importance of flavonoids

***'Leave your drugs in the chemist's pot if you can cure the patient with food.'*- Hippocrates, 420 BC.**

Several plant-derived agents have been used in clinical trials due to their anticancer, antioxidant, antidiabetic, antimicrobial and anti-inflammatory potentials (10). Although it takes a considerable effort and time to uncover the biological mechanisms of these naturally occurring molecules, some of them have already been brought to market. A striking example to those of plant-derived medicines is taxol, which is currently the world`s best-selling anti-cancer drug (11).

Flavonoids as plant secondary metabolites are mainly present in fruits, vegetables, nuts and grains. They have received a considerable amount of interest for many years since they are believed to have an effect on human health (2, 8, 12). The first report proposing the existence of a particular type of flavonoid called Vitamin P was published in 1936 by Szent-Gyorgy and Rusznyak (13). Since then, a large number of epidemiologic studies have established a correlation between fruit and vegetable intake in the diet and reduced risk of various chronic diseases (13-16). One of the most comprehensive epidemiologic investigation on cardiovascular heart disease (CHD) with the participation of 84251 female and 42148 male was carried out by Joshipura et al. (17). This research reported a reduced risk of CHD for participants who consumed a high amount of fruit and vegetable in their diet. Following epidemiologic studies, clinical investigations were conducted under both *in-vivo* and *in-vitro* conditions to gain a better understanding of the therapeutic potentials of flavonoids.

Here, it should also be mentioned that there is a growing awareness for drug-free treatments and replace drugs with plant-derived natural products. Statistically speaking, the efficiency of a drug, for achieving the desired results is expressed as the number needed to treat (NNT) (18). In other words, the NNT is a measure of how well a drug is likely to treat a patient suffering from a particular health condition and the potential for harm. In 2003, Allen Roses who used to be the worldwide vice-president of genetics at GlaxoSmithKline (GSK) stated that almost 90% of the drugs work only for 30-50% of people, indicating that the drugs available on the market do not work for everybody (19). Moreover, two researchers independently confirmed that only 1 in 250 people could be helped by the drug statin, (which is the most widely prescribed drug in the world for lowering cholesterol) before one heart attack is prevented. On the other hand, for statin therapy, side effects occur in 5% of patients, which in turn shows that a patient is 12.5 times more likely to be harmed by this drug than to be helped (20, 21).

Above-mentioned studies imply that medicating with conventional drugs is becoming the default procedure and hence natural products such as flavonoids might be an alternative to pharmaceuticals in the treatment of various diseases. Some of the reported health benefits of flavonoids that are mentioned in the current study are summarised in **Table 1**, and briefly discussed below:

1.2.1 Antioxidant properties

Biochemically, oxygen is essential to produce energy from food compounds, such as sugar and fat. However, highly reactive molecules called free oxygen radicals can be formed due to the interactions between oxygen and certain molecules (22, 23). The cells in the body are subject to constant oxidative stress caused by external influences, such as the environment, air and also UV exposure from sunlight. Such influences can also trigger free radicals which

can further lead to cellular damage, inflammation, and as a result, can lead on to an increased risk of various chronic diseases (23-25).

Natural endogenous defences in the body can neutralise free radicals to cope with their destructive effects and the oxidative stress (22, 26). Although these endogenous antioxidants have a substantial role for cellular functions to be maintained, they may not be sufficient if there is an increase in the level of oxidative stress. Under this condition, the beneficial compounds such as vitamins and flavonoids can be taken exogenously as a supplement to the diet to protect the body against the damaging effect of oxidative processes (27, 28).

The potential protective features of flavonoids acting as antioxidative agents have been extensively studied in the literature (29, 30). Several groups have reported that flavonoids may inhibit the enzymes that play a role in the activation of carcinogens, and affect cell signalling mechanisms (31, 32). Flavonoids have also been reported to protect lipid biomembranes by inhibiting the lipid peroxidation process and scavenging free radicals (33). The potential antioxidant activity of flavonoids has been attributed to their structural features, in particular to the (i) catechol group on B-ring, (ii) hydroxylation at C-3 and carbonyl group at C-4 and (iii) the presence of a double bond between C-2 and C-3 (34). Nevertheless, due to their limited solubility, low bioavailability and extensive metabolism into glucuronides and sulphates metabolites, which have reduced antioxidant capacity, there exists a need for more evidence whether the flavonoids have a direct reactive oxygen species (ROS) scavenging antioxidant activity. Some of the reported findings regarding the potential antioxidant activity of flavonoids are given below:

Antioxidant activity of quercetin has been widely studied and well-described by both *in vitro* and *in-vivo* models. Patil *et al*. investigated the cognitive performance of quercetin in both

aged and lipopolysaccharide (LPS) treated mice for Alzheimer's disease (AD) associated dementia. Intraperitoneal (i.p.) injection of quercetin in mice for seven days improved the memory and learning abilities of mice by inhibiting the cyclooxygenase-2 enzyme (35).

A recent study investigated the antioxidant action of a quercetin glycoside, rutin, on the DPPH (2,2-diphenyl-1-picrylhydrazyl) radical scavenging activities. DPPH is a commonly used free radical to monitor the antioxidant activity of a compound. Two forms of rutin, alone and in a mixture of lysine in the Maillard reaction (MR), were studied. Rutin alone showed a high DPPH radical scavenging activity. Further measurements were conducted with the rutin–lysine MR product using Cu^{2+} induced HepG2 cells that are most prone to oxidative stress. Rutin-lysine treated HepG2 cells exhibited an enhanced free radical scavenging activity compared to rutin alone (36).

Tiliroside antioxidant activity has also been reported through both *in-vitro* and *in-vivo* studies. Chicaro *et al*. demonstrated the protective effect of tiliroside (25 μmol dm^{-3}) against linolenic acid peroxidation which was induced by 2,2-azobis (2-amidinopropane) dihydrochloride in micelles of sodium dodecyl sulphate. (37). A more recent *in-vivo* study looked at the antioxidant protective mechanisms of tiliroside in BV-2 microglia cell line with a combination of lipopolysaccharide (LPS) and gamma interferon (IFNγ). Tiliroside (6 μmol dm^{-3}) has been reported to reduce the ROS significantly from BV2 cells and activated the Nrf2/HO-1 antioxidant protective mechanism (38).

1.2.2 Antihistamine & anti-inflammatory properties

Due to its potential ability to prevent the release of histamine from mast cells, quercetin has been suggested as a natural antihistamine agent and has been marketed as a food supplement (39). Horcajada *et al*., for example, suggested that quercetin is a better mast cell stabiliser than Cromolyn, which is the only related pharmaceutical available in the market for

asthma disease (40). It was proposed that quercetin could regulate allergic reactions by limiting the release of mediators that trigger the allergy, such as histamine, prostaglandin DS (PGD2), tumour necrosis factor (TNF) and several cytokines like IL-8 (40). Similarly, rutin, a glycoside of quercetin, was suggested to serve as an anti-inflammatory agent in the treatment of osteoarthritis, as monitored through the decrease in the serum level of a type II collagen biomarker, Coll2-1 (41).

1.2.3 Antimicrobial activities

Flavonoids, in particular, catechins, have been widely studied for their antimicrobial properties. The proposed antimicrobial mechanisms of catechins are due to their ability to damage the cell membrane through binding to the bacterial lipid bilayer (both gram-positive and gram-negative bacteria) and to inhibit the enzyme activity and fatty acid synthesis (42). An *in-vitro* study with kidney epithelial cells evaluated the antimicrobial effects of catechin-rich green tea leaf extract using various pathogenic bacteria that cause skin infections. The study proposed that catechins in the extracts might inhibit the ability of bacteria to adhere and host cell membrane surfaces; hence they prevent bacterial growth (43).

It should also be mentioned that apart from the specific interactions of flavonoids with several enzymes and receptors as mentioned above, there are an accumulating number of studies, reporting the non-specific interactions of flavonoids with biomembrane lipids. These studies demonstrate that flavonoids can change the biomembrane physical properties such as fluidity/rigidity and thickness. Alterations in membranes` structural properties, i.e., fluidity changes have been linked to the therapeutic potentials of some flavonoids; therefore they are particularly important (44). Moreover, some studies have shown that flavonoids, through their interactions with biomembrane lipids, can influence the lifetime of model ion channels, such as gramicidin A (45, 46).

1.2.4 Dietary consumption of Flavonoids

The estimated daily intake of flavonoids can vary depend on the food type and flavonoids consumed by populations. According to a US-based study in adults, estimated mean total intake of flavonoids was 344.83 ± 9.13 mg/d, which 18.09 ±0.82 mg comes from flavonols (47). A more recent study by European adults (18-64 years old from 14 countries) reported similar results in the overall mean intake of total flavonoids which was 428±49 mg/d with an average of 23 ±2 mg coming from flavonols (48). Considering the flavonols used in the current study (M_W kaempferol = 286 – the smallest and M_W rutin = 664.56 – the largest) and the amount of water that enters the Gastrointestinal tract (GIT) per day is approximately 9 L, biological concentrations of flavonols is estimated to be in between 3.8-10 µM. However, this concentration can rise significantly to extremes. For example, 1 cup serving buckwheat tea contains around 675 mg rutin which corresponds to around 100 µmol dm^{-3} rutin consumption. Moreover, luminal concentrations (ileal and cecal lumens) of flavonoids are known to be much higher compared to the amounts in plasma. Suzuki *et al*. calculated the luminal flavonoid concentration in rats - higher than 40 µmol dm^{-3} whereas it is lower in plasma, i.e. 10 µmol dm^{-3} (49). Estimated daily intake of flavonoids mentioned in the current study, including their primary dietary sources is summarised in **Table 1**.

Table 1.1 Potential health benefits, dietary sources and estimated daily consumption of flavonoids mentioned in the current work.

Flavonoid Class	Flavonoids	Reported health benefits	Typical Dietary Source	Estimated dietary consumption (mg/d)
Flavonols	Quercetin	Supports respiratory health[40], balances blood pressure[50] and supports cardiovascular health [51]	Berry,onion	16 mg/d in adults (18 to 64 years) in the UK [48]
	Kaempferol	Antioxidant, anticancer, anti-inflammatory activity[52]	Apple, broccoli	8 mg/d in adults (18 to 64 years) in the UK [48]
	Tiliroside	Suppress obesity-induced metabolic disorders[53] Inhibiting of neuroinflammation[38]	Rosehip, potentialla species	NA
	Rutin	Anti-inflammatory agent[41]	Buckwheat	10 mg/d in adults in Sweden [54]
Flavanones	Naringenin	Antioxidant, anti-inflammatory and chemoprotective activity[55]	Citrus fruits	2 mg/d in adults (18 to 64 years) in the UK [48]
	Hesperetin	Antioxidant, anti-inflammatory, blood lipid and cholesterol lowering activity[56]	Citrus fruits	6 mg/d in adults (18 to 64 years) in the UK [48]
	Naringin	Antioxidant, anti-inflammatory and chemoprotective activity[55]	Citrus fruits	NA
Catechins	(+) – Catechin	Anticancer(57), antibacterial (58), aeuroprotective.	Green tea, red grapes	14 mg/d in adults (18 to 64 years) in the UK [48]

1.3 Absorption and metabolism of Flavonoids

Human intervention studies, including *in-vivo* and *in-vitro* testings, have been conducted to understand the absorption and metabolism mechanisms of flavonoids in the human body. Physicochemical properties, i.e. conjugation, structural configuration, molecular size, solubility and hydrophobicity have been reported to play a role in the flavonoid absorption released from the food (59).

Flavonoids are released from food initially by chewing before they make their way to the stomach. Walle *et al*. observed that some flavonoid glycosides, i.e. quercetin-3-rutinoside (rutin), quercetin-3-glucoside, quercetin-3-rhamnoglucoside, quercetin-4`-glucoside, and naringenin-7-rhamnoglucoside, can be hydrolysed to their parent aglycones by human saliva within two hours (60). The same authors also collected saliva samples incubated with genistein-7-glucoside from 17 different participants and reported a significant difference in the extent of hydrolysis for each sample (61). Here, it should be noted that the residential time for food in the mouth is considerably short. Therefore it might greatly limit the hydrolysis and metabolism of flavonoids. Hence it can be assumed that most flavonoids would remain intact before reaching the stomach (60).

The metabolism of flavonoids in the stomach showed a rapid absorption of some flavonoids. For example, administration of quercetin (aglycones) to a rat`s stomach was recovered after 20 min in bile. In contrast, no absorption or deglycosylation was reported with quercetin glycosides, rutin and quercetin-3-O-glucoside (62). Similarly, no absorption occurred with isoflavones in the stomach. Rios *et al*. conducted a human study using a nasogastric tube to detect whether the procyanidin polymers and flavanol monomers are absorbed in the

stomach after the consumption of a cocoa beverage. Quantification of samples via HPLC showed no difference in the profile up to an hour proposing very little or no absorption of procyanidins in the stomach (63). In general, the results mentioned above suggest that most of the flavonoids remain intact in the stomach.

The small intestine is an important site for flavonoid absorption. Although initial studies suggested an intact absorption of flavonoid glycosides from the small intestine and hydrolysis to the corresponding aglycones in the colon (64), it is now well-accepted that some flavonoid glycosides would be hydrolysed to their parent aglycones before absorption. This was first evidenced by Day *et al*. who identified that lactase-phlorizin hydrolase (LPH), a well-known enzyme hydrolysing milk, is also responsible for hydrolysing quercetin glucosides prior to their transport into the enterocyte cells (65). Day then suggested that flavonoids that are not a substrate for LPH can be deglycosylated into the colon by microorganisms. This finding was further supported by many other studies (66, 67).

Upon absorption from the enterocyte cell membrane in the small intestine, flavonoids may undergo phase I and phase II metabolism. Phase I metabolism involves hydrolysis, oxidation, or reduction reactions using mainly the cytochrome 450 (CYPs) enzymes. Whereas phase II metabolism involves conjugation reactions, i.e. glucuronidation, sulfation and methylation, which requires the enzymes, the UDP-glucuronosyltransferases (UGTs), sulfotransferases (SULTs) and catechol-O-methyltransferase (COMT), and cofactor SAM, respectively (64).

Compartments involved in the flavonoid metabolism are shown in **Figure 1.3**.

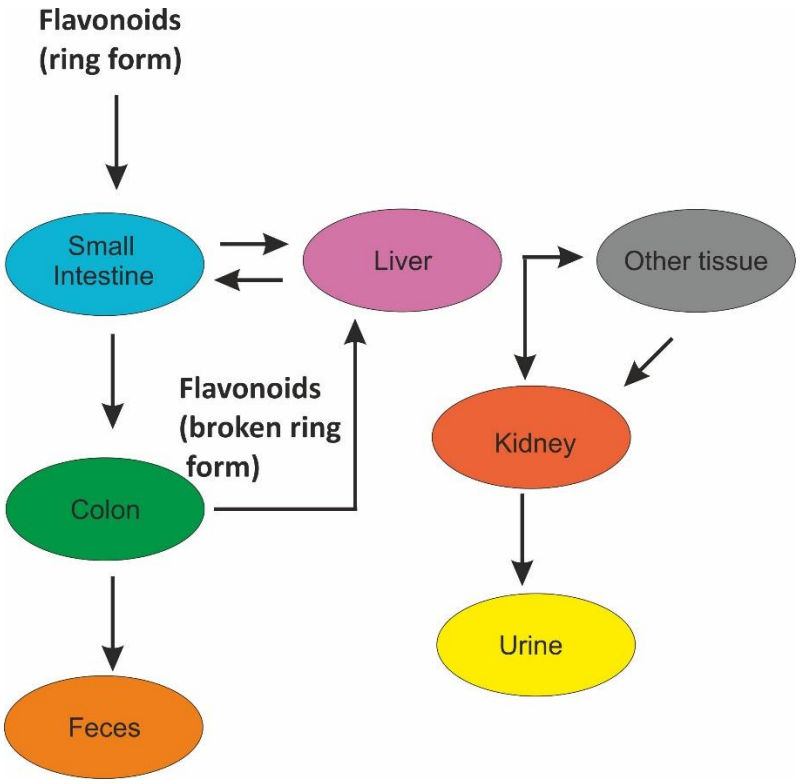

Figure 1.3 Compartments involved in the flavonoid metabolism (3).

1.4 Cell membranes

The current fluid mosaic membrane model was proposed by Singer and Nicholson (68). Based on the direct observation of cell membranes via electron microscope, in this model, membranes consist of two phospholipid layers in which proteins and carbohydrates are embedded and orient their hydrophobic and hydrophilic parts with the respective lipid counterparts. Asymmetrical distribution of protein and lipid molecules in the inner and outer leaflet of the membrane and lateral mobility were suggested. Further works modified the model with the lipid raft hypothesis by Simon (69) and Brown (70). According to these authors, instead of forming a homogenous fluid phase, lipids and proteins are sequestered into small phase-separated domains known as lipid rafts. In general, all biomembranes consists of lipids and proteins, and some membranes also include carbohydrates in the

composition. **Figure 1.4** shows the fluid mosaic model of a biological cell cytoplasmic membrane.

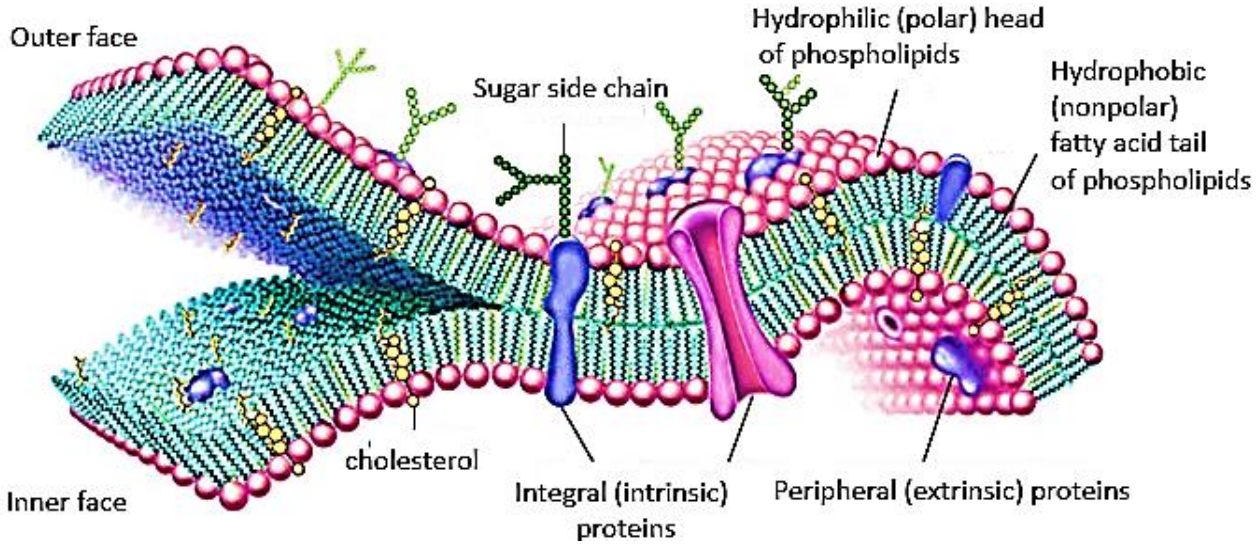

Figure 1.4 The fluid mosaic model of a biological cell cytoplasmic membrane. Original image modified from a source image by courtesy of Encyclopaedia Britannica, Inc., (Chicago, Illinois, USA), Copyright 2007; used with permission.

1.4.1 Lipids, sterols and proteins

Lipids are defined as water insoluble amphiphilic biomolecules with a variety of biological roles from serving as building blocks of membranes to being an energy reserve, and they constitute approximately 50% of the cell membranes (71). In eukaryotic cells, the endoplasmic reticulum (ER) is the site where membrane lipids are mainly synthesised. The three most abundant types of membrane-forming of lipids in eukaryotic cells are phospholipids, glycolipids, and cholesterol (72).

Phospholipids are the most abundant lipid type in cell membranes. Phospholipids are lined up into two parallel layers to form the phospholipid bilayer. They consist of a polar head group and two apolar tails. The tail is made up two fatty acid chains which may differ in length. The number of carbon atoms of each chain typically varies between 14 and 24. The fatty acids are

joint together by a glycerol head. Glycerol is a three-carbon molecule, and together with the phosphate group, forms the polar head group (72).

The fatty acyl chains may be classified as saturated (all carbons in the chain are bonded to each other by single covalent bonds) and unsaturated (with one or more double bonds in the chain). The cis double bond introduces a kink in the tail as shown in **Figure 1.5**. The kinks prevent tails packing tightly which in turn causes an increase in the membrane fluidity (73). Hence, apolar interactions between unsaturated tails become less strong compared to the apolar interactions with saturated chains. This situation explains the difference between the physical states of vegetable oil and butter. At room temperature, highly saturated fats are solid whereas highly unsaturated fats are liquid (74). Temperature affects the fluid state of membranes. Upon heating, the individual lipids are more mobile. Hence, the phase transition of lipids such as dipalmitoylphosphatidylcholine (DPPC) that are in gel solid/state at room temperature change their phase to liquid/mobile above their phase transition temperature (37 ^{o}C).

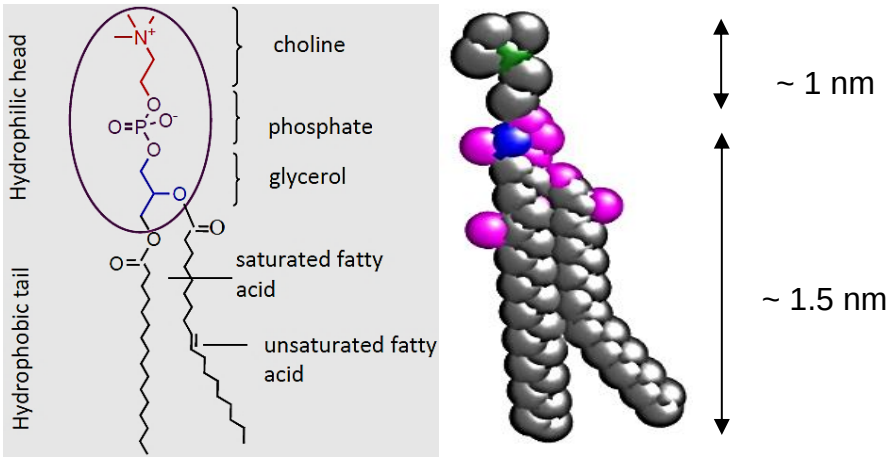

Figure 1.5 Structure of a phospholipid with one unsaturated tail and its space-filling model.

Glycerol-based phospholipids - glycerophospholipids or phosphoglycerides - are the most common ones in biological membranes. The alcohol moieties of phosphoglycerides determine their category. Depending on the alcohol group, some common phosphoglycerides found in mammalian membranes are given in **Figure 1.6(a).** These are phosphatidylethanolamine (PE), phosphatidylserine (PS), phosphatidylcholine (PC) and phosphatidylinositol (PI) (75).

Another phospholipid type found in membranes is sphingolipid which is derived from sphingosine alcohol and consists of a long (18-carbon) unsaturated hydrocarbon chain. See **Figure 1.6(b**) for sphingomyelin (SM) and glucosyclceramide (GlcCer) (72).

Among sterols, cholesterol is the most common in animal tissues and acts as a regulator of biomembrane fluidity. Literature findings suggest that while relatively low cholesterol content (1-5 mol %) induces membrane fluidisation, higher concentrations (above 10 mol%) lead to membrane rigidification (76).

Another type of sterol is ergosterol, which is primarily found in the membrane of fungi, where it serves a similar role to that of cholesterol (77).

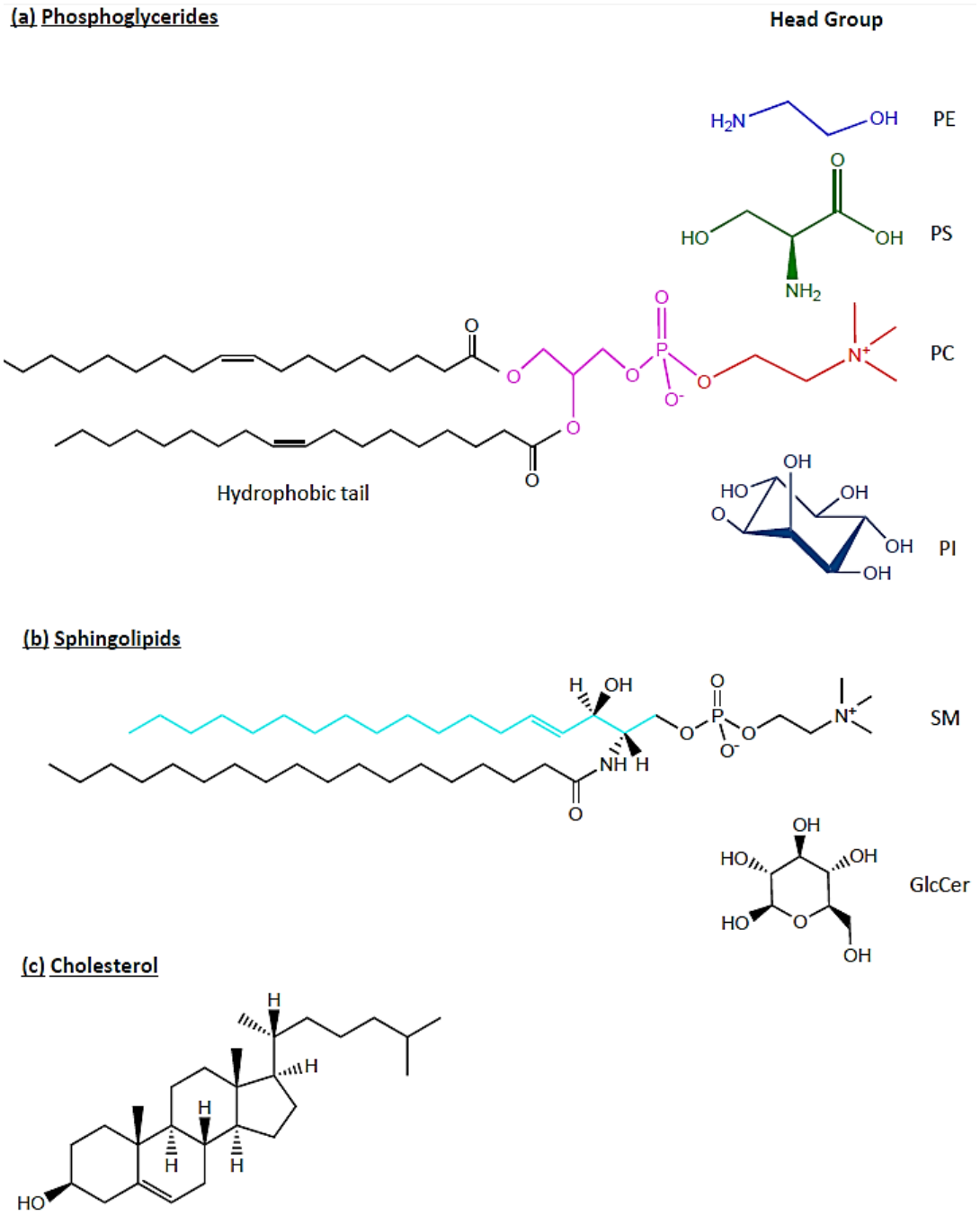

Figure 1.6 Lipid types and classification.

Proteins are another principal components of membranes, and can broadly be classified as transmembrane and surface-bound proteins. Transmembrane proteins, also known as integral membrane proteins, span the entire phospholipid bilayer and reach the aqueous

phases on both sides of the membrane. Surface-bound proteins are associated or anchored on one side of the membrane surface without contacting the opposite monolayer leaflet (75).

1.5 Model membranes

Phospholipid bilayers act as boundaries for controlling the passage of molecules that can move across the membrane. Nutrients in food, drugs or toxins have to cross membranes to exert their beneficial or harmful effects. However, membranes in living cells are highly complex and dynamic structures, and hence it is challenging to understand the interactions between molecules of interest and the membrane lipids. It is therefore of great importance to work with artificial membranes that can mimic natural cell membrane behaviour. And in doing so, it is possible to simplify the heterogeneity of intact cells to document the role of a single component, such as phospholipids, which actually form the fundamental skeleton of biomembranes. Physical properties of membranes, i.e. thickness, fluidity/rigidity, lipid packing behaviour and mechanical properties, including bending and stretching, can be studied in this way (78)

Biomimetic membranes, whose composition, size and geometry can be tailored, provide a highly manipulable model to examine the required processes under controlled conditions. Model membranes can serve as an effective tool particularly for the pharmaceutical industry, since they can quickly be produced with reduced costs compared to live cells, such as the ones in the preclinical testing of a newly formulated drug with respect to its cell membrane interaction (79). Free-standing lipid monolayers, i.e. Langmuir monolayers at the air/water (A/W) interface, and bilayers, i.e. black lipid membranes (BLM) and solid-supported, (i.e. platinum, gold) lipid monolayers and bilayers have commonly been used as biomimetic models (75). The membrane models employed in the current study are (i) 1,2 dioleoyl-sn-

glycero-3-phosphocholine (DOPC) monolayer coated Hg electrode, (ii) free-standing Langmuir monolayers and (iii) multilamellar vesicles (MLVs), respectively. A brief introduction to describe each membrane model is given below.

1.5.1 Solid substrate supported phospholipid monolayers

Self-assembled monolayers (SAMs) can be fabricated on a supporting material, which provides a stable and robust platform for monolayer films. Substrate-supported monolayers (and bilayers) are preferred systems for bionanotechnological applications, such as sensors due to their stability. The solid substrate, on which the thin film is deposited provides an easy manipulation of the chemical and physical properties of the monolayers. Most commonly used supporting materials are silica, borosilicate glass, gold, mica and platinum (78, 80).

Unlike the closed structure of vesicles, SAMs form planar structures on the supports and represent half of a bilayer. Hence, only the upper leaflet is exposed to the aqueous solution. The over-riding advantage of these systems arises from their high stability even under high flow rates. Moreover, depositing a membrane on to a solid substrate would allow employing a number of surface specific analytical techniques, such as Förster resonance energy transfer (FRET). On the other hand, the possible limitation of such systems is caused by possible interactions between the solid support and membranes (81).

Electrochemical studies have been widely employed to understand the structural characteristics and functionality of supported SAMs (82-86). The idea of depositing lipid layers on Hg electrode was initially put forward by Miller *et al*. (87, 88). Miller`s technique inspired Nelson and, in a similar approach, Nelson *et al*. deposited SAMs on the substrate surface coated with mercury (Hg) for the toxicity prediction in aqueous media (please see review by Nelson (82) for detailed information). Hg has several advantages over other substrate

materials of electrodes (82, 89): First of all, the Hg electrode is an ideally polarised electrode because electrode reactions are kinetically impeded within a certain potential window (double layer range); and hence it exhibits a capacitor type behaviour. More importantly, Hg is (i) hydrophobic in nature and, (ii) a liquid at room temperature. All these characteristics mentioned above render Hg highly compatible with fluid phospholipid layers. Therefore, it provides an ideal platform for supporting stable phospholipid monolayers (83) as depicted in **Figure 1.7**. Due to the fluid nature of phospholipids, they can undergo structural changes in the electrified fields. Such structural changes, in other words, phase transitions, appear as sharp capacitance peaks, (82) which will further be discussed in the next chapter (section 2.2.4).

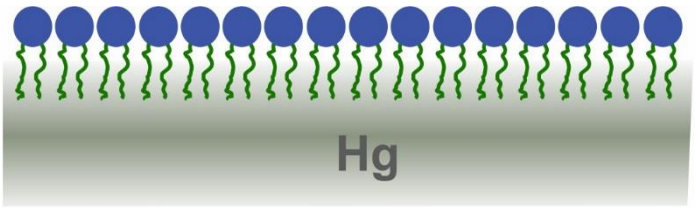

Figure 1.7 Monolayer coated Hg electrode.

1.5.2 Free-standing Langmuir monolayers

Langmuir monolayers are attributed as excellent tools for interaction studies of amphiphilic molecules. As depicted in **Figure 1.8**, Langmuir monolayers are formed at the A/W interface by spreading an organic solution of a known number of phospholipid molecules over the water surface. The membrane forming lipid molecules pack together into well-defined, insoluble thin films at the surface, which resembles half a membrane in order to mimic the processes at membrane surfaces (90).

This technique has vital importance in understanding the packing behaviour of different lipids and their mixtures. It allows characterisation of lipid-lipid or lipid-surface-active compound

interactions at various physical phases (liquid-liquid, gaseous phase, etc.) in two-dimensional (2D) arrangements. The composition of lipid mixture, subphase conditions i.e. temperature and pH can be defined depending on the experimental requirements (79).

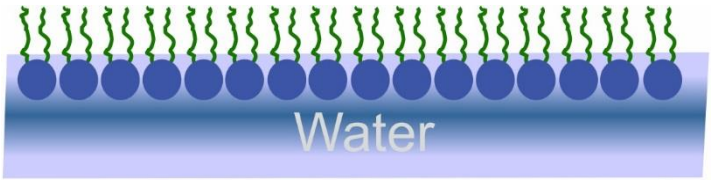

Figure 1.8 Free-standing Langmuir monolayer at the A/W interface.

Generally therefore, ultra-thin films of monolayers (both free-standing and supported monolayers) are attributed as powerful experimental tools for modelling biomembrane function. In a way they mimic bilayer systems since compressed films of lipids were shown to exhibit the same chemical potential and molecular areas with bilayer systems in equilibrium (79).

1.5.3 Multilamellar vesicles

Due to their self-assembly properties, lipid molecules are organised into different morphologies spontaneously in aqueous solutions. Bilayers, in the form of vesicles, vary by size from nanometer levels, i.e. small unilamellar vesicles (SUV) to micron level, i.e. giant unilamellar vesicles (GUV). They can also be configured as multilamellar vesicles (MLVs), and large unilamellar vesicles (LUVs) (79). Such final form depends on the preparation method, for example, LUVs and SUVs can be produced from the MLV dispersions via sonication and extrusion through a porous membrane respectively (75, 79). **Figure 1.9** depicts the multilamellar vesicle structure.

Depending on the preparation method, the most likely disadvantage of lipid vesicles might arise from the membrane lifetime (short life span), which in turn, might result in the formation of vesicular aggregates and clumps over a long period (79).

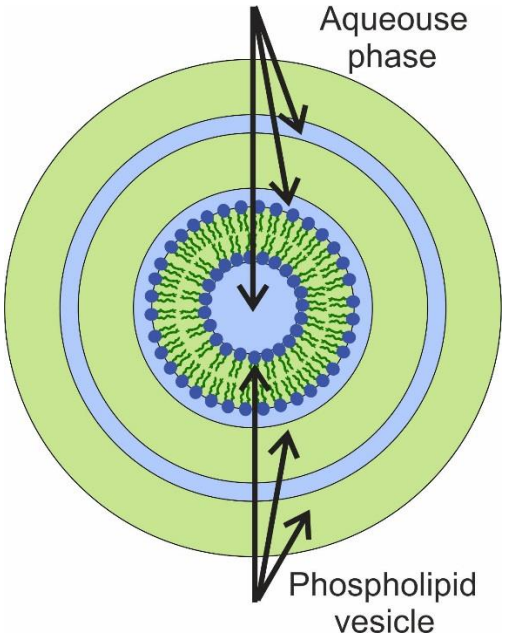

Figure 1.9 Multilamellar vesicles or liposomes.

Lipids can also arrange themselves in a variety of lamellar and nonlamellar structures such as bio continuous cubic phase, lamellar bilayer, spherical and inverse micelles, hexagonal and inverted hexagonal phases (71). Each of these aggregates is characterised by the certain curvature of the surface. The surface curvature and the volume of each molecule determine the geometric packing and control the shape of each aggregate formed (75, 91).

1.6 Surface properties of membranes

1.6.1 Surface tension

As shown in **Figure 1.10**, the intermolecular attractions between the water molecules in bulk are in all directions, which means that the attractive forces between them are balanced. However, water molecules at the surface experience an imbalance of forces as they have no neighbours above them to balance the molecular attraction. This disruption in the equilibrium of forces at the air/water interface results in a higher attraction of a molecule towards the bulk liquid than the air phase. Hence, the molecules located at the A/W interface create a net downward attractive force which causes the surface to minimise its area and results in what is called as surface tension and is represented by gamma, γ (92).

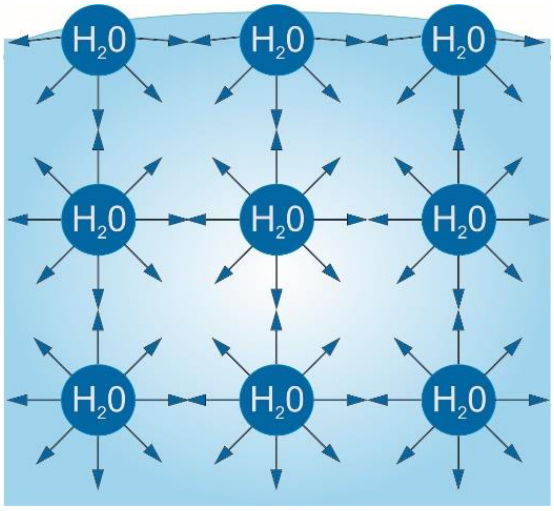

Figure 1.10 Illustration of water molecules in bulk and at the A/W interface.

Surface tension (γ) can be better explained based on the surface thermodynamics. Since the force (F) created is against the work done to extend a liquid surface, an overall increase in the free energy of the system is observed. The surface tension is described as the force per length and is usually expressed in units mN m^{-1} (93).

$$\gamma = \frac{F}{2L} \qquad (1.1)$$

Unlike the most other liquids, water has a high surface tension of 72.8 mN m^{-1} (20 ^{o}C) due to the strong intermolecular interactions of its molecules. Because of such a high surface tension, it can be used as an ideal subphase for monolayer studies. The surface tension decreases when the surface-active molecules, i.e. amphiphilic molecules are introduced to the interface. Amphiphilic molecules can form insoluble monolayers with their polar head groups facing towards aqueous phase and apolar tails facing towards the air. These apolar and polar groups determine their affinity for the interface, i.e. molecules with a short hydrocarbon chain, or a large polar head group, are not able to form a stable monolayer as the molecule would be expected to dissolve into the bulk phase (92, 93).

1.6.2 Surface pressure

As depicted in **Figure 1.11 A,** the behaviour of phospholipids at the interfaces (air/water or oil/water) can be characterised by measuring the alterations of the lateral surface pressure (π) as a function of the area (A) available per molecule. A two-dimensional phase diagram/isotherm is obtained as a result of monolayer compression which gives integral information on the lipid - phase transition. The monolayer morphology can further be characterised employing optical microscopy techniques such as BAM and fluorescence microscope (90). The BAM principle and measurements will be detailed in the next chapter.

Formation of an insoluble monolayer film by amphiphiles at an A/W surface also called Langmuir film, lowers the surface tension due to the interaction of polar part of the amphiphiles with water surface molecules. As depicted in **Figure 1.11 (B)**), when the molecules initially spread over a liquid surface (which is deposited in a Langmuir trough), the distance between the molecules is large in the gaseous phase. Hence the monolayer does not cause significant alterations in the surface tension. When the monolayer is compressed at a

constant temperature, amphiphiles start to interact with each other strongly. The area that is available for each amphiphile decreases. As a result, surface tension decreases and surface pressure increases (see **Figure 1.11 B**) (75, 92, 94).

The surface pressure is simply defined as a change of the surface tension between pure liquid (water) and the one with an adsorbed film as shown by the **equation 1.2**,

$$\pi = \gamma_o - \gamma \qquad \textbf{(1.2)}$$

where γ_o and γ refer to the surface tension of pure liquid and surface tension of film-adsorbed surface.

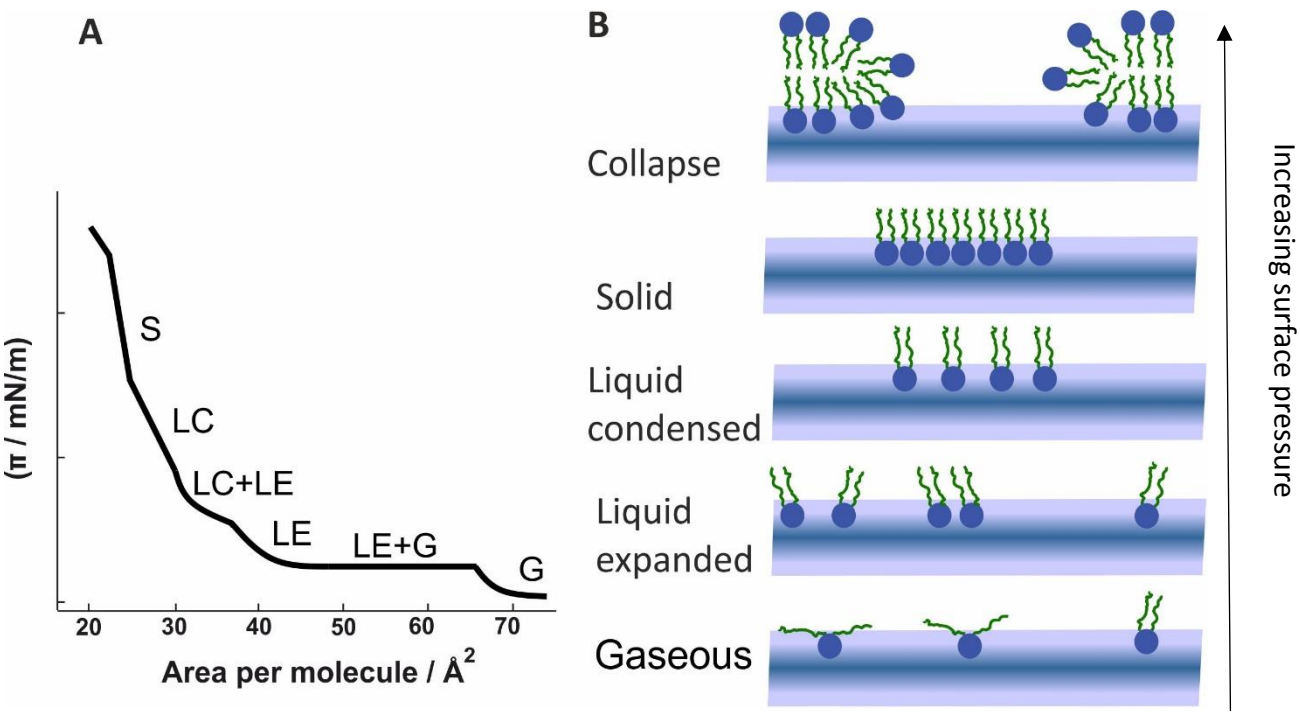

Figure 1.11 Surface pressure / molecular area Isotherm with corresponding monolayer phases. Figure modified from Lyklema[94]

1.7 Electrical properties of membranes

Lipid bilayers act as a barrier to the prevention of free movement of most molecules i.e. ions across the membranes. Due to this characteristic property, cell membranes can be attributed as excellent electrical insulators. Transportation of chemicals across the plasma membranes can occur via different pathways for instance through passive diffusion or active transport (95). Passive diffusion is driven by the concentration difference between extra and intracellular membrane. On the other hand, active transport involves the use of energy from ATP. As a result of ion movement, an electrical field or potential differences occur at interfaces which, in a sense render the interface properties electrical in nature (95).

1.7.1 (Bio)membrane capacitance

As mentioned briefly in the previous section, cell membranes can act as electrical insulators by keeping the charged molecules separated across the membranes, and hence they can be modelled as capacitors. In other words, cell membranes can be described as a dielectric material in between the interior and the exterior region of the membrane which consists of a mixture of ions dissolved in aqueous media and act as conductors (95). Membranes as a dielectric can be polarised upon applying an external electric field. (96).

The dielectric constant of biomembranes determines the membrane`s response such as ion permeability to externally applied electrical fields through different techniques, i.e. cyclic voltammetry (84), and impedance spectroscopy (97). Such a response provides information about the interfacial properties between the membrane and the liquid surface, i.e. adsorption and penetration of molecules within the membrane.

In biological membranes, ion channels and pumps are responsible for voltage difference, and the voltage across a membrane is described as the membrane potential. At rest, cells have a

potential range from -40 to -80 (inside relative to outside). Since the interior and the exterior of the cell membrane are surrounded by ions at different concentrations, ion channels allow ions to move from an area of higher concentration to an area of lower concentration. Ion pumps on the other hand play role to actively push ions across the membrane against their concentration gradient. Ion channels and ion pumps can, therefore, be represented as electrical equivalent batteries or resistors embedded in the membrane (98, 99).

In electrochemistry, charge transportation occurs between electrodes via charge carriers, i.e. ions in an electrolyte solution. Electric current is produced as a result of a flow of electric charge over a period. The relationship between electric charge and current is provided in the equation of 1.3,

$$\boldsymbol{I = \frac{Q}{t}} \qquad \textbf{(1.3)}$$

Where *I*, *Q* and *t* represent current in amps, charge in coulombs and time in seconds; respectively. Current can be measured only in the presence of a voltage applied across a conductor (100). The charge can be stored to be used later; such a device is called as capacitor, visualised as composed of two separated plates. As the capacitor is charged, one of the plates will become positively charged while the other becomes negatively charged and the voltage builds up across the plates. The charge on each plate of the capacitor continues to flow until the voltage potential of the capacitor becomes equal to the voltage source. It is possible to determine the amount of charge stored in a capacitor by the equation of 1.4,

$$\boldsymbol{Q = \frac{C}{V}} \qquad \textbf{(1.4)}$$

where *Q* and *C* represent charge and capacitance in Coulombs and Farads, respectively while *V* is the voltage across the plates (99, 100).

The capacitance is directly proportional to the surface area (A) of the plates (conductors) and inversely related to the distance (d) that separates the plates.

The ability of a dielectric to support an electric field is called permittivity, and this is a measure of how easily a dielectric material can become polarised in response to the electric field.

Two plates of the capacitor are separated by a distance *d.* The substance separating two plates should be an insulator that does not allow electrons to flow. This insulating substance is called as dielectric and the value for dielectric constant ε, or relative permittivity, is specific to the nature of each material. Hydrophilic environments possess high ε values i.e. water (ε ~ 78.5) whereas hydrophobic environments i.e. phospholipids' alkyl tails possess low ε values i.e. (ε ~ 2) (101). The following equation gives capacitance C (SI units Farads), between two plates with distance *d;*

$$\boldsymbol{C = \frac{\varepsilon \varepsilon_0 A}{d}} \qquad \textbf{(1.5)}$$

Where ε_0 is the permittivity constant for free space, ε is the relative permittivity of the insulating material, and *A* is the area of plates in square metres (99).

1.7.2 Membranes as RC circuits

As mentioned cell membranes exhibit a variety of electrical properties and they can be modelled as a resistance-capacitance circuit (RC circuit) as shown in **Figure 1.12** where C_m is membrane capacitance and R_m is membrane resistance, and R_s is total resistance of the bathing solution and electrodes (102).

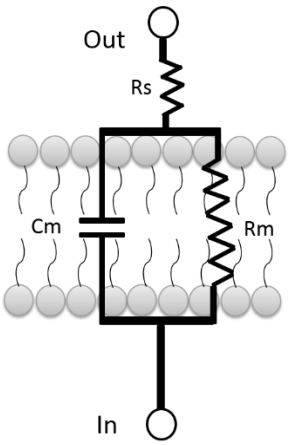

Figure 1.12 Equivalent resistor-capacitor circuit (RC) for a membrane model.

An electrical potential *V* can be applied across the membrane, and hence the charge (Q) could be separated. Upon applying a potential from *V* = 0 to *V,* the *V* gets dissipated through the resistor (R_s) and capacitor (C_M). The voltage drop in the resistor is measured to measure how much *V* is dissipated;

$$\boldsymbol{V_R = iR_S} \qquad \textbf{(1.6)}$$

the potential drop across the capacitor (C_M) is

$$\boldsymbol{V_{Cm} = \frac{q}{C_M}} \qquad \textbf{(1.7)}$$

The potential drop for the circuit is therefore,

$$\boldsymbol{V = V_R + V_C} \qquad \textbf{(1.8)}$$

Note that equivalent resistor-capacitor circuit (RC) for a membrane model can be more complex than described in this section.

1.7.3 Electrical double layer

Two types of processes occur between the electrode surface and solution; Faradaic and non-Faradaic processes. Faradaic processes, which are not of interest to the current study, are used to study redox properties of the materials arising from charge transfer across the

metal/electrode interface. However, between a particular range of potentials, no electron transfer is observed on the metal/electrode interface, but adsorption and desorption of ions can occur (103). This process is called as a non-Faradaic process, and in this case, electrode/solution interfaces have the ability to act as capacitors due to their double layer properties (104). Helmholtz in 1879 coined the model `electrical double layer` (DL) as a simple capacitor type of structure; having two sheets of charge at an interface with an opposite polarity separated by a distance of one molecule. Following equation describes the relationship between the stored charged density (σ) and the voltage drop (V) between the plates.

$$\boldsymbol{\sigma = v\ \frac{\varepsilon\varepsilon_0}{d}} \qquad \textbf{(1.9)}$$

Where ε is the dielectric constant of the medium, ε_o is the permittivity constant, and d is the interplate spacing. Hence differential capacitance is given as;

$$\boldsymbol{\frac{\partial\sigma}{\partial V} = C_d = \frac{\varepsilon\varepsilon_0}{d}} \qquad \textbf{(1.10)}$$

According to this model, a single layer of ions is adsorbed on the charged electrode surface as depicted in **Figure 1.13** and no electron transfer reactions occur at the electrode. The charge at the electrode surface is neutralised by opposite sign counterions placed close to the electrode surface. This model only considers electrostatic interactions between the ions at both electrode surface and in solution.

A significant contribution to Helmholtz model was made by Louis Georges Gouy and David Leonard Chapman by introducing a diffuse model of DL in addition to electrostatic forces. (103). As a result of building up a high concentration of ions at the electrode surface, ions would have a tendency to diffuse up to the bulk. Electrostatic forces would then pull the ions towards the surface whereas the diffusion would pull the ions back in the solution. In other

words, this theory proposes the presence of an interplay between electrostatic and diffusion processes which then maintain a layer of counterions on the charged surface. This leads a diffuse layer of counterions and called as the diffuse double layer.

In this model, ions do have a thermal motion due to Boltzmann distribution but size is considered as point charges, and Gouy Chapman theory neglected the adsorbed ion layer and failed for the highly charged double layer (103). This theory was further modified by Stern who developed a more sophisticated theory by combining the predictions from both Gouy Chapman and Helmholtz models. The interface in Stern model in a way signifies as two series connected capacitors. As seen in **Figure 1.13**, there is an inner layer (Stern layer) and an outer diffuse layer in this model (103, 105).

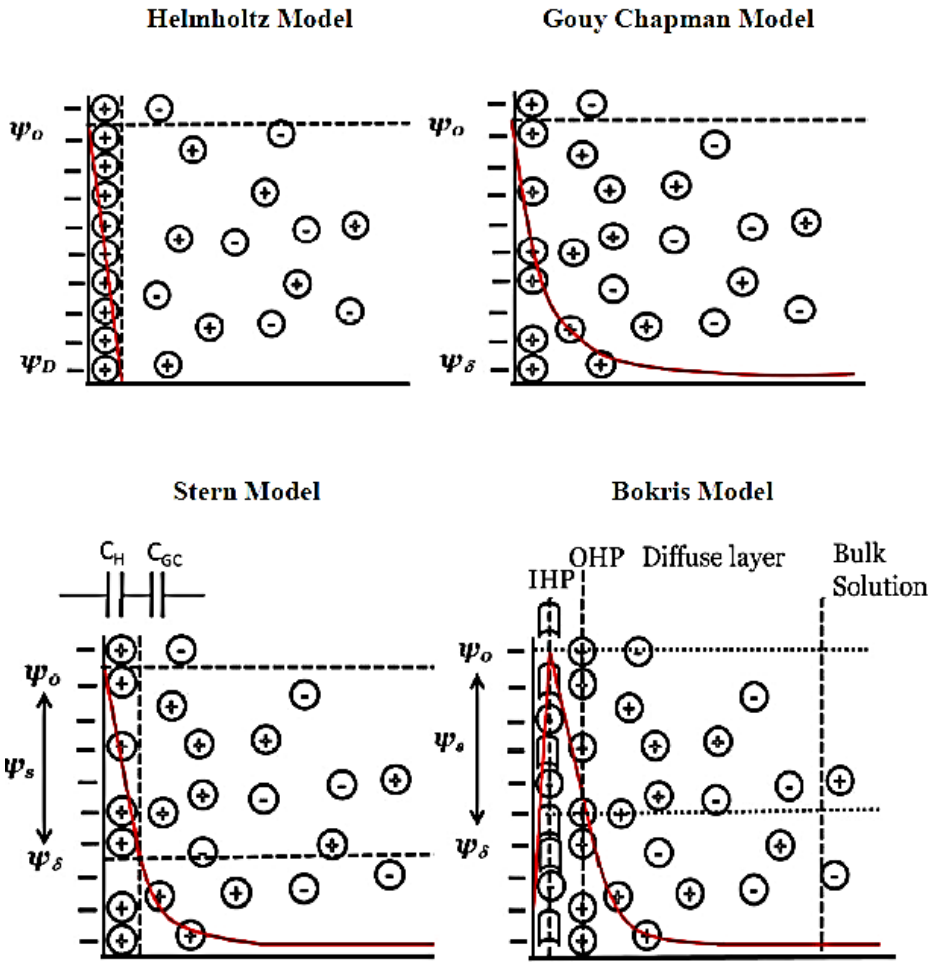

Figure 1.13 Different models of electrical double layer .

1.8 Interactions of flavonoids with membranes

The molecular mechanism of action of flavonoids is a longstanding debate. Although their mechanism has been widely attributed to specific interactions involving protein–flavonoid binding, recent studies have intimated that flavonoids alter biomembrane organisation, which might then lead to modifications in membrane protein function (106, 107).

The simplest techniques that can be used to test this hypothesis involve the use of biological membrane models with associated biophysical techniques. As mentioned in section 1.5 of this chapter, the advantages of these model systems arise from their reduced complexity and improved experimental control compared to cell cultures.

Various techniques have been employed to investigate the molecular mechanism behind flavonoid-membrane interactions using model systems. These include spectroscopic techniques such as electron paramagnetic resonance (EPR) (108), nuclear magnetic resonance spectroscopy (NMR) (109), fluorescence spectroscopy measurements (110), electrochemical methods (111), and differential scanning calorimetry (DSC) (112). Each of these techniques provides understanding into a particular aspect of the interactions, such as membrane fluidity/rigidity, membrane localisation of flavonoids, and their structure-activity relationship .

One of the very first studies about flavonoid-membrane interactions with biomimetic membranes was published by Saija *et al*. in 1994. Since then many other reports have investigated the effect of flavonoids on phospholipid membranes. Ollila *et al*. (113) employed noncovalent immobilised artificial membrane (IAM) chromatography to probe the interactions between DPPC bilayers and eight different flavonoids with varying degree of hydroxylation. The findings suggested that flavonoids which are rich in hydroxyl groups exhibited higher interactions with the DPPC membrane interface. Van Dijk et al. (114) studied the affinity of flavonoids for liposomes via quenching measurements. Flavonoids which are planar in configuration i.e. quercetin and morin exhibited higher affinity for liposomes compared to flavonoids which are tilted in configuration. Interestingly this study is also the only study, reporting that flavonoid glycosides (naringenin and eriodictyol) showed a higher affinity towards liposomes compared to their parent aglycones.

Studies have also reported the effect of flavonoids on membrane fluidity alterations and their location within the membranes. However, the results in this context remain controversial. While some studies suggested a membrane-rigidifying effect of flavonoids accompanied with

their location in the membrane hydrophobic core, many others assumed an opposite effect - fluidising membranes along with a tendency to localise at the lipid/water interface. The results in this context will be discussed in the further sections of the thesis.

In summary, literature findings reported a number of parameters that have a role in flavonoid-biomembrane interactions. Structural properties such as the configuration, the number and position of OH- groups, the existence of glycosidic moiety, together with the hydrophobicity of flavonoids have been reported to have an influence in their biomembrane activity. However, in spite of the work done looking at the biological activity of flavonoids, the interaction mechanism between flavonoids and model biological membranes has not yet been fully understood, and the literature so far remains controversial. Flavonoid concentration and lipid membrane composition, as well as the diversity of techniques employed, could contribute to the variation of the results (115).

The results of the current work and the comparison with the previous reports in terms of structure-activity relationship, membrane alterations with flavonoids, and their proposed membrane localisation will be discussed in depth in throughout this thesis.

1.9 Aims and objectives

The main goal of this research work was to develop a better understanding of the flavonoid-biomembrane interactions in a cross-platform approach. For this, we employed distinctively different techniques to extract complementary information regarding the interactions.

- One key objective of this study was to investigate the interactions of flavonoids with the self-assembled phospholipid monolayers on microfabricated electrodes. By this, we aimed to reinforce the electrochemical sensing system for the food ingredients for

the first time. A successful application of this sensing device allowed establishing a structure-activity relationship (SAR) of a variety of flavonoids with membranes to elucidate the structural characteristics responsible for their membrane activity. Moreover, we intentionally avoided the influence of an additional variable involved in flavonoid-membrane interactions. Hence, unlike many conventional membrane models of liposome bilayers, this study aimed to use monolayer membrane models in proof-of-concept experiments with one lipid type; 1,2 dioleoyl-sn-glycero-3-phosphocholine (DOPC) to screen flavonoid interactions.

- Another motivation of this study was to correlate the findings obtained by the electrochemical membrane sensor with a very fundamental technique; Langmuir monolayers of DOPC at air/water interface. Langmuir monolayers are excellent systems to monitor film stability. Exploring the effects of flavonoids on the film stability is especially important in investigation of the therapeutic effects of flavonoids that involve cell-stabilisation.
- Finally, we aimed to characterise flavonoid-membrane interactions with lipid vesicles which are more realistic representative of the biological membranes. A powerful structural method; Small Angle X-ray Scattering was employed to obtain complementary structural information, in particular, membrane fluidity and thickness alterations with flavonoids.

Chapter 2 Experimental materials and methods

2.1 Materials

DOPC with the purity of > 99% was purchased from Avanti Polar Lipids (USA). The flavonoids quercetin dihydrate, rutin trihydrate (quercetin-3-β-D-rutinoside), naringenin, hesperetin, (+) - catechin hydrate and naringin were supplied by Sigma-Aldrich (Germany). Kaempferol and tiliroside were obtained from Extrasynthese (France). Phosphate buffered saline (PBS) powder was used to prepare the pH 7.4 buffer solution and was obtained from Sigma-Aldrich. For monolayer studies, one batch of PBS was dissolved in 1 L of Milli-Q water (Millipore Inc., Ω = 18.2 MΩ.cm) to give 0.01 M phosphate, 0.138 mol dm^{-3} NaCl + 0.0027 mol dm^{-3} KCl. Ethanol (absolute, AR, Merck) and dichloromethane (anhydrous, ≥ 99.8%, Sigma-Aldrich) were used as received without further purification. A stock solution of flavonoids dissolved in ethanol and a stock solution of DOPC (2 mg ml^{-1}) in PBS buffer were freshly prepared prior to experiments.

For confocal imaging experiments, lipid soluble Rhodamine B (λ_{exc_RhoB}= 554nm and λ_{em_RhoB} = 579nm), with a product number of 509-34-02, was supplied from Sigma (Sigma-Aldrich Company Ltd., Dorset, UK) and used as a fluorescent probe to label vesicles. Rhod B solution was made up by dissolving the dye powder in 1% EtOH and added to the vesicle solution at a molar ratio of (dye/lipid) 0.5%. Bovine serum albumin, purchased from Sigma- Aldrich was used to provide a stable matrix for the vesicles.

2.2 Electrochemical experiments

2.2.1 Rapid cyclic voltammetry (RCV)

An electrochemical sensor system (patented by the University of Leeds); (116) composed of a phospholipid monolayer coated mercury (Hg) film on fabricated Pt electrode was interrogated by rapid cyclic voltammetry (RCV). Voltammetric experiments in this thesis were used to obtain information about test samples (flavonoids, in this case) interacting with the phospholipid layer through monitoring the current (I) as a function of the potential (V) applied to an electrode over a specified period (t). Cyclic voltammetry (CV) is one of the most common electrochemical technique, in which a triangular voltage waveform (**Figure 2.1(A)**) is applied to the working electrode that generates a resulting current (117). The voltage is reversed to its initial potential after reaching a switching potential, and the current response is measured. The scan rate for the current measurements was fixed to 40 Vs^{-1} since capacitance current is measured which is proportional to the scan rate.

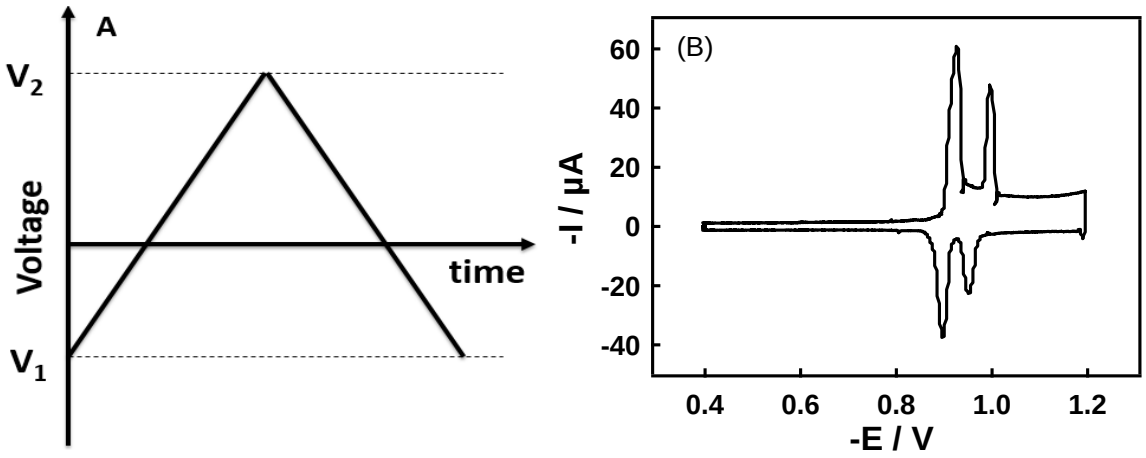

Figure 2.1 Applied potential vs. time in cyclic voltammetry (A) and a typical voltammogram (B).

A typical voltammogram obtained from the current RCV technique is depicted in **Figure 2.1(B)** with a constant capacitance baseline region from -0.4 V to -0.95 V followed by two sharp and

well-defined cathodic capacitance current peaks with a reverse anodic process. In the current study of the non-faradaic process, the CV was used to detect the alterations in the monolayer structure created by flavonoids. These alterations can either appear as peak suppression and peak shift or as an increase in the low capacitance baseline region which is an indicator of membrane permeability. This will be detailed in the following section of 2.2.4 (phase transitions).

In the case of non-faradaic reactions, the CV current is proportional to the capacitance of the interface, where the interface acts as a simple parallel plate capacitor.

2.2.2 Electrochemical flow system Setup

Electrochemical set-up consisted of a flow cell that was custom made as shown in **Figure 2.2.** The choice of the flow cell material was plexiglass, also known as acrylic (118). The flow cell accommodates an electrolyte (PBS buffer in this case) and a three electrode system: a working electrode (WE), a reference electrode (RE), and a counter (auxiliary) electrode (CE). By employing the reference electrode, a stable and reproducible potential is produced and measured at the working electrode with no or little current passing through it. A silver/silver chloride (Ag/AgCl), 3.5 mol dm^{-3} potassium chloride (KCl) was used as a reference electrode (VWR International Ltd.), and fitted into the cell.

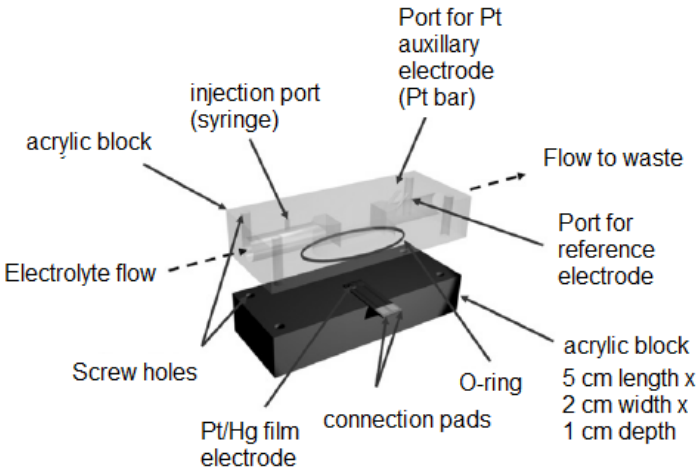

Figure 2.2 The flow cell where the Pt/Hg electrodes are placed (119).

The counter electrode, also known as the auxiliary electrode was made of platinum (Pt) rod to conduct current flow. An identical current flow is carried through the working electrodes. Counter electrode has a much larger surface area compared to working electrode i.e. the working electrode has a diameter of 0.01 cm^2, and the counter electrode is a sheet of Pt with a surface area of 4 cm^2.

The microfabricated Hg film electrode (MFE) deposited on the Pt electrodes (Tyndall National Institute, Ireland) embedded on a 28 x 28 mm^2 silicon wafer substrate were used as working electrodes as shown in **Figure 2.3** (119). Each Pt electrode is addressed via Si_3N_4-insulated interconnections to 2.54 mm Pt electrical contacts. The MFE was connected to an Autolab PGSTAT 30 potentiostat (Eco Chemie, Utrecht, Netherlands) interfaced to a PowerLab 4/25 signal generator (AD Instruments Ltd.) monitored by ScopeTM software. Current vs. potential RCV scans were recorded via the software at a scan rate of 40 Vs^{-1}. A peristaltic pump was used to maintain a constant buffer flow (PBS) over the electrode with a flow rate of 5-10 cm^3 min^{-1}.

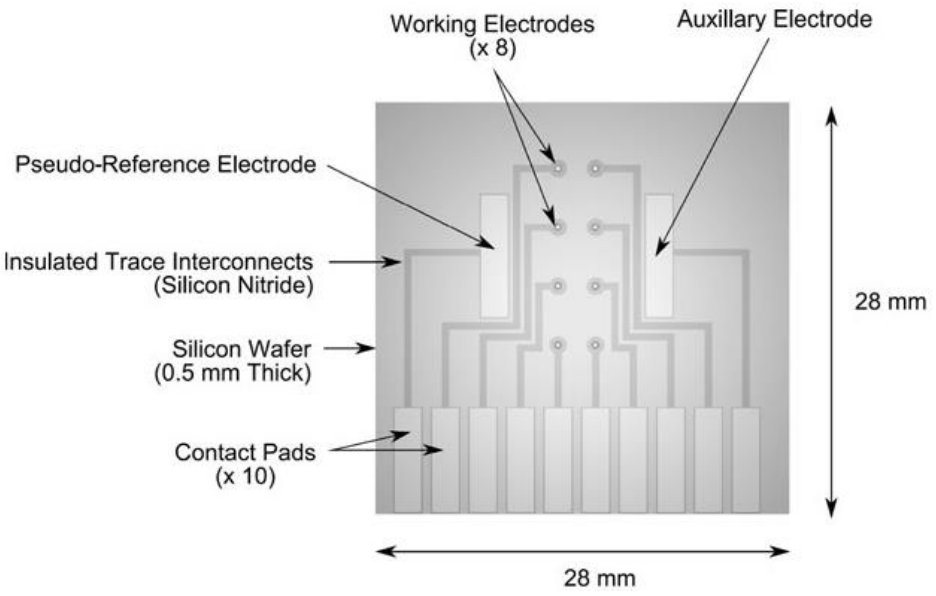

Figure 2.3 Schematic representation of microfabricated Pt chip electrode (119).

Three individual solutions of (i) control buffer (PBS), (ii) DOPC dispersion in buffer and (iii) test samples in buffer were introduced into the flow cell separately (each solution at one time). Electrolyte and sample solutions were stirred with magnetic stirrers throughout the experiments. A blanket of argon gas (Air Products) was turned on 60 minutes prior to experiments and maintained throughout each experiment to effectively remove the oxygen (O_2) from the electrolyte, lipid dispersion and test sample solutions.

2.2.3 Electrode pretreatment and DOPC deposition on Hg

The working electrodes were cleaned using a mixture of H_2SO_4 (Fisher Scientific) and 30 % H_2O_2 (Fluka) (piranha solution) in a ratio of approximately 3:1, respectively and rinsed with plenty of Milli-Q (18.2MΩ) water, successively, before drying under nitrogen (N_2) (118). After cleaning, Hg was deposited on the Pt electrode manually. Such deposition was performed in a fume hood using an Eppendorf microliter pipette and has been clearly detailed previously (118, 120). The Hg deposited Pt electrode is subsequently referred to as Pt/Hg electrodes

throughout the text. Once coated, Hg on the Pt electrode is very stable, and are reusable up to six months.

Prior to lipid deposition, control PBS was drawn from the electrolyte reservoir to pass through the flow cell by repetitive cycling from -0.4 to -3.0 V to clean the Hg surface in-situ. This process was repeated until the capacitive current peaks due to the previous sample completely disappeared. It should be noted that a one-two minute period is usually sufficient to clean any soluble/insoluble adsorbed organic material from the Hg surface. However, the cleaning period could be extended up to five minutes for the removal of the memory effect from the analysis of persistent samples (83). After obtaining a satisfactorily clean Hg surface, the DOPC dispersion was deposited on Hg as follows: (i) A DOPC dispersion (0.2 mg cm^{-3}, 100-200 µL) was injected into the system with a continuous potential excursion from -0.4 V to -3 V at 40 Vs^{-1}. (ii) 1-2 seconds after the DOPC injection, the characteristic voltammetric lipid peaks appeared, and the RCV was terminated. (iii) Following that, RCV was initiated with an altered potential excursion from -0.4 to -1.2 V to test the quality and stability of the lipid monolayer. In the case of poor monolayer coverage/quality, the coating procedure was repeated (118, 120). **Figure 2.4** is a schematic representation of the RCV setup.

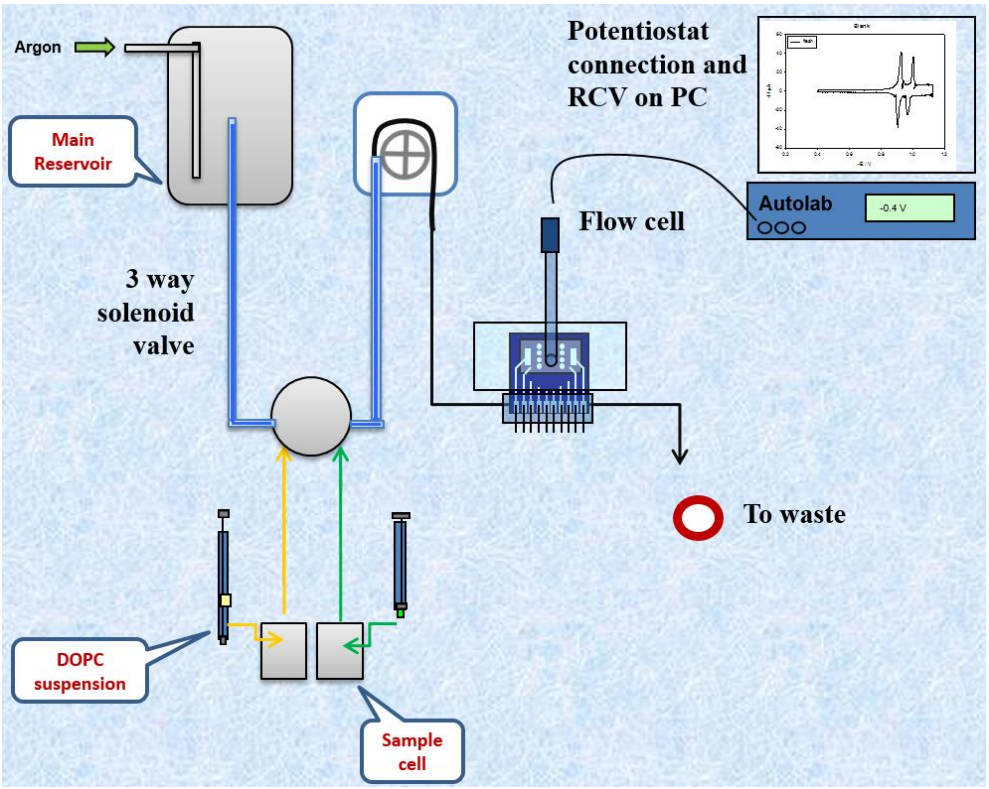

Figure 2.4 Schematic diagram of the flow cell-based sensing device. Pathways are represented by black arrows.

2.2.4 Phase transitions

Several processes such as adsorption and reorientation of amphiphiles and the displacement of molecules can occur as a function of potential in adsorbed surfactant films on the electrode surface. DOPC monolayers on Hg electrode undergo two characteristic, non-faradaic discontinuous phase transitions manifest as sharp voltammetric peaks in an applied potential window within -0.4 and -1.2 V (84). Such transitions which appear as potential induced capacitance peaks are dependent on several parameters such as the potential applied, the type of phospholipid and the electrolyte solution used.

Nelson *et al*. extensively investigated and interpreted the mechanisms behind these phase transitions. Following the initial work by simulation studies (118), Vakurov *et al*. directly characterised the fluid DOPC assemblies at electrified Hg surfaces via Atomic Force Microscope (AFM) studies (84) which significantly contributed to our understanding of the phase transition behaviour. The general consensus on these phase transitions is that they correspond to the structural changes of DOPC monolayer on Hg, i.e., poration and eventual `desorption`. Using AFM, Vakurov *et al*. observed that (i) between the potentials -0.4 V and until about -0.95 V, phospholipid molecules arrange themselves as a complete monolayer on the Hg, representing half a bilayer, with their apolar tails positioning to the Hg surface and the polar heads positioning to solution, (ii) the first capacitance current peak appears (–0.95 to -1.0 V), and represents the electrolyte penetration into the monolayer and initial desorption of the layer from the electrode surface (iii) the second capacitance peak (-1.1 V) corresponds to the readsorption of bilayer patches on to the electrode surface taking place by a nucleation and growth process (84) (iv) a group of additional current peaks also appear at more negative potentials (between -1.35 V and -1.7 V) which correspond to the collapse of organised phospholipid structures on the Hg surface.

2.2.5 Electrochemical characterisation of interactions

Nelson developed the above-mentioned electrochemical sensor device to screen the interactions of bioactive compounds with model monolayer membranes. Although this sensing device was previously used to screen a variety of bio-actives such as nanoparticles and aromatic apolar compounds including toxins, peptides, steroids, and pharmaceuticals, the current work reinforced the sensing system for food ingredients; flavonoids for the first time (120-123).

Studies with the current electrochemical sensor have established that it is an effective technique to reveal the relationships between the structure of the compounds of interest and their extent of interaction with the monolayer sensor element. Using the current membrane sensor, such modifications could be selectively detected through the alterations in the peak suppression, peak shift, and baseline capacitance height. This can be done since changes in the nature and extent of the phase transitions are related to alterations in the self-organisation of the layer, and compound interaction with the monolayer changes its organisation (84).

Once Hg was successfully coated with DOPC, the flavonoid solutions (dissolved in ethanol) were introduced into the flow cell at the predetermined concentrations, and alterations in the lipid monolayer were monitored for 5 minutes by cycling the potential from -0.4 to -1.2 V. The ethanol concentration did not exceed 1 % in the final solution, and all controls in this study refer to the control with 1 % ethanol alone.

Different behaviour in the monolayer response following the interaction with different compounds could be explained through their adsorption and penetration mechanism. For example, a definite increase in the baseline capacitance current along with suppression of the

capacitive current peaks strongly indicates a penetration or disruption of the layer by the compounds of interest (118). The increase in the baseline capacitance could be explained according to the following equation; ($C_d = \varepsilon\varepsilon_o/d$), where capacitance ($C_d$) is directly proportional to dielectric constant (ε) and inversely proportional to the thickness of dielectric (*d*). As a result of penetration of a compound, the low dielectric constant of the monolayer's apolar core is disturbed. It is therefore tempting to assume that an increase in capacitance could be due to monolayer thinning and/or increase in dielectric constant.

2.3 Langmuir trough experiments

A specialist in-house Langmuir film balance whose essential features are illustrated in **Figure 2.5** was used throughout this work. A rectangular polytetrafluoroethylene (PTFE) trough of dimensions 25 X 35 X 4 cm accommodates a rhomboidal shape PTFE barrier which has four sides of 15 cm long and 4 cm high**,** and all the sides are hinged at the corners. Such feature provides a leak-free enclosure and hence renders this barrier advantageous compared to conventional square shape barrier set ups. The PTFE pegs underneath the walls of the barrier provide the liquid (buffer in this case) flow. The barrier is connected to a Powermax P22 stepper motor (Unimatic Engineers, London, U.K.) from the two opposite sides. Compression or expansion is conducted with the help of these two barriers. As a result, the interfacial area inside the barrier is altered. The interfacial tension/pressure is measured by a Wilhelmy plate of roughened mica (~3 cm) which was dipped into the subphase at the centre of the trough and suspended from a strain gauge based force transducer (Maywood Instruments, Basingstoke, U.K.). Further details of the experimental arrangement can be found in the patent (124).

EtOH and dichloromethane (DCM) mixture at the ratio of 1:9 was used to prepare the stock solution of lipid DOPC. DOPC solution (0.2 mg/mL) was then spread over the subphase of PBS buffer (pH, 7.4) in order to form a monolayer. Following solvent evaporation for 15 minutes, the monolayer was slowly compressed at the rate of 8.6 mm^2 s^{-1} (corresponding to 3.6 $Å^2$ min^{-1}), starting from an initial (maximum) through area of 22 500 mm^2. This compression rate is considered to be slow enough to represent the "true equilibrium" isotherm since decreasing the compression rate further created no difference in the π–A isotherms. The monolayer was compressed to π = 30 mN m^{-1}, which corresponds to a typical biological membrane pressure (125) and flavonoids were injected beneath the monolayer to give a final subphase concentration of 10 μmol dm^{-3}. The system was then allowed to stabilise for around 20 minutes after flavonoid injection, and the film stability was monitored as a function of the change in the trough area by maintaining the pressure constant at 30 mN m^{-1} for an hour. Measurement of area loss at π = 30 mN m^{-1} was detected for DOPC monolayer alone and in the presence of flavonoids by extrapolating the trough area (A) at time t, relative to the initial starting area (Ao), i.e. A/Ao, as a function of time.

At the end of 1 h, the monolayer was expanded to its initial area and recompressed to the collapse point. Recompression was done to observe any changes in the π-A isotherm indicative of flavonoid-monolayer interactions.

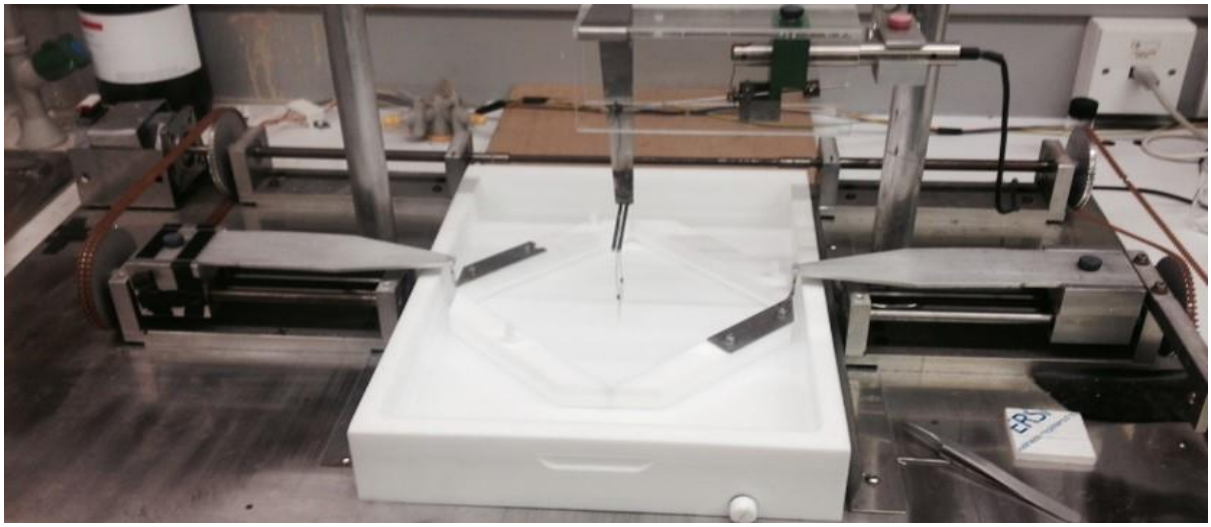

Figure 2.5 Photo of the Langmuir trough setup used for the current study.

2.4 Brewster angle microscopy (BAM)

Brewster angle microscopy is a widely used technique for studying thin film structure on liquid surfaces. Although the lateral resolution of the BAM2 images is considerably less (~2 μm) compared to fluorescence microscopy (FM), its advantage arises from being a completely noninvasive technique without requiring sample labelling (126).

2.4.1 Apparatus and set-Up

The BAM images help in direct observation of the structural changes occurring in the monolayer. In principle, when an incident beam hits a surface, it usually is reflected. However, if a p-polarised light encounters an air-water interface, no reflection occurs at the Brewster angle. This angle for the air-water boundary is ~53.15^{o}, and the surface of pure water appears as a black image due to the no reflection of light (127). On the other hand, if a thin film is present at the interface such as in the case of a lipid film, a small amount of light is reflected due to the refractive index differences created by the adsorbed film at the Brewster angle as illustrated in **Figure 2.6**. The data from such reflected intensity of a p-polarized light is collected as images by the detector of BAM.

The BAM system and its operation described in detail elsewhere (128) and only brief details are presented here. A BAM2plus Brewster Angle Microscope (NFT, Gottingen, Germany), combined with the Langmuir trough above was employed to visualize the morphology of the DOPC monolayers before and after flavonoid addition. The whole assembly was enclosed with metallic walls for safety reasons. The shutter speed for the camera was fixed at 1/50 at the Brewster angle for the pure A-W interface. Above this speed, very thick interference lines were observed. The laser output power was kept constant at 18% for all experiments and polarizer and analyser angles were set to zero. Background compensation was done to increase the image quality by subtracting the image for air/water surface from the images of the studied compounds. Thus, the overall appearance of the image has become more homogenous by reducing the brightness in the central region while increasing it at the edges. Same setting conditions were applied for all the measurements to avoid introducing variabilities in comparing the data. The images of the flavonoid trated and untreated spread films were recorded every minute starting from zero time until the end of collapse pressure. The images were also collected an hour after reachin collapse pressure.

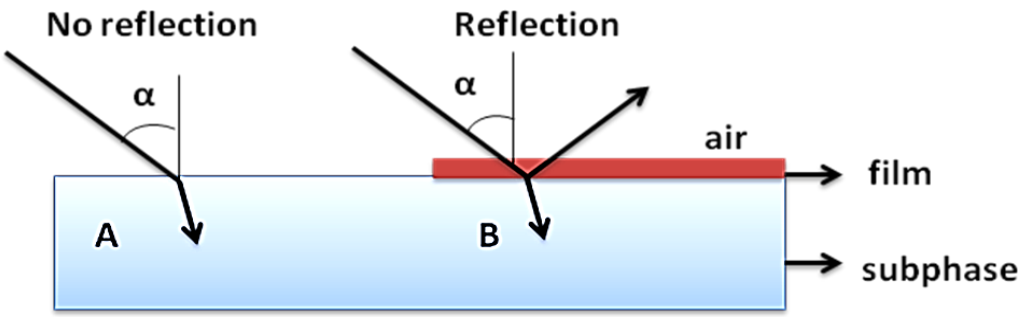

Figure 2.6 Reflection and refraction of p-polarised incident beam in the absence (A) and presence of a film (B) produced by the BAM.

2.5 Small angle X-ray scattering (SAXS) experiments

Structural characteristics of DOPC multilamellar vesicles (MLVs) in the absence and presence of flavonoids were investigated via small X-ray scattering (SAXS). Scattering techniques such as SAXS have been widely used to characterise the structural properties of MLVs that are based on the regular piling up of lipid dispersions. Spontaneously formed MLVs with several well-defined lamellar phase lipid bilayers are easy to produce and highly homogeneous (129, 130). MLVs with a limited number of lamellae are equally spaced in a stack and give rise to additional Bragg peaks (131).

DOPC is one of the most preferred phospholipid types in producing MLVs for SAXS studies. The advantage of this phospholipid over the other membrane forming lipids arises from its ability to form a stable lamellar liquid crystalline (Lα) phase - the most biologically relevant phase – over a range of temperatures (129).

2.5.1 Setup, sample preparation and X-ray structure analysis

As seen from the schematic illustration in **Figure 2.7**, an incident beam from the X-ray source hits a sample. This sample could be a liquid solution of particles, a solid powder or a gel. Photons interact with the electrons in the sample, and contrast is created due to the electron density differences between the sample and its environment.

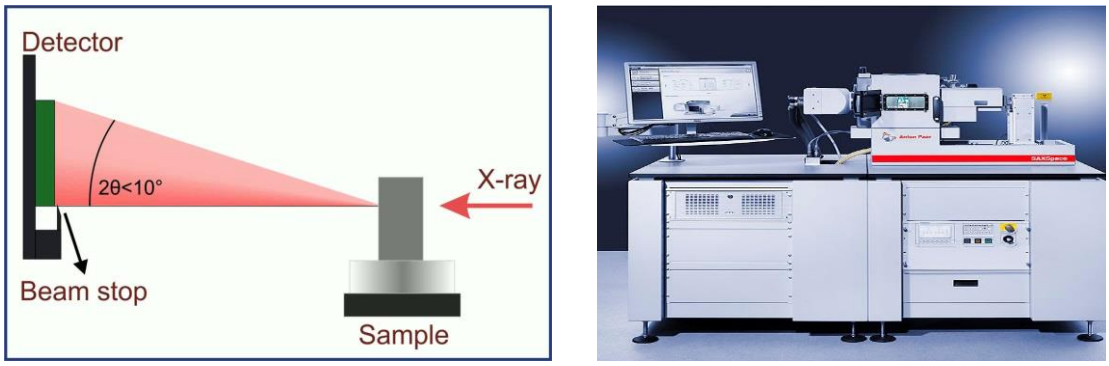

Figure 2.7 Schematic illustration of X-ray scattering and SAXSpace system.

MLVs were prepared according to standard protocols (132). Briefly, a DOPC stock solution was made by dissolving 10 wt % of lipid in ethanol. Similar ethanol stock solutions of flavonoids (quercetin, rutin, or tiliroside) were also prepared and then each mixed with the DOPC solution, resulting in a final concentration of 6 mol % of flavonoid. Each mixture was vortexed for 2 min, and the solvent was evaporated in a vacuum oven for 24 h. After obtaining dry thin films at the bottom of the sample tube, 90 µL of water of approximately 0.1 mM ionic strength, pH 7.1 (PBS buffer diluted 100× to prevent osmotically induced inhomogeneity of MLV bilayer stacking), was added into the sample tube to fully hydrate the films (111). The operated SAXS camera setup (SAXSpace, Anton Paar, Austria) is described in great detail elsewhere (133) Briefly, a collimation block unit vertically focuses a line-shaped beam of Cu Kα radiation with a wavelength λ = 0.154 nm onto the detector plane. For the SAXS experiments, the high-resolution mode was chosen, which permits detection of a minimum scattering vector, qmin, of 0.04 nm−1 ($q = (4\pi/\lambda) \sin \theta$, where 2θ is the scattering angle). All studied samples were filled into the same vacuum-tight, reusable 1 mm quartz capillary to guarantee exactly the same scattering volume. The experiments were performed at 25 °C with a temperature stability of 0.1 °C. A Mythen X-ray detector (Dectris Ltd., Baden, Switzerland) system was used to record the 1D scattering patterns. SAXStreat software (Anton Paar, Graz, Austria) was used to fine-tune the primary beam position, before subtracting the background from water, capillary, and air using the SAXSQuant software (Anton Paar, Graz, Austria). Background subtracted SAXS patterns have been analysed according to the modified Caillé theory. The technique and underlying premises have been described previously in depth (134, 135) (for reviews see Rappolt *et al*. (136) and Pabst *et al*. (137)). The bilayer model used to interpret the data, and its applications have also been described previously (138). Lamellar

repeat distance *d* and the head-to-headgroup thickness, d_{HH}, were directly obtained from the fits to the scattered intensities. SAXS analysis of lipid membrane systems was performed via Global Analysis Program (GAP) (137, 139). Scattered intensity is recorded as a function of scattering factor, and it is usually represented by q. The scattered intensity of a stack of layers is shown by

$$I(q) = \frac{<S(q)|F(q)|^2>}{q^2} \qquad \textbf{(2.1)}$$

(S(q)= structure factor; F(q) = form factor). Caillé theory characterises both stacking and bending disorders of the stack of fluid bilayers. The position of the membrane is clearly defined by its movement so that would give a contribution to its uncertainty in position. Also, whole membrane itself, can move up and down as it is in water. Hence, additional to the stacking disorders which arise due to the positional uncertainty, Caillé theory has also included the undulations of the membrane. The bending fluctuation or Caillé parameter is given by

$$\eta = \frac{\pi k_B T}{2d^2\sqrt{BK_c}} \qquad \textbf{(2.2)}$$

As given in the equation 2.2, the Caillé parameter or bending fluctuation is directly related to the membrane bending rigidity, K_C, and the bulk compression modulus, *B* (140). Mean fluctuations of the membrane position, *σ*, were derived from the Caillé parameter, *η,*

$$\boldsymbol{\sigma = \sqrt{\eta}\frac{d}{\pi}} \qquad \textbf{(2.3)}$$

Note that, the uncertainty in membrane position depends on the forces that keep the membrane in place which are attractive and repulsive forces (141). The only attractive forces are the Van der Waals attractions between dipole head groups of two membranes (142) and

repulsive forces arise from the undulations (141). If there are no charges in the system these are the two main contributions causing fluctuations.

2.5.2 Electron density profile (EDP)

Electron density profiles (EDPs) extracted from X-ray studies with the calculation of Fourier transform show the plot of polar head groups and terminal methyls (see **Figure 2.8)**. Electron density maps use the contrast between regions of "electron-rich" and "electron-poor" atoms (139). Based on this contrast, the lowest electron density is observed at the bilayer centre where terminal methyl groups are located (143). Whereas polar head groups that are rich in electrons such as oxygen and nitrogen, are associated with the two highest electron density contrast positions. This is seen as the phosphate to phosphate distance in electron density profiles as depicted in **Figure 2.8**, and it gives one of the most important structural parameter, membrane thickness, d_{HH} $2(z_H)$ (75). If stearic bilayer thickness is in subject, then this term refers to the full extension of the membrane and given by

$$d_B = d_{HH} + 4\sigma_H \qquad \textbf{(2.4)}$$

where d_{HH} is the thickness between the two head groups and σ_H the width of the Gaussian applied to a model electron density profile of the headgroup region (134). σ_H is fixed to a constant value and is usually nominated as 9Å for phosphatidylcholines (144). Note that, in the current study we have not considered the head group extension and hence bilayer thickness is equal to d_{HH} $2(z_H)$.

From the fits, we directly obtain the *d* –spacing (lamellar repeat distance), *d,* which is further subdivided into the membrane thickness, d_{HH}, and the water layer thickness, d_W.

The electron density distribution is characterised by the form factor, and *f(q)* is given by the Fourier transform of the electron density profile along the z axis.

$$|F(q)|^2 = 2\pi\left[2\sigma_H exp\left(-\frac{\sigma_H^2 q^2}{2}\right) cos(qz_H) - \sigma_C \rho_R exp\left(-\frac{\sigma_c^2 q^2}{2}\right)\right]^2 \qquad \textbf{(2.5)}$$

the parameter z_H indicates the centre of the head-group Gaussian and σ_H shows the width of the head-group Gaussian ρ_R in the equation represents the width and the relative amplitude of the hydrocarbon chain Gaussian $\rho_R = (\rho_C / \rho_H)$.

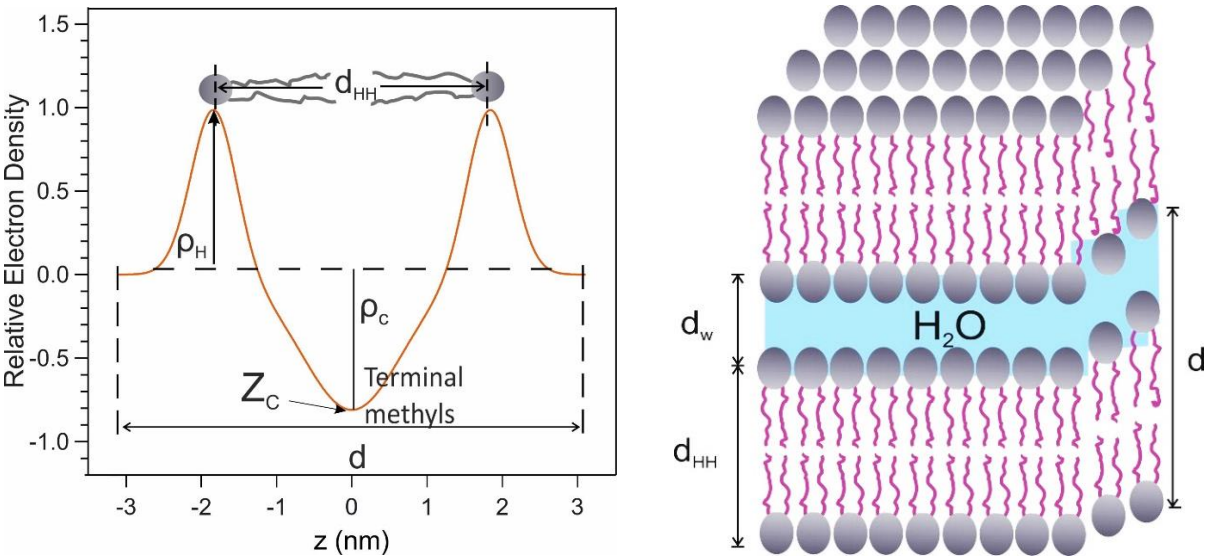

Figure 2.8 EDP of DOPC vesicles at 25 °C and schematic bilayer structure with an illustration of structural parameters; *d*, d_{HH} and d_w.

2.6 Confocal laser scanning microscope (CLSM) experiments

Confocal Laser Scanning Microscope (CLSM), using a Leica TCS SP2 microscope, mounted on a Leica Model DM RXE microscope base, was operated in fluorescence mode was employed to visualise the MLVs in the absence and presence of flavonoids.

2.6.1 Sample preparation and methodology

For Confocal experiments, DOPC MLVs (10 wt%) were prepared in the absence and presence of flavonoids as described in section 2.5.1. 1% of bovine serum albumin solution was added to vesicle solution to immobilise the vesicle movement by increasing the solution viscosity. Approximately 1 ml. of vesicle sample in the tube were transferred into confocal cell (diameter of 19 mm and 3 mm depth) via an Eppendorf microliter pipette. A cover slip with a thickness of 0.17 mm was placed on top of the cell, ensuring that there was no liquid leakage yet air trapped between the cover slip and sample. The images were recorded at room temperature using a 40X oil-immersion objective lenses with a resolution of 1024 X 1024 pixels. Fluorescence from the sample was excited with 476 nm Ar and 543 nm HeNe laser lines for flavonoids (naturally fluorescent) and the Rhod B respectively. Morphological changes in vesicles comprised of flavonoids can, therefore, be monitored based on the contrast created due to the excitation wavelength differences between the flavonoids and the dye solubilised in lipid.

2.6.2 Apparatus and set up

The diagram and the main components of CLSM are shown in **Figure 2.9**. CLSM has a pinhole which is different than other microscopes. The laser beam light passes through the pinhole aperture (illumination pinhole) and goes through a dichroic mirror. The dichroic mirror enables a certain wavelength of light to pass and reflects the light with a longer wavelength. The transmitted light is focused on a small point on the target sample by an objective lens. The wavelength coming from that particular focal point of the sample travels backwards through the same path that the laser travels. Light from other regions of the sample is eliminated by the detection pinhole (145).

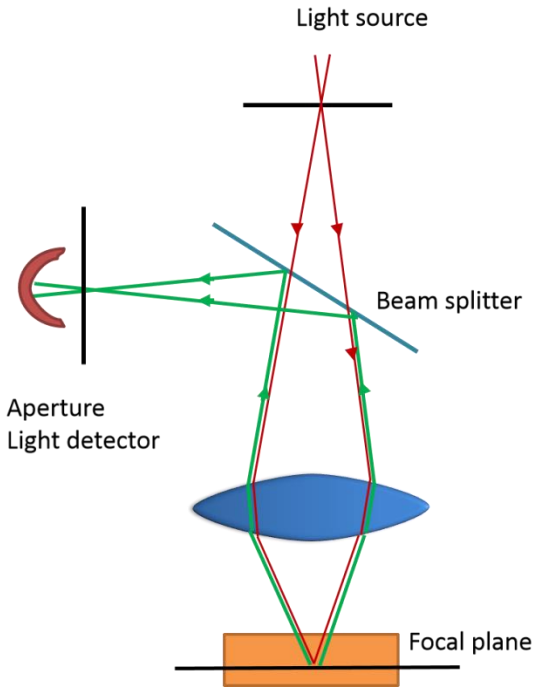

Figure 2.9 The principal and schematic illustration of images formed in confocal laser scanning microscopy (CLSM).

2.7 Light scattering experiments

Solution state of flavonoids was investigated by Dynamic Light Scattering (DLS) on a Nano-ZS Zetasizer (Malvern Instruments Ltd., UK), measuring the volume (%) - size distribution of flavonoids in 0.1 mol dm^{-3} PBS for both freshly dispersed and aged (for 5 hours) solutions. Light scattering occurs when a laser interacts with a particle or molecule within a cell, and the intensity of the scattered light is measured through a detector (detection optics were at the position of 173 ^{o}C). The signal obtained from the detector is passed to a where the light scattering intensity at successive time intervals is compared to derive the rate at which the intensity is varying. The correlator sends this information to a computer where the Zetasizer software analyses and presents the size distribution data. The aim of using DLS was to assess whether there was any detectable flavonoids particles/ precipitates in the solution.

Particles suspended in a solution are in constant, random motion (Brownian motion) An important feature of Brownian motion and DLS measures the diffusion coefficient (*D*) of the particles. Stokes-Einstein equation defines the relationship between the radius (assuming that the particle is spherical) of a particle and its diffusion coefficient (how quickly a particle moves) (146).

$$\boldsymbol{D = \frac{K_B . T}{6\pi\eta r}} \qquad \textbf{(2.6)}$$

Where K_B is the Boltzmann's constant, T is the temperature and η the viscosity of the continuous phase.

On the other hand, vesicle size distribution was investigated by Mastersizer 3000 (Malvern Instruments Ltd., UK). The average droplet size of the pure and flavonoid loaded vesicles was characterised in terms of volume weighted mean diameter d43 defined by

$$d_{43} = \frac{\Sigma\, n_i d_i^4}{\Sigma n_i d_i^3} \qquad \textbf{(2.7)}$$

Where n_i is the number of vesicles of diameter d_i. The refractive indices of water and phospholipid were taken as 1.330 and 1.450, respectively.

Chapter 3 Interactions of flavonoids with mercury supported DOPC monolayers

3.1 Introduction

This chapter will discuss the interactions of eight structurally varying flavonoids with DOPC monolayer on a Hg film electrode using an electrochemical biomimetic membrane sensor; Hg-supported phospholipid monolayer. The most significant advantage of this technique over conventional methods arises from its rapid response time (from seconds to a couple of minutes). Several authors have used bilayer models to characterise the flavonoid interactions with a range of techniques. However, there is no study reporting a systematic investigation of flavonoid interactions with phospholipid monolayers.

Self-assembled monolayers on a Hg electrode is a powerful membrane model which allows an online, high-throughput investigation of bio-actives with phospholipids. This study reinforces the current sensor technology in the screening of food ingredients - flavonoids, for the first time. With this approach, a number of flavonoids have been systematicaly characterised to build a structure-activity relationship. The structural parameters such as the configuration, the number of hydroxyl groups, the presence of double bond between C2-C3, and the presence of glycosidic moiety play a role in membrane activity of flavonoids. The importance of these parameters that are known to affect the extent of interactions has been investigated in this chapter.

As mentioned in detail in the previous chapter, DOPC monolayer on a Hg electrode forms two consecutive current peaks between the voltage -0.4 V and -1.2 V. The degree of flavonoid interaction with the DOPC phospholipid assemblies was characterised by a depression in either or both of these peaks and an enhancement in the baseline capacitance layer. Such alterations created on DOPC monolayer can be seen from the `fingerprint images` obtained. Moreover, the interactions have been quantitatively analysed with detection limit calculations and a rank order have been established.

3.2 Results and discussion

3.2.1 Stability and reproducibility of DOPC monolayer

Performing experiments with a high-quality phospholipid control are of crucial importance. Hence, first and foremost, the stability and reproducibility of the lipid control were studied. Phospholipid monolayers of DOPC supported on the Pt/Hg electrode were shown to be in a stable and reproducible configuration throughout the experiments**. Figure 3.1** displays the stability of the monolayer over 10 minutes.

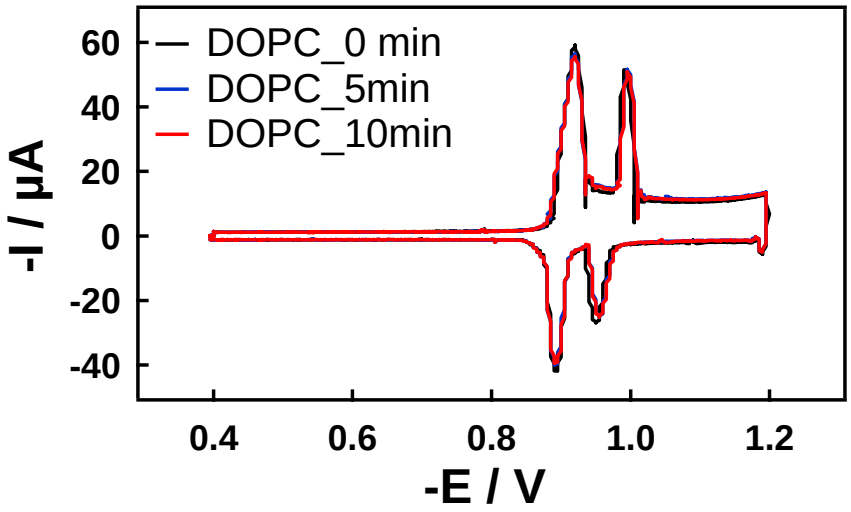

Figure 3.1 RCVs recorded at 40 V s^{-1} of a DOPC-coated Pt/Hg electrode at 0 (black line), 5 (blue line) and 10 minutes (red line).

In the current study, 5 minutes exposure time was sufficient to differentiate the effect created on the current-voltage curve of DOPC monolayer by each flavonoid. Therefore, prior to each experiment, a scan of a DOPC monolayer supported on the Pt/Hg electrode was taken at the end of 5 minutes, and this scan was used as a control.

3.2.2 The choice of solvent

Flavonoids are soluble in organic solvents such as DMSO, ethanol and methanol. **Figure 3.2** shows the RCV images of DOPC monolayer exposed to 1% ethanol, 1% methanol and 0.5% DMSO, recorded at the end of 5, 5 and 1 minute exposure time; respectively.

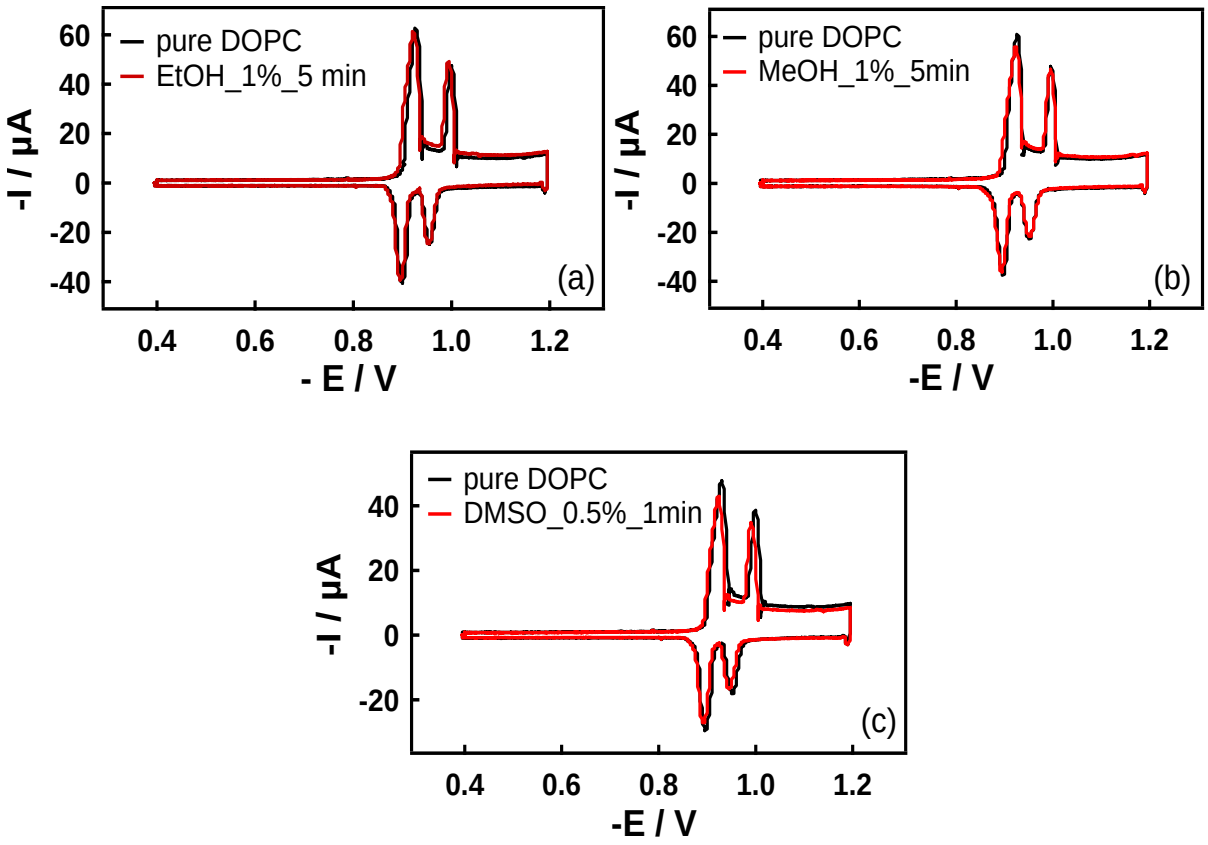

Figure 3.2 RCVs recorded at 40 V s^{-1} of a DOPC-coated Pt/Hg electrode (black line) in PBS at pH 7.4 and exposed to 1% EtOH (a), 1% MeOH (b) and 0.5% DMSO (c) (red line).

Upon introducing 1% EtOH and MeOH **(Figures 3.2 (a) and (b))** to the system for 5 minutes, a negligible peak suppression was observed. However, when monolayer was exposed to 0.5 % DMSO for 1 minute, a slightly higher peak suppression (suppression ratio is around 10%) was seen **(Figure 3.2c)**. Although DMSO is a commonly used solvent to dissolve flavonoids in cell culture studies (147), it dissolves acrylic of which the flow cell is made and which is why the DMSO exposure time was kept fivefold shorter with a lower concentration in the current experiments. Also, DMSO strongly interacts with the membrane surface and creates considerable modifications in the lipid membrane structure even at low concentrations of 0.3 mol % (148). Therefore, DMSO is not a compatible solvent to use with the current membrane model system.

Ethanol and methanol are very weakly surface active and widely used solvents to dissolve flavonoids (114, 149). A study measuring the solubility of quercetin in both ethanol/water and methanol/water systems observed a slightly improved solubility of quercetin in ethanol/water system (150). Another study stated that the solubility of luteolin in DMSO and ethanol has the same order of magnitude (149). Furthermore, it has been reported that at concentrations up to 4%, ethanol does not significantly alter the configuration of (DM)PC vesicles (151). Because of these reasons, ethanol was chosen as a solvent in preparing stock solutions of flavonoids throughout the experiments. The RCV plot in **Figure 3.3** shows the effect of ethanol exposure (concentrations above 1%) on the DOPC coated Pt/Hg electrode.

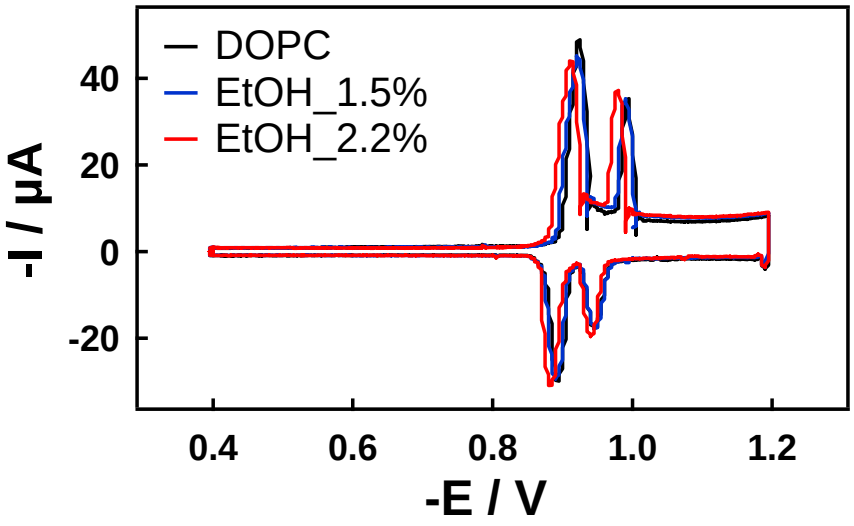

Figure 3.3 RCVs recorded at 40 V s^{-1} of a DOPC-coated Pt/Hg electrode in PBS at pH 7.4 (black line) being treated by ethanol at 1.5 % (blue line) and 2.2 % (red line). The images were taken at the end of 5 minute exposure time.

EtOH, at the concentrations of 1.5% and 2.2%, suppressed the first peak by 7% and 10%, respectively. As seen, a slight increase in EtOH concentration created a slightly more depression in the capacitative current peak along with a very slight shift to less negative potentials. In cases where the flavonoid was added to a concentration of 10 µmol dm^{-3}, the

ethanol percentage in the final solution did not exceed 1%. When added to give higher flavonoid concentrations of 35 µmol dm^{-3}, and to maintain the solution of flavonoids with higher molecular weight i.e. rutin and tiliroside, ethanol concentration reached a maximum of ~ 1.5%. For RCV experiments, measurements with phospholipid control were taken before introducing flavonoid solutions to the system, and this control refers to the DOPC monolayer on the Pt/Hg electrode, exposed to ethanol at the given concentrations.

3.2.3 Electrochemical characterisation of flavonoid – DOPC monolayer interactions

As mentioned previously, in response to the applied electric fields, phospholipid monolayers of DOPC on Pt/Hg undergo reproducible phase transitions which are manifested by the consecutive current peaks on the RCV plot. Any alteration occurring in the phospholipid monolayer`s organisation results in modifications in the phase transitions and thus the peak height, position and shape of the current peaks. Such response is unique to the structure of each compound and hence gives a characteristic "fingerprint" RCV profile. **Figure 3.4** presents the RCV profiles of the Hg-supported DOPC monolayers (the black line) following exposure to the flavonoids at the concentrations of 10 µmol dm^{-3} (red line) and 35 µmol dm^{-3} (blue line). Here, it should be noted that the RCV results of this research can be considered as extremely reproducible due to the multitude of repetitions carried out in this research.

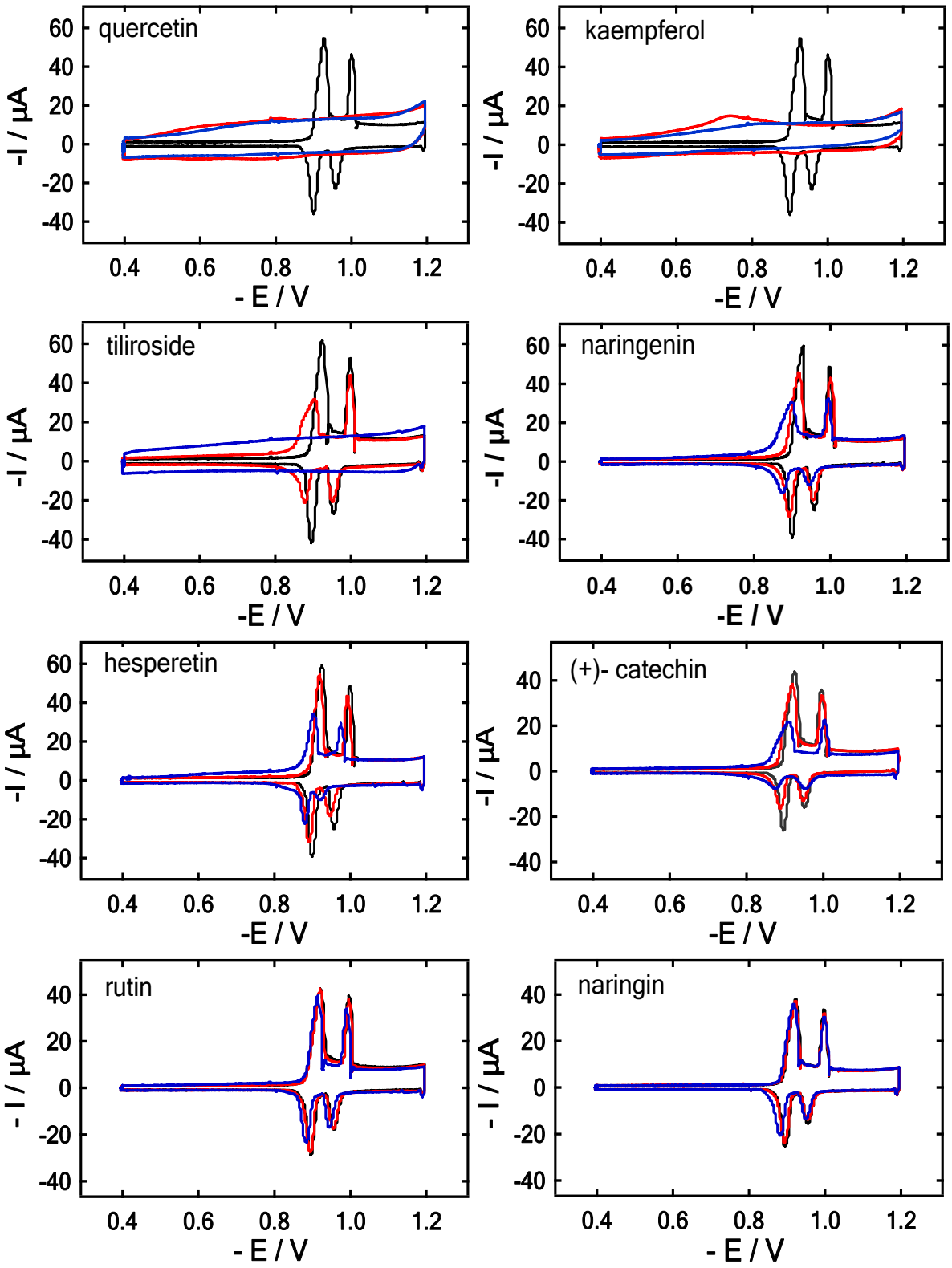

Figure 3.4 RCVs at 40 V s^{-1} of a DOPC-coated Pt/Hg electrode (black line) in the presence of flavonoids studied at concentrations of 10 µmol dm^{-3} (red line) and 35 µmol dm^{-3} (blue line) in PBS at pH 7.4.

It can clearly be seen that introduction of some flavonoids leads to significant modification in the monolayer structure. At the concentrations of 10 µmol dm^{-3} (red line in **Figure 3.4**), quercetin and kaempferol induced the most significant changes in DOPC properties with significant penetration of the monolayer. Compound penetration to the monolayer can be characterised as a total capacitance peak current suppression along with an increase in capacitance baseline height. A similar interaction pattern to those of quercetin and kaempferol was also observed with tiliroside at higher concentrations of 35 µmol dm^{-3}, while this flavonoid showed a smaller interaction at lower concentrations of 10 µmol dm^{-3}. On the other hand, naringenin, hesperetin and catechin interacted less strongly with DOPC which is seen as an intermediate peak suppression. Finally, rutin and naringin displayed no significant interaction with DOPC (111). It should also be noted that, although rutin did not create any visible peak suppression, it created an indistinct hump formation on the baseline capacitance at 35 µmol dm^{-3}**.** A suppression of the capacitance current peaks with little effect on the capacitance current baseline is representative of species adsorbing on the monolayer surface as shown by previous studies (118, 152). Using this argument, the voltammetric peak suppression following naringenin, hesperetin and catechin interaction indicates that they adsorb on the surface of the DOPC monolayer (111).

The results above show that the interactions are directly related to the flavonoid structure. Quercetin and kaempferol, which display the strongest interaction with significant penetration of the DOPC monolayer, possess two coplanar rings whereas the third ring is oriented at right angles. Presumably, the planar two rings facilitate the interaction and penetration of the flavonoid within the ordered structure of lipid membrane. Flavonoids showing intermediate interaction with and no penetration of the DOPC monolayer include

naringenin, hesperetin and catechin: which have a common structural characteristic where the second ring of the two-ringed structure is kinked which hinders interaction (111).

The insignificant interactions of rutin and naringin with DOPC can be related to the two glycoside groups attached to quercetin and naringenin respectively, which sterically hinders the adsorption and/or penetration of these glycosylated flavonoids into DOPC monolayer. Indeed, tiliroside has also one glycoside group positioned between the flavonoid moiety and a further ring, however, unlike the other glycosidic flavonoids, it is significantly active on the DOPC monolayer. The factors behind tiliroside's high response might be due to the reasons as follows: In the first case, unlike rutin and naringin, tiliroside only has one sugar moiety. Secondly, from the previous argument, its two ringed planar configuration will account for a stronger interaction. Thirdly, tiliroside, in spite of the presence of a sugar group, possesses has even a higher $\log_{10}P$: 2.7 (153) than most of the aglycones used in this study. Hence, in the case of tiliroside, both structural properties and a high $\log_{10}P$ seem to favour its monolayer activity (111).

The molecular basis as to what structural features render quercetin and kaempferol planar in configuration compared to the slightly twisted structure of naringenin and hesperetin was detailed by van Acker *et al*. who investigated the antioxidant activity of flavonoids by quantum chemical calculations (154). Interestingly, six of the flavonoids used in their study were the same as those used in the present study; namely quercetin, kaempferol, naringenin, hesperetin, rutin and (+) – catechin (154). Acker`s study highlighted the importance of several structural parameters in determining planar/or non-planar configuration. These parameters; the presence of 3-OH, a double bond between C-2 and C-3, and the glycosidic moiety attached on the 3-OH seemed to have an effect in the torsion angle of the B-ring and, in turn, the

coplanarity of the structure. For example, the findings showed that the presence of 3-OH group such as in the case of quercetin and kaempferol helped maintain the ring in the same plane with respect to the rest of the molecule (torsion angle closer to zero). However, the lack of a 3-OH group such as in the case of naringenin and hesperetin resulted in the loss of hydrogen bonds and hence caused a slightly twisted configuration with the remainder of the molecule. Comparable results were also observed with different flavonoids.

An exception to this was observed with (+) – catechin. Despite the presence of 3-OH moiety, (+) – catechin displayed a higher torsion angle and hence slightly twisted conformation compared to quercetin. This was explained by the absence of double bond in the C-ring of (+) – catechin, which possibly affected the magnitude of the torsion angle (155). Moreover, the introduction of a sugar moiety on the 3-OH group of rutin was reported to result in the loss of coplanarity of the B-ring with respect to the rest of the molecule.

The findings of the current monolayer study are commensurate with the findings from the previous flavonoid-membrane interaction studies that use lipid vesicles as model membrane architectures. One of the very first studies on this subject was published in 1995 by Saija *et al*., who investigated the interactions between; quercetin, rutin, naringenin, hesperetin and DPPC model membrane using differential scanning calorimetry (DSC) (156). Out of the flavonoids, the highest membrane affinity observed with quercetin was attributed to its planar structure. This finding was supported by further studies by van Dijk *et al*., (114) who probed the affinity of a set of flavonoids towards artificial vesicles via a quenching membrane probe 1,6-diphenyl-1,3,5-hexa-triene (DPH). Flavonol of quercetin displayed a significantly higher affinity for vesicles compared to flavanone of naringenin due to its planar configuration. The authors concluded that the tilted configuration of flavanones renders them

less likely to intercalate into the ordered structures of the phospholipids unlike the planar conformation of flavonols.

In addition to the studies that compare the membrane activity of different aglycones, several groups have also explored the interactions of flavonoid glycosides with biomimetic membranes (157, 158). Except for the study by van Dijk, which reported a higher membrane affinity with 7-glucosides of both naringenin and eriodictyol compared to their parent aglycones (114), the existing studies concur with the view that the presence of glycoside moieties hinder the interactions of flavonoids with lipid membranes (156, 157, 159). The less significant interactions with flavonoid glycosides have been attributed to their structural configurations and lower lipophilicities. As explained previously, the introduction of a sugar group in the molecule might decrease the coplanarity, and hence such a structure confers higher flexibility to conformational changes (154). Furthermore, since the existence of glycoside groups render the molecules more hydrophilic, flavonoid glycosides possess lower octanol/water partition coefficient indexes compared to their corresponding aglycones (157, 160).

The absorption phenomena of aglycones and glucosides of soy isoflavones in humans were also investigated (161). Isoflavone aglycones not only revealed a more rapid absorption, but also their plasma concentrations in humans were approximately five times higher than their glucosides.

It is also interesting to see *in-vitro* cell culture studies in the concept of flavonoid membrane interactions (159, 162-166). These studies have mainly used enterocyte Caco-2 cells for the flavonoid transportation across the cell membrane and attributed the flavonoid mechanism to their specific interactions with enzymes, receptors, transporters and ion channels. Tian *et*

al. investigated 36 flavonoids for their structure-permeability relationships, transportation and uptake using Caco-2 cell monolayers (163). The study reported a passive diffusion pathway for most of the flavonoids studied. Moreover, rutin did not permeate across the cell monolayer.

Tammela *et al*. investigated permeability characteristics and membrane affinity of flavonoids via transport studies in Caco-2 cells and phospholipid vesicles (159). Cellular uptake studies with Caco-2 cells correlated well with the membrane affinity measurements i.e. quercetin with high membrane affinity exhibited poor apical to basolateral transport.

The only study regarding absorption and transportation of tiliroside and related flavonoids (kaempferol, kaempferol-3-glucoside and p-coumaric acid) on and across Caco-2 cell membranes, at a concentration of 10 µmol dm^{-3} was published by Luo *et al*. (167). 1% of tiliroside was found to diffuse passively across the membrane despite its conjugating side chain (coumaroyl-glucoside). This finding contradicts with many studies that claim no passive diffusion of glycosides across the membrane. The authors of this research extrapolated behind this unpredictable behaviour of tiliroside was attributed to its high $\log_{10}P$ index which seems to facilitate its passive transportation (167).

3.2.4 The effect of flavonoid exposure time on the RCV plot

The effect of flavonoids on DOPC monolayer properties was investigated at different exposure times 1 minute and 5 minutes, respectively.

For quercetin and kaempferol, the effect of exposure time was tested at low solution concentrations of 3.5 µmol dm^{-3} to obtain a distinctive interaction pattern with visible peaks. Otherwise, both flavonoids completely suppressed the peaks at higher concentrations. Also

for tiliroside, 10 µmol dm^{-3} concentration was chosen since no visible peak was observed at higher concentrations. For the rest of the flavonoids, 35 µmol dm^{-3} was used.

Figure 3.5 shows that flavonoid-DOPC monolayer interactions were time-dependent. Except for tiliroside, whose effect remained nearly the same throughout all the exposure times, a higher response was observed with all other flavonoids after a longer exposure time.

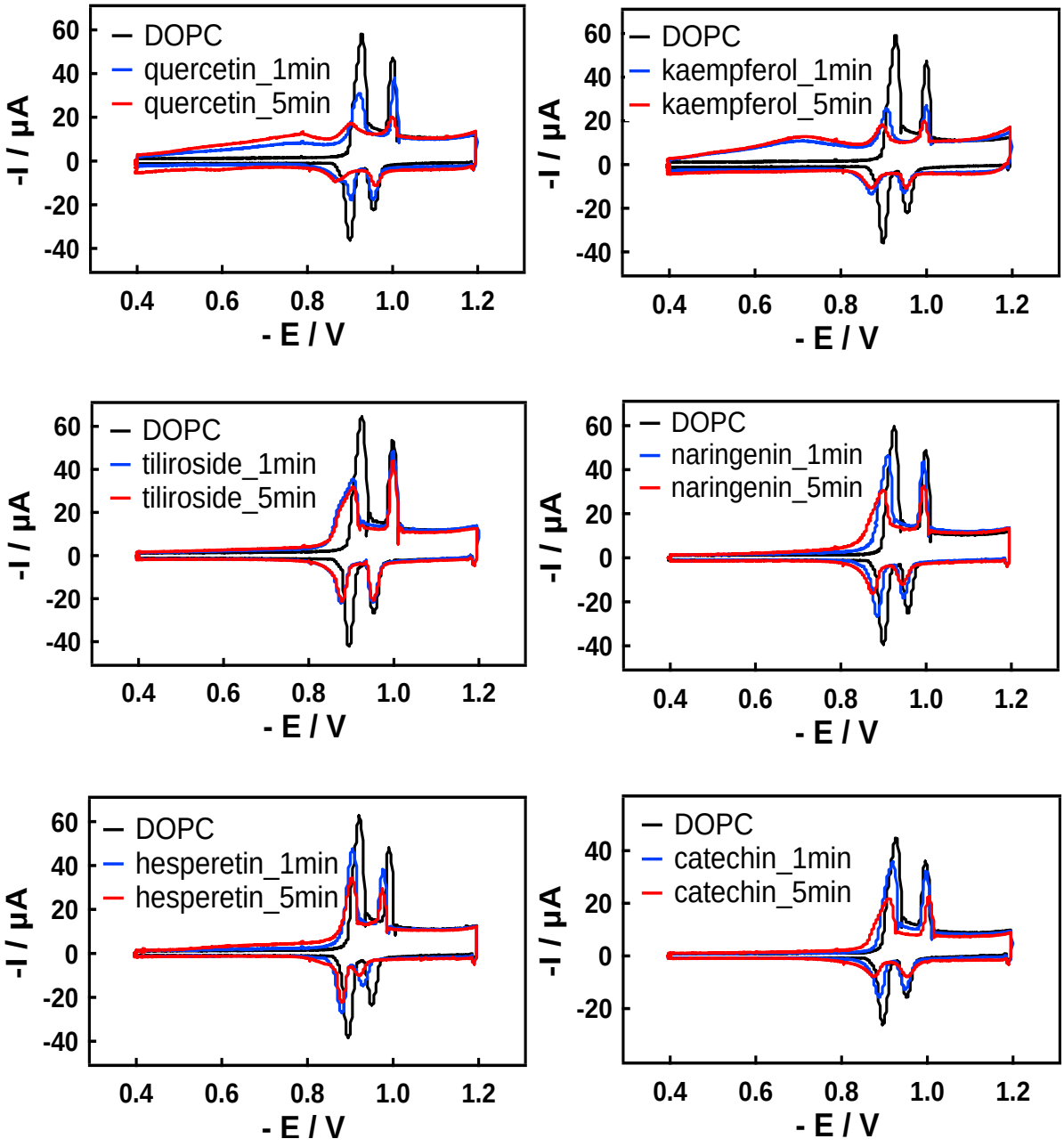

Figure 3.5 The effect of flavonoid exposure time; 1 minute (blue line) and 5 minutes (red line) on the RCV plots. RCVs recorded at 40 V s^{-1} of a DOPC-coated Pt/Hg electrode (black line) in the presence of 3.5 µmol dm^{-3} of quercetin and kaempferol, 10 µmol dm^{-3} of tiliroside, and 35 µmol dm^{-3} of naringenin, hesperetin and catechin in PBS at pH 7.4.

Figure 3.5 clearly shows that, at the end of 1 minute exposure time, kaempferol revealed the highest peak suppression, whereas, at increased exposure times, quercetin caused a more intensified peak reduction. **Table 3.1** shows the effect of flavonoids on the first peak height reduction relative to the control peak with DOPC monolayer as a function of exposure time. This table also shows the molecular properties of flavonoids such as molecular weight and topological surface area as these features might help to interpret the effect of exposure time on the monolayer alterations. For example, the molecular weight (M_W) of a molecule could be a factor controlling its adsorption rate (168). It is noticeable that tiliroside has a higher M_W than the other flavonoids studied and hence, the membrane adsorption and penetration might be retarded for this flavonoid which is already large.

Table 3.1 Relative (% of control) decrease of the RCV first peak height due to flavonoid/DOPC interactions.

Flavonoids	Exposure time (1-min)	Exposure time (5-min)	Molecular weight
Quercetin	% 47	70.4	302.236 g/mol
Kaempferol	% 56.7	68	286.23 g/mol
Tiliroside	% 45	49.7	594.525 g/mol
Naringenin	% 21.7	48.6	272.257 g/mol
Hesperetin	% 21	% 43.3	302.27 g/mol
Catechin	%19.9	% 41.6	290.26 g/mol

3.2.5 Detection limit calculation

The limit of detection (LoD) is the minimum quantity (or concentration) of a compound that statistically exerts a response with a given analytical technique (169). LoDs of RCV, therefore, provide more quantitative evaluations for the effect of each flavonoid on the DOPC layers.

LoD calculation with RCV has been described in detail previously (170). According to the procedure, the first capacitive current peak height of the control DOPC was used for LoD estimation, and the reproducibility of this peak was estimated by taking ten replicates. The three times standard deviation (SD) of the control peak height was calculated. A decrease in the first peak height, following interaction with the respective flavonoid was used in LoD estimations by extrapolating a calibration curve of peak height vs. flavonoid concentration in solution. Graphical interpretation of the detection limit of flavonoid interaction except for rutin and naringin, (LoDs of rutin and naringin could not have been determined due to their insignificant effects on the peaks) are given in **Figure 3.6**, and a rank order of the LoD values is displayed in **Table 3.2.**

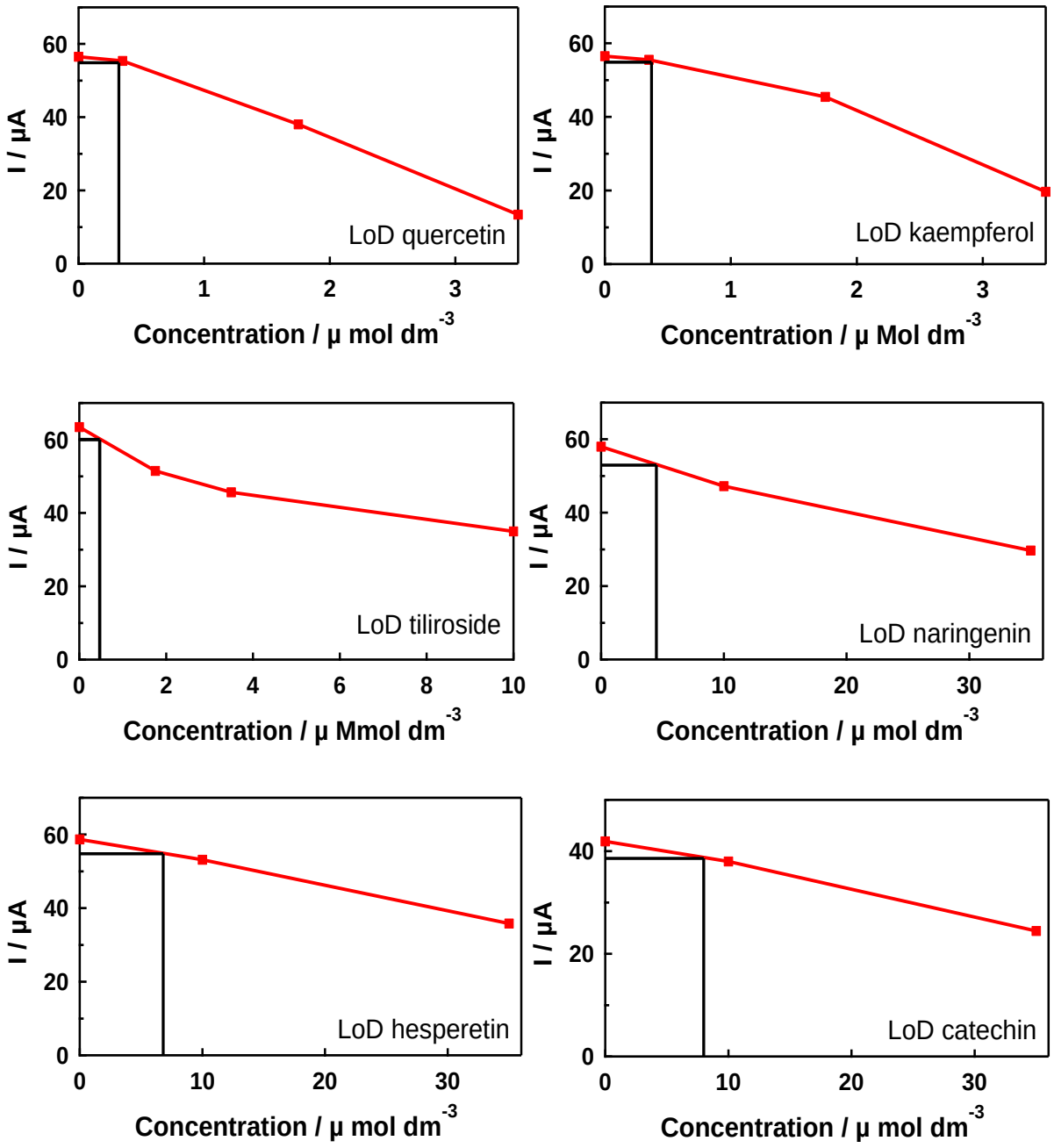

Figure 3.6 Characterisation of the detection limit (LoD) for the interaction of flavonoids with DOPC monolayers on Hg. The black horizontal line represents three times standard deviation of the first capacitive current peak from RCV of unmodified DOPC. LoD is determined as the concentration where the horizontal line intersects with the concentration curve (red line).

As seen in **Figure 3.6,** the LoDs of flavonoids follows the general order of flavonoid-DOPC interaction with RCV. The first peak suppression with quercetin seems to be slightly more pronounced than kaempferol at a concentration range of 0.35 - 3.5 µmol dm^{-3}. However, the difference between the LoDs of both flavonoids is not significant (see **Table 3.2**). A detailed study by Ulrih *et al*. compared the effect of quercetin and kaempferol on lipid membranes using a combination of techniques (171). Unlike many other studies (172) that suggest a higher membrane activity with quercetin, the authors observed a slightly more noticeable activity from kaempferol.

Many people assumed a relationship between the hydrophobicity of flavonoids and their membrane activity. For flavonoids, the octanol-water partition coefficient / $\log_{10}P$ (153, 173) and olive oil-water partition coefficients have been previously determined (114). **Figure 3.7** shows **t**he plot of the estimated LoD values in the current study against the corresponding $\log_{10}P$ values of flavonoids in literature. This figure clearly shows that when $\log_{10}P$ is used as a measure of hydrophobicity, there is no reliable correlation between the LoDs and the flavonoid hydrophobicity. For example, as given in **Table 3.2**, naringenin, a less membrane interactive flavonoid possess a higher $\log_{10}P$ compared to quercetin (153).

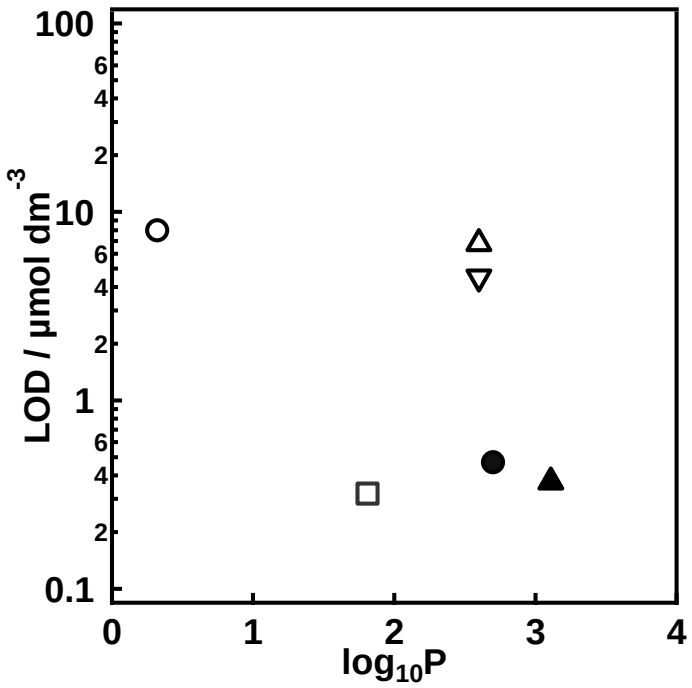

Figure 3.7 Scatter plot to show the compound`s respective LoD values at DOPC-coated Hg electrode in PBS at pH 7.4 vs. their respective $\log_{10}P$ values for the following compounds: quercetin (open square), kaempferol (filled triangle), tiliroside (filled circle), naringenin (inverted triangle), hesperetin (open triangle) and (+) - catechin (open circle).

In literature, a linear correlation between the LoDs of RCV to ionic liquids (ILs) and their EC_{50} values was reported (121). It should be noted that EC_{50} is commonly used as a measure of a compound`s i.e. drug and toxin potency and it refers to the plasma concentration required to obtain 50% of a maximum response *in-vivo*. Due to the relationship between the toxicity of ILs to living organisms and their influence on the DOPC monolayer, the study proposed that the phospholipid membrane is likely to be the primary target of toxic action with ILs.

EC_{50} is comparable with IC_{50} which represents the concentration of an inhibitor, for example, a drug to inhibit a specific biological function for half maximal effect *in vitro*. A study by Ofer *et al*. investigated the effect of flavonoids on carrier-mediated transport process of xenobiotics. More specifically, they probed the inhibitory potency of flavonoids to organic

cation transporters (OCT) in the tetraethylammonium (TEA) uptake assay of talinolol using a Caco-2 cell monolayer (174). The flavonoids studied inhibited OCT-mediated transport with a rank order of IC_{50}-values: quercetin< kaempferol< naringenin< rutin< hesperetin< naringin. The numerical IC_{50} values (logarithmic) of these flavonoids and the LoDs of flavonoid/DOPC interaction from the current study are listed in **Table 3.2** and also plotted in **Figure 3.8** shows a correlation between $Log_{10}(IC_{50})$ values of OCT inhibition assay and LoDs of RCV to the flavonoids is seen in **Figure 3.8** with a linear correlation coefficient, r = 0.95.

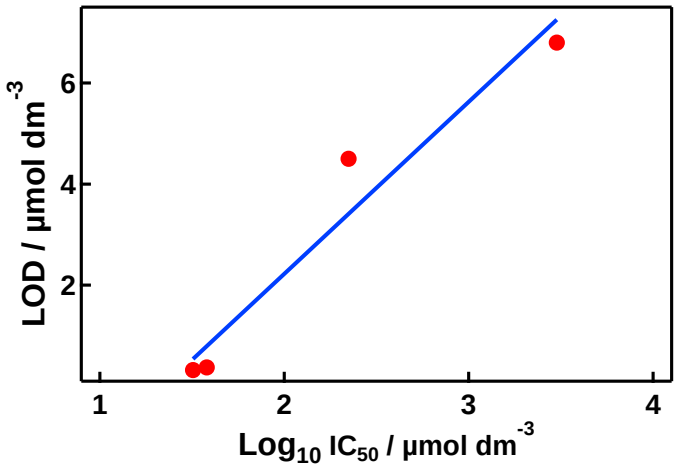

Figure 3.8 Correlation of $Log_{10}(IC_{50})$ values in OCT inhibition assay with LoD obtained from the current study.

Table 3.2 $Log_{10}P$ and IC_{50} values of flavonoids from the literature and LoDs of RCV to the flavonoids from the current study.

Flavonoids	Experimental $Log_{10}P$	LoD / µmol dm^{-3}	Configuration	2,3 double bond	IC_{50} logarithmic
Flavonol					
Quercetin	1.82[a]	0.32	Planar	Yes	1.51[f]
Rutin	-0.87[b]	-	Planar	Yes	>3[f]
Kaempferol	3.25[c]	0.37	Planar	Yes	1.58[f]
Tiliroside	2.7[c]	0.47	Planar	Yes	-
Flavanone					
Naringenin	2.70[c],2.60[a]	4.5	Non-planar	No	2.35[f]
Naringin	-0.13[c]	-	Non-planar	No	>3.7[f]
Hesperetin	2.60[d]	6.8	Non-planar	No	>3.47[f]
Flavan-3-ols					
Catechin	0.32[e]	8	Non-planar	No	

[a]Experimental $log_{10}P$ from Rothwell *et al.*(173). [b]$log_{10}P$ from DrugBank(175). [c]Experimental $log_{10}P$ from Luo *et al.*(153). [d]Experimental $log_{10}P$ from Cooper *et al.*(176). [e]Experimental $log_{10}P$ from Shibusawa *et al.*(177). [f]Experimental IC50 values from Ofer *et al.*(174)

3.2.6 State of solution

It is also important to assess the solution state of flavonoids. This was determined by Dynamic Light Scattering (DLS) on a Nano-ZS Zetasizer (Malvern Instruments Ltd., UK), measuring the volume (%) - size distribution of flavonoids in 0.1 mol dm^{-3} PBS for both freshly dispersed and aged (for 5 hours) solutions. The aim was to assess whether there was any precipitation of the flavonoids from the very dilute solution.

Volume-size distribution of flavonoids (35 μmol dm^{-3}) in PBS solution in **Figure 3.9** shows the presence of some detectable precipitates. When the analysis was repeated after 5 hours, the peaks remained more or less in the same position for some of the flavonoids. For example, quercetin implied no significant change in the particle size. The average of the three repetitive DLS measurements from both freshly prepared flavonoid solutions and aged dispersions are given in **Table 3.3**. This table also presents the literature data on flavonoid solubility in water.

As seen from the **Table 3.3**, a slight increase in size is observed over time. These measurements imply that at the concentration studied (35 μmol dm^{-3}) the flavonoids are not all molecularly dissolved, and there are some detectable precipitates in the system. However, the size is not significantly changing over the course of the experiment. Hardly any change in size over time indicates that flavonoid dispersions are quite dilute systems.

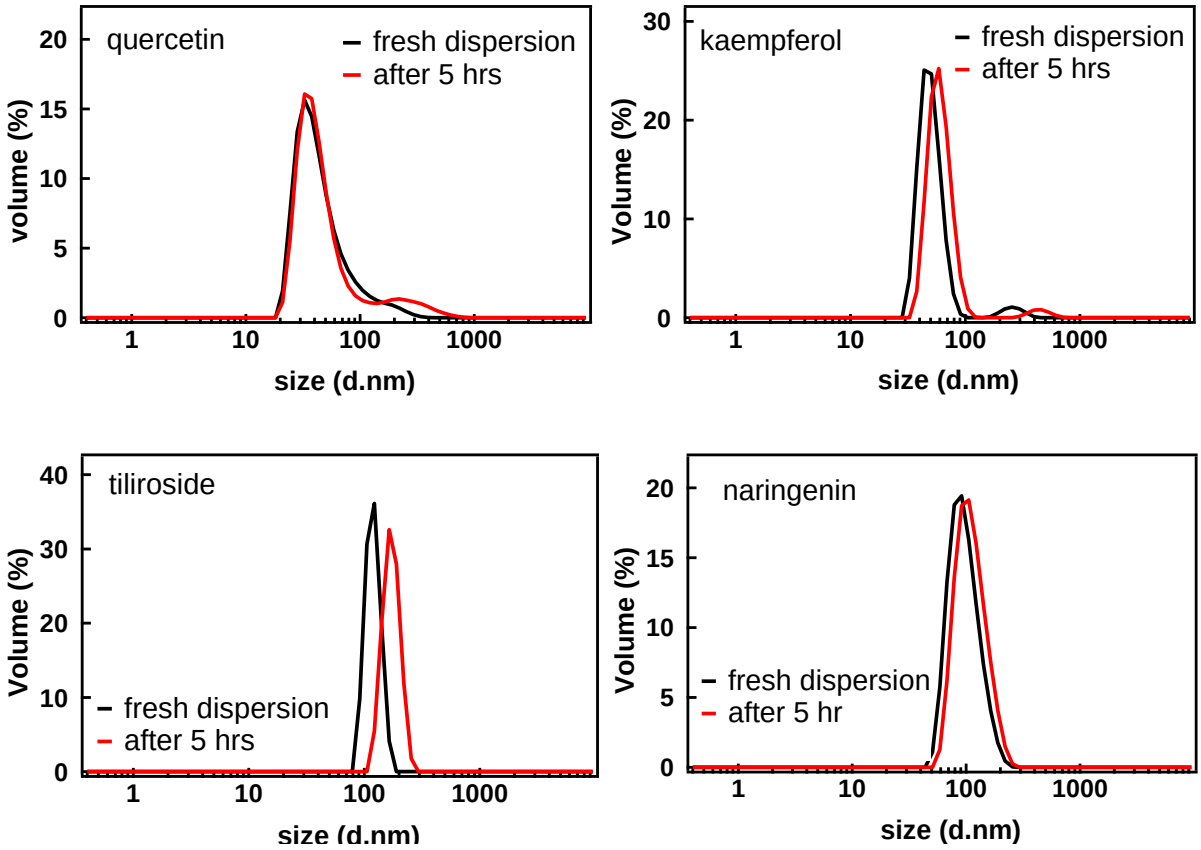

Figure 3.9 Volume (%) - size distribution of flavonoids at the concentration of 35 µmol dm^{-3} in 0.1 mol dm^{-3} PBS for both freshly dispersed and aged (for 5 hours) solutions.

It should also be said that when flavonoid dispersions were filtered through 1-micron filter (Whatman syringe filter, GF/F Glass Microfiber Membrane Filter), no particles were detected by DLS in the filtrate. Obtaining no reading might be due to some interaction between flavonoids and the filter material or the absence of particles in the solution.

Table 3.3 Particle size (d_{43}) and water solubility of flavonoids

Dispersions	D43 (nm)	Water solubility
Quercetin freshly dispersed	49.63	0.26 mg/mL[175]
Quercetin aged solution	58.3	
Kaempferol freshly dispersed	48.2	0.18 mg/mL[175]
Kaempferol aged solution	54	
Tiliroside freshly dispersed	148.8	No data available
Tiliroside aged solution	172.15	
Naringenin freshly dispersed	88.9	0.21 mg/mL[175]
Naringenin aged solution	100.1	
Hesperetin	-	0.138 mg/mL[175]
Catechin	-	Soluble in water
Naringin	-	No data available

Significantly repetition of the RCV experiment with a 5-hour aged-solution (35 µmol dm^{-3}), showed no change in the interaction profile. **Figure 3.10** illustrates the fingerprint scans of quercetin taken from both freshly dissolved (blue line) and aged solutions (red line). The scans are identical showing that the dissolved flavonoid fraction does not change with time.

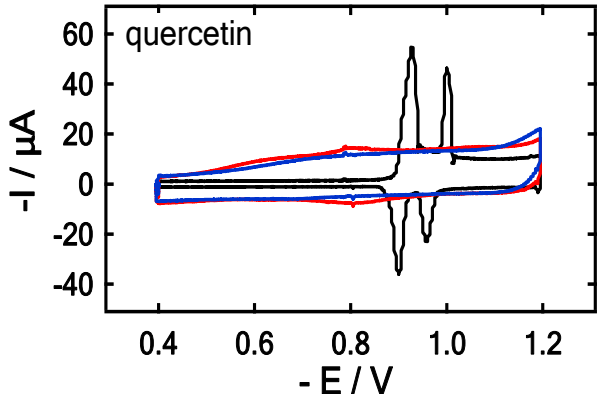

Figure 3.10 RCV of DOPC-coated Pt/Hg electrode (black line) following exposure to quercetin (35 µmol dm^{-3}). The blue line shows the freshly dispersed solution, and the red line shows aged solution for 5 hours, in PBS at pH 7.4.

3.2.7 Lipid recovery results

The integrity and recovery of DOPC monolayer exposed to flavonoids were determined once flavonoid exposure was discontinued and the system was flushed with buffer solution. This process is known as `recovery` (121, 178) and in general, it gives information on whether there is any "memory" effect caused by test compounds which are reversibly adsorbed on the phospholipid on the Pt/Hg electrode. The RCV scans can show full, partial or no recovery upon introduction of compounds of interest. The extent of recovery is related to the degree of DOPC structure restoration which in turn relates to the reversibility of the interactions.

The degree of reversibility of flavonoid interaction was shown in **Figure 3.11**. The red line illustrates the effect of each flavonoid at the concentration studied and the blue line shows the recoveries. After physically flushing the system with buffer in the absence of flavonoid exposure, the lipid recovered, and the peaks returned, indicating these interactions are almost completely reversible. This shows that flavonoids can easily be washed away from the phospholipid environment and hence they reorient back to their original profile.

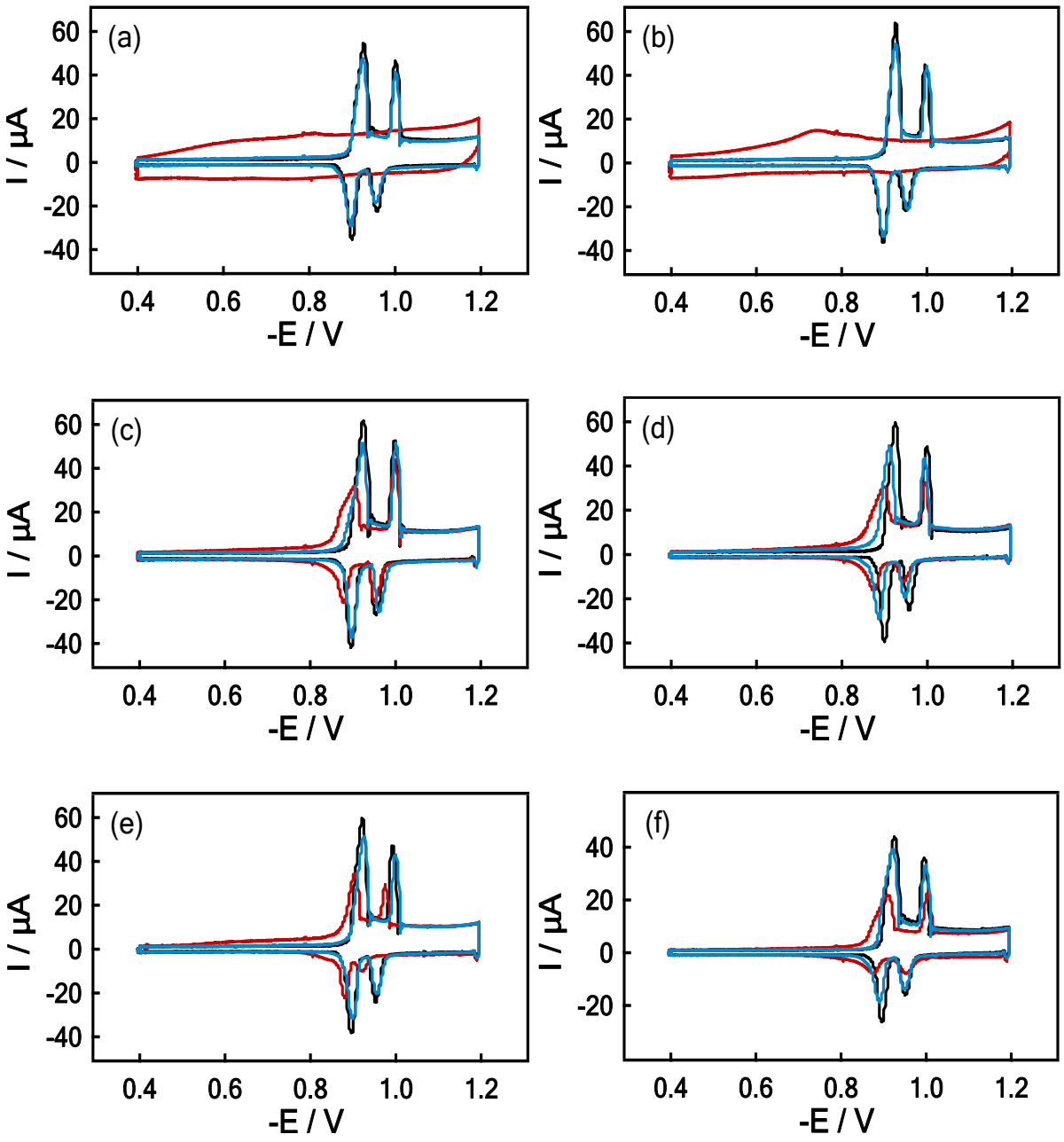

Figure 3.11 RCVs at 40 V s^{-1} of a pure DOPC-coated Pt/Hg electrode in PBS at pH 7.4. (black line) in the presence of 10 µmol dm^{-3} quercetin (a), kaempferol (b), tiliroside (c) and 35 µmol dm^{-3} naringenin (d), hesperetin (e) and catechin (f) (red line). Capacitive current peaks are recovering after testing flavonoids (blue line).

From the recovery data, one can deduce that the flavonoid/DOPC interaction relates to the interaction of soluble flavonoid with the DOPC monolayer. The reference concentration of 10

µmol dm^{-3} used in this study has already been reported in the solubility range (54). For example, solubility for tiliroside and related flavonoids such as kaempferol and kaempferol-3-glucoside was indicated as around 10 µmol dm^{-3} by Luo *et al*.

3.3 Conclusions

With RCV study we aimed to systematically investigate the structure-activity relationship of eight flavonoids using an electrochemical membrane model in proof-of-concept experiments. The current work reinforced the application of the electrochemical membrane model of DOPC monolayers supported on Hg electrode for screening food ingredients. Due to its high-throughput configuration, this sensing device can be used for rapid screening of not only flavonoids but also many other food ingredients such as proteins and peptides for their membrane activity. Hence, this technique can serve as a new screening tool in developing new formulations for future applications in industries like food and beverages.

The key findings of the study can be summarised as follows:

(i) The membrane activities of flavonoids are directly related to their structure, and to their conformations. Flavonols with two co-planar rings showed more intensified interactions compared to interactions of non-planar flavanones with DOPC monolayers. Penetration of quercetin, kaempferol and tiliroside into the DOPC monolayer is evidenced by an increase in the capacitance baseline height on the RCV plot along with substantial peak suppression.

(ii) Rutin and naringin with two sugar groups showed no noteworthy effect on the monolayer structure which implies that the presence of a sugar moiety hinders the interactions. However, another glycoside tiliroside created a very pronounced effect on DOPC monolayer. Note that unlike other glycosides, tiliroside has only

one sugar group and surprisingly, it possesses a high $\log_{10}P$ value (2.7). Such high hydrophobicity along with its structural configuration might contribute to its stronger interaction with the lipid monolayer.

(iii) Comparison between the extent of flavonoid interaction with the DOPC monolayer and the flavonoid $\log_{10}P$ shows that there is no reliable correlation between the biomembrane activity of flavonoids and their $\log_{10}P$. However, detection limits of RCV to flavonoids well correlated with their published IC_{50} values.

(iv) Hydrogen-bonding between –OH group of flavonoids and carbonyl and polar groups of phospholipids at the membrane interface whereby planarity allows an easier fit into the monolayer might be the driving force behind the interactions. Also, electrostatic forces from aromatic rings and associated polarisability contribute o the interactions.

Chapter 4 Interactions of flavonoids with Langmuir monolayers of DOPC

4.1 Introduction

Subsequent to the initial RCV screening, three flavonoids; quercetin, rutin and tiliroside were chosen amongst the eight to further characterise the interactions through classic spread Langmuir monolayers at the air−water (A−W) interface. The rationales for choosing these three flavonoids are as follows. (i) Quercetin is the most widely studied flavonoid for its membrane activity, and hence it was chosen as a reference compound to help understand and interpret the mechanisms involve in interactions. (ii) Rutin was chosen as a negative control because although it is a quercetin glycoside formed by replacing one of the hydroxy group at position C-3 with glucose and rhamnose sugar groups, it did not exhibit a significant activity on DOPC monolayer with RCV. (iii) Finally, tiliroside was selected because despite bearing one sugar moiety, it showed a strong activity on DOPC monolayer with an intensified effect at high concentrations which makes it intriguing for further analysis. **Figure 4.1** reminds the structures of the flavonoids used for further characterisation.

Free-standing Langmuir monolayers at the A/W interface are well-defined and fundamental interfacial systems and, hence suitable models to study the interactions at interfaces. Moreover, Langmuir monolayers are excellent systems to monitor film stability, and this information is especially useful in the investigation of the therapeutic effects of flavonoids. The aim of using such a conventional approach was to determine whether the findings from

free-standing Langmuir monolayers correlate with the findings from the previous technique; Hg-supported DOPC monolayer.

In this chapter, surface pressure (π) versus area per molecule (A) isotherms facilitated the study of the adsorption and penetration of the flavonoids on and into DOPC monolayers. In addition, the effect of the flavonoids on film stability was monitored at a constant pressure of 30 mN m^{-1}, by recording the alterations in monolayer area as a function of time. Moreover, a direct observation of the stability behaviour of the DOPC film with and without flavonoids was characterised by Brewster angle microscopy (BAM).

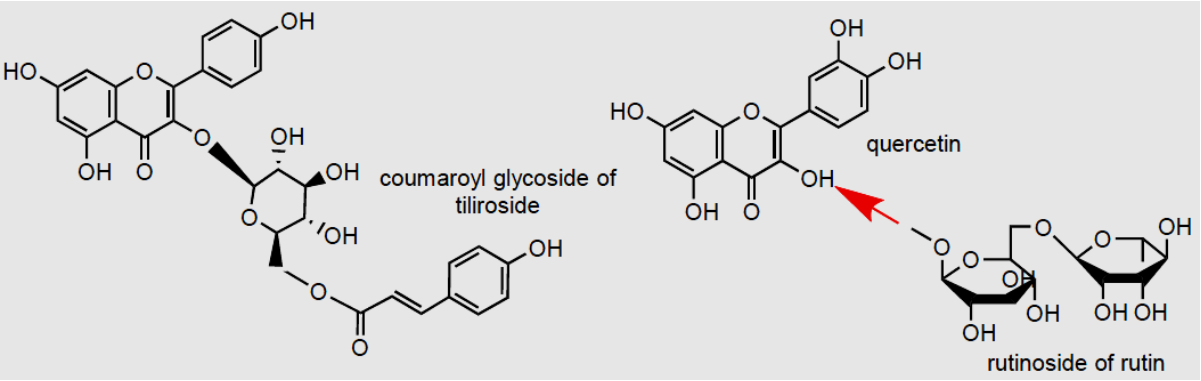

Figure 4.1 The structures of flavonoids used for follow-up experiments.

4.2 Results and discussion

4.2.1 π-A Isotherms of octadecanol

Octadecanol (synonyms: Stearyl alcohol, n-Octadecanol, Octadecan-1-ol) with the formula of CH_3 $(CH_2)_{16}CH_2OH$ is a long chain alcohol and classical monolayer-forming material. Since octadecanol monolayers reveal distinct phase transitions which have been characterised by several groups (179, 180) we first produced the π-A compression isotherm of octadecanol before proceeding the experiments with the main phospholipid of this study, DOPC.

A typical π-A isotherm for octadecanol monolayer is shown in **Figure 4.2**, for an aqueous surface of the water (Milli-Q) at 24.5 ^oC. The-low pressure region of the isotherm extrapolates to an area of about 22-24 $Å^2$/molecule. The molecules in this region are loosely packed due to the large distance between them, and hence the film is more compressible. When the film compression starts, a sharp kink occurs and the slope increases until about π = 10-15 mN m^{-1}. This region of the curve corresponds to a discontinues change in the tilt of the molecules towards the direction of the next nearest neighbour (179, 181). At higher pressures, a second abrupt transition in the isotherm is observed with a very steep curve. In this region, where the molecules in the film are more closely packed, a decrease in the tilt angle of the alkyl chains from the normal to the interface is observed (179). Upon increasing the pressure, a well-aligned configuration occurs with the chain axes are vertically oriented (179). Finally, collapse phenomenon occurs at further increased pressures with smaller surface areas (92).

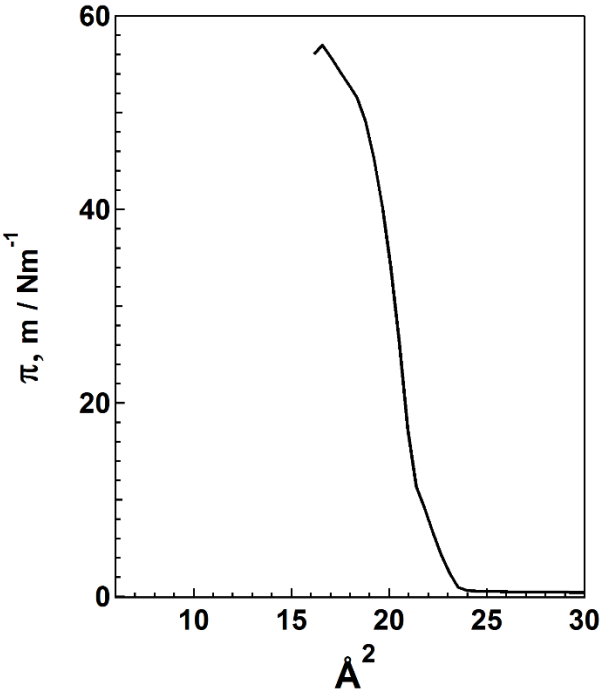

Figure 4.2 π-A isotherms of octadecanol monolayers on an aqueous surface of the water (Milli-Q) at 24.5 ^{o}C.

4.2.2 π-A Isotherms of DOPC

Figure 4.3 shows the π-A isotherms of DOPC monolayer produced over ultrapure deionized water (black line), (Millipore Inc., Ω = 18.2 MΩ.cm, pH 6.9), and PBS buffer (red line) with pH 7.4 and ionic strength 0.01 M. Surface pressure for both isotherms displays a gradual increase along with a decrease in the area per DOPC molecule.

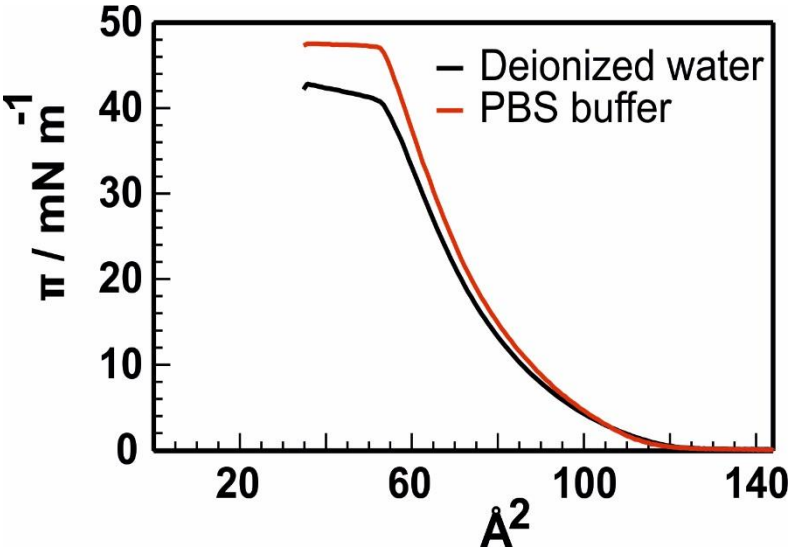

Figure 4.3. π-A isotherms for DOPC monolayers produced over ultrapure deionized water with pH 6.9 (black curve) and PBS buffer with pH 7.4 and ionic strength 0.01 M (red curve) at 25.5 ^{o}C**.**

π-A isotherm of DOPC monolayer is characterised by liquid expanded (LE) phase up to the monolayer collapse. Cis double bond in the middle of each hydrocarbon chains of DOPC weakens the molecular interactions. Therefore, under all experimental conditions, this phospholipid only forms a fluid, LE phase with no appearance of phase transition until the collapse pressure (182, 183).

The black line in **Figure 4.3** shows that the area per DOPC molecule at π = 30 mN m^{-1} and collapse point (roughly 40 mN m^{-1}) is around 62.5 Å^2/molecule and 53.4 Å^2/molecule, respectively. These findings well correlate with the previous reports (184).

As seen from the π-A isotherm in **Figure 4.3**, subphase conditions created an effect on the DOPC compression isotherm. Exchanging the aqueous solution from ultrapure deionized water to the PBS buffer caused a higher collapse pressure (π_c), i.e. from $\pi_{c\ \text{deionized water subphase}}$ = 40.3 mN m^{-1} to $\pi_{c\ \text{buffer subphase}}$ = 46.4 mN m^{-1}. This increase in π_c might be due to a higher film stability with buffer subphase. Also, a slight shift is seen towards a larger extrapolated molecular area. However, this shift remained within the experimental error (4%). For example, at π = 30 mN m^{-1}, DOPC occupies 62.5 $Å^2$/molecule and 65 $Å^2$/molecule over the subphase of water (Milli-Q) and buffer (PBS), respectively.

π-A compression isotherms for DOPC monolayer were also recorded through repetitive compression-expansion cycles. Each time, the film was compressed up to π = 30 mN m^{-1} where the pressure was maintained constant for an hour, before its expansion to the maximum trough area. The same cycle was repeated at least three times over the subphase of water (Milli-Q) and buffer (PBS), to record the compression isotherms of DOPC as well as monitor the film stability (film stability will be described in detail in the following section.

Figure 4.4 shows the three repetitive measurements of compression isotherms of DOPC spread over PBS buffer solution at pH 7.4, ionic strength 0.1 M. After each compression-expansion cycle, the number of the lost molecules were calculated and subtracted from the initial number of molecules spread. This value was used as the number of molecules, which spread for the next cycle. Otherwise, if all spread molecules were assumed to remain at the A/W interface, a shift of the isotherm curve towards slightly lower molecular area would have been observed.

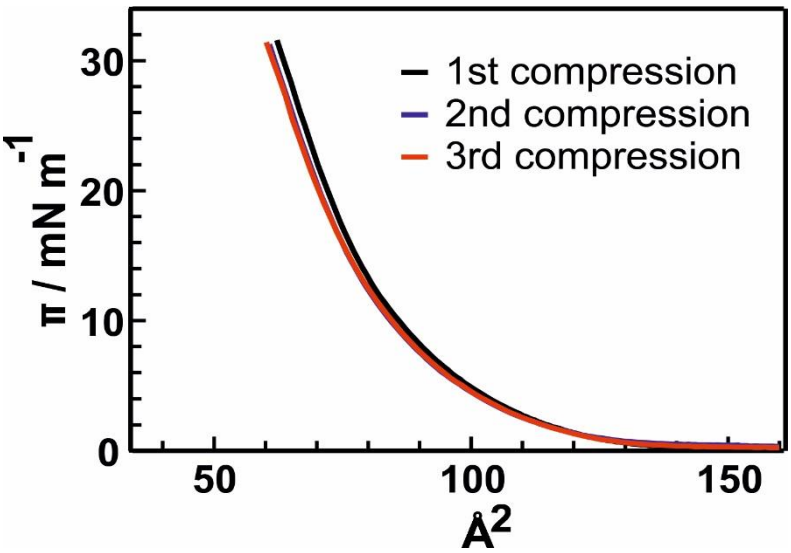

Figure 4.4. Repetitive π – A isotherms for DOPC monolayers spread at the A/W interface at temperature 25 ºC over PBS buffer at pH: 7.4 and ionic strength 0.1 M.

Repetitive compression-expansion cycles for Langmuir monolayers of DOPC were extensively investigated by Niňo *et al*. (185). They reported no hysteresis in the monolayer up to π = 30 mN m^{-1} indicating that the isotherms produced until π = 30 mN m^{-1} are completely reproducible. Hysteresis began at surface pressures above 30 mN m^{-1}, and the isotherm shifted towards the lower molecular area which is an indication of an irreversible molecular loss in the monolayer (185).

Previous studies also investigated the effect of the pH of the medium on the phospholipid isotherms before and after the monolayer collapse. Here it should be noted that the surface pressure to which monolayers can be compressed before they collapse is defined as equilibrium surface pressure (π_e). Both Niňo (185) and Lucero (183) reported that π_e is pH-independent for DOPC monolayer between pH 5 and 9. Based on these findings, the authors suggested that for DOPC monolayers, the packing behaviour is mainly determined by the ordering of the acyl chains instead of the ionisation of the polar head groups.

On the other hand, Kuroda *et al*. studied the effect of pH on the phospholipid isotherms at lower pH values; 3,5 and 5,6, respectively (186). A decrease in the pH of the medium from 5.6 to 3.5 shifted the DOPC compression isotherm towards lower molecular areas which was explained due to a possible reduction in the magnitude of the zeta potential of DOPC membrane. The electrical neutral point of DOPC membranes was reported near pH 4.0 which means that the repulsive force between lipid molecules is the weakest in this pH range. As a consequence of the weak repulsive forces between molecules in low pH (pH<4), one might expect reduced area coverage of the DOPC monolayer.

4.2.3 Monolayer stability – constant pressure experiments

If a monolayer film is maintained at a constant surface pressure or constant area for a certain period, an inevitable film loss and hence contraction of the spread films is observed. The loss in the monolayer film area is an indication of how stable a monolayer is. **Figure 4.5(a) and Figure 4.5(b)** show the DOPC film contraction; as a measure of the decrease in the relative trough area versus time, produced over ultrapure deionized water, (Ω = 18.2 MΩ.cm, pH 6.9) and PBS buffer (pH 7.4, ionic strength 0.01 M)**,** respectively**.** These measurements were conducted through successive compression-expansion cycles for three times.

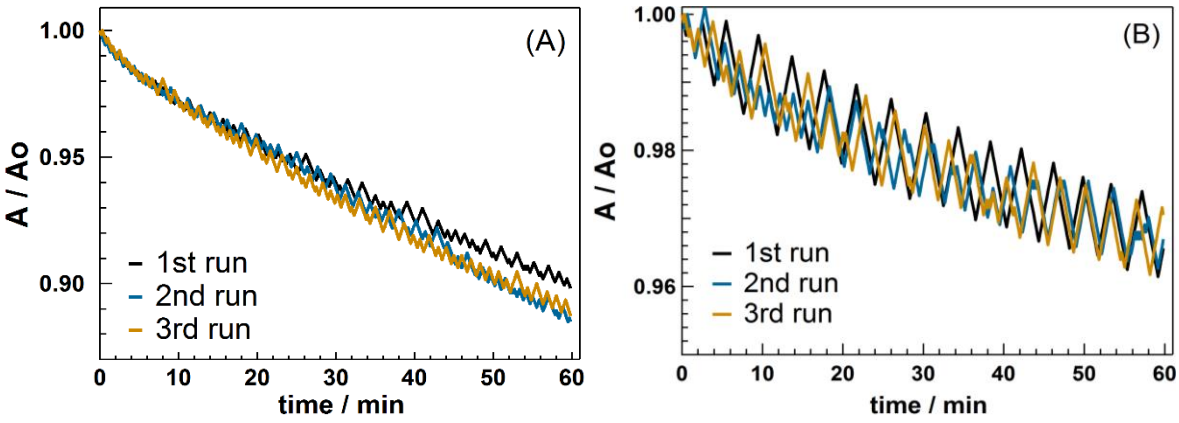

Figure 4.5 Film stability as a function of time for pure DOPC monolayers (a) produced over ultra-pure water and (b) produced over PBS buffer. (Note that the sawtooth appearance is due to the discrete time step between alterations of the barrier position to maintain constant π = 30 mN m^{-1}).

As seen in **Figure 4.5(A)** and **Figure 4.5(B)**, contraction of the relative trough area for DOPC monolayer was around 10% and 3.5%, respectively. In the presence of PBS buffer, there is a less reduction in the film area and hence better stability. The improved stability of the phospholipid film is probably due to the influence of subphase salt. Upon introducing the salt to the subphase, ions from the solution become attracted towards the head group region of the lipid molecules. For example, positively charged sodium (Na^+) and negatively charged chloride (Cl^-) ions in the solution have an affinity towards the negatively charged phosphate and positively charged choline in the head group region, respectively (187). This probably results in a shielding of the internal electrostatic interactions that causes a reduction of the interaction between each pair of DOPC phospholipid (186).

The mechanisms underlying the film loss and the monolayer stability of different phospholipids and fatty acids have been investigated by several groups (185, 188, 189). These

studies used the equilibrium surface pressure (π_e) as a key parameter in elucidating the mechanism. As described previously, π_e is defined as the surface pressure to which monolayers can be compressed before they collapse.

At the pressures above and below π_e, Niño *et al*. investigated the stability behaviour of monolayers comprised of two phospholipids; DOPC and DPPC at the A/W interface (185). When a monolayer film is maintained at pressures above equilibrium spreading pressure ($\pi > \pi_e$), the film loss was reported due to the collapsing into the bulk phase which is in agreement with previous reports (189). On the other hand, when a monolayer film is maintained at surface pressures lower than equilibrium spreading pressure ($\pi < \pi_e$), the molecular loss was suggested because of the desorption mechanism i.e. desorption of molecules into the bulk phase (185). This loss was shown depend on the properties of amphiphiles i.e. the degree of unsaturation and the number of C atoms.

Recent studies also proposed that because phospholipid molecules become more soluble when they are oxidised, and oxidation may accelerate the lipid loss (188, 190). Although the membrane damage caused by oxidation remains relatively unclear, in a general manner, unsaturated lipids were proposed to be more prone to peroxidation compared to saturated ones. Wong-Ekkabut investigated the oxidation mechanism of lipids with different degree of unsaturation (191). They measured the sum frequency intensity of the vinyl CH stretch at the double carbon bonds by maintaining a constant pressure for a certain period. Lipid degradation was attributed to lipid oxidation mediated by different species in the air, such as oxygen and ozone. The proposed mechanism was given as follows: Following the vinyl CH stretch disappearing, oxidised functional groups are introduced to lipid which then increases the solubility of molecules due to the H-bond formation with the surrounding water (191).

4.2.4 Effect of flavonoids on π-A Isotherms of DOPC monolayers

On the basis of the RCV results, the aglycone (i.e., without the sugar) quercetin, and two glycosides - tiliroside (one sugar moiety in the structure) and rutin (two sugar moieties in the structure) - were selected for follow-up experiments with Langmuir monolayers, since they appeared to exhibit particularly representative effects of varying degrees of interaction.

Figure 4.6 shows the effects of adding quercetin, rutin and tiliroside at 10 μmol dm^{-3} beneath Langmuir monolayers of DOPC at π = 30 mN m^{-1}. Introducing flavonoids did not change the shape of the isotherm. However, it did affect the molecular area available per molecule with quercetin (**Figure 4.6(a))** and tiliroside (**Figure 4.6(b))**. In other words, the increase in the molecular area upon introducing quercetin and tiliroside agrees with the insertion of these flavonoids into the LE state.

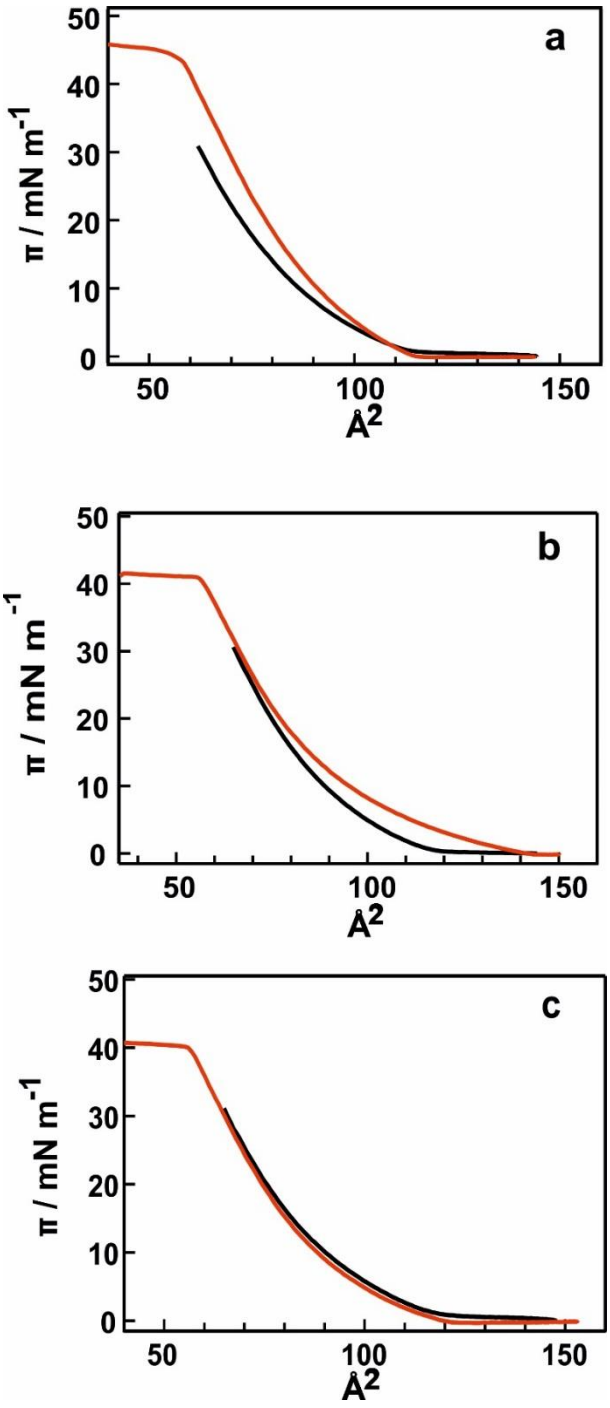

Figure 4.6. π-A isotherms of DOPC monolayer at the air-water interface in the absence (black line) and the presence of 10 µmol dm^{-3} (a) quercetin, (b) tiliroside and (c) rutin in the subphase (red line).

As shown in **Figure 4.6(a),** the introduction of quercetin (10 µmol dm^{-3}) into the subphase did not provoke an immediate increase in the monolayer area at low surface pressures (below 5

mN m^{-1}). However, the monolayer exhibited a more expanded isotherm when the pressure was increased further. Quercetin introduction shifted the isotherm towards a larger area per (DOPC) molecule (~67 $Å^2$) compared to that of the pure DOPC monolayer (~60 $Å^2$). It is assumed this shift occurred due to the area occupied by quercetin molecules inserted into the monolayer and is observed all along the isotherm indicating that the molecule remained in the monolayer at even higher surface pressures (111). This result is in agreement with the only other study of quercetin interacting with Langmuir monolayers of phospholipid (DPPC), published recently (192). Similar to the present findings, the authors reported an increase in surface pressure due to the effective incorporation of the molecule into the model lipid membrane (192).

In the same study, a π-A isotherm for pure quercetin spread on the air/water interface was also produced with a maximum surface pressure of just above 20 mN m^{-1} before the collapse (192). Based on the area per quercetin molecule (A_{flav} = 89 $Å^2$) at π = 20 mN m^{-1}, taken from the study, we attempted to quantify the amount of adsorption of quercetin into the DOPC monolayers, assuming ideal mixing. In other words, the mole fraction of quercetin (f_{flav}) in the mixture was calculated via:

$$\mathbf{A_{total} = (1\text{-}f_{flav})\, A_{lipid} + f_{flav} * A_{flav}} \qquad \mathbf{(4.1)}$$

: where, A_{total} (78 $Å^2$), A_{lipid} (72 $Å^2$) and A_{flav} (89 $Å^2$) signify the area per molecule in the mixed monolayer, area per lipid molecule and area per quercetin molecule, respectively. In the current study, f_{flav} was found around 35 % which shows a high passive adsorption of quercetin molecule into DOPC monolayers.

Figure 4.6(b) shows the compression isotherm of DOPC monolayer in the presence of tiliroside (10 µmol dm^{-3}). Unlike quercetin, surface pressure rises rapidly with tiliroside, when

it is injected at π =30 mN m^{-1}, signifying that the molecules are very close to each other. The distinct increase in the π vanishes upon further compression of the lipid film (111).

At first glance, **Figure 4.6(c)** displays no significant effect of rutin injected beneath DOPC monolayers, implying there is no definitive interaction. However, further surface characterisation via BAM indicates significant effects of this compound on the monolayer (see later in **section 4.2.6**). A recent study pointed to a similar behaviour of pure DOPC monolayers in the presence of the cationic photosensitizer methylene blue (MB) (193) that has almost the same $\log_{10}P$ (194) as rutin (~ -0.9). Although the surface pressure of DOPC remained unaltered with MB incorporation, further analysis using polarisation-modulated infrared reflection-absorption spectroscopy (PM-IRRAS) revealed the adsorption of MB onto the polar surface which then further leads its binding close to the double bonds of the hydrophobic chains (111).

4.2.5 Effect of flavonoids on the stability of DOPC monolayers

The effect of flavonoids on the film stability of DOPC monolayers is demonstrated in **Figure 4.7** at a constant π of 30 mN m^{-1}. Here, note that the sawtooth appearance in this figure is due to the discrete time step between alterations of the barrier position to maintain constant π = 30 mN m^{-1}.

The striking monolayer-stabilising action of quercetin, suggesting the lack of phospholipid desorption from the monolayer, is observed in **Figure 4.7(a)**. A similar stabilising effect was also observed with tiliroside **Figure 4.7(b)**.

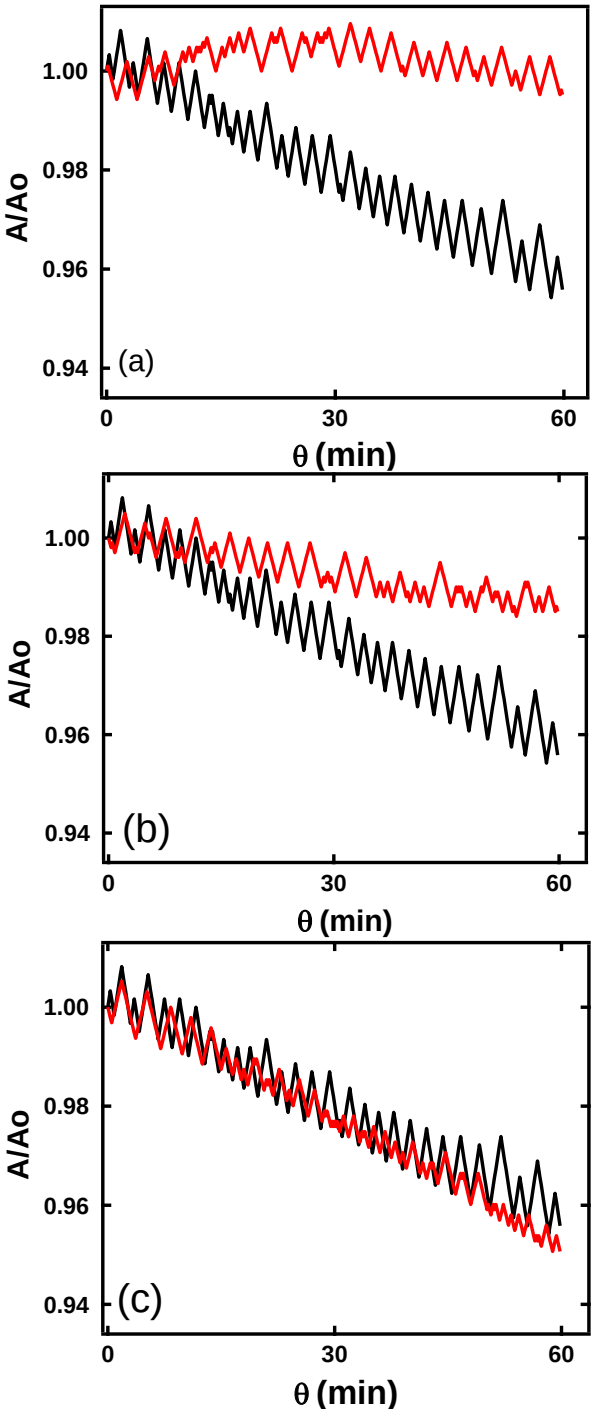

Figure 4.7 Film loss at constant pressure of 30 mN m^{-1} in DOPC monolayers (black line) in the presence of 10 µmol dm^{-3} **(a)** quercetin, **(b)** tiliroside and **(c)** rutin in the subphase (red line).

Studies showing the monolayer-stabilising action of flavonoids using Langmuir monolayers are quite limited. The first study to ever show such an action was with milk thistle flavonoids; dihydroxyquercetin (taxifolin) and silybin through Langmuir monolayers of lecithin (195). Both flavonoids exhibited different mechanisms of action; with dihydroxyquercetin stabilising the lecithin monolayer through its adsorption to the monolayer-air interface and silybin being immobilised in the apolar core of the lipid monolayer (195).

Membrane stabilisation is an important phenomenon since it is believed to be a key mechanism by which some drugs exert their beneficial effects. For example, certain allergic reactions such as allergic asthma can only be controlled using mast cell stabilisers, preventing the release of histamine and related mediators from mast cells. Unfortunately, Cromolyn is the only drug available in the market acting as a mast cell `stabiliser`. The effect of Cromolyn was compared with quercetin using human cultured mast cells for their ability to inhibit the key mediators from the cells. Also, a human study was conducted to observe the effect of quercetin on the contact dermatitis and photosensitivity. Interestingly, quercetin was found more effective than cromolyn in stabilising the cells by limiting the release of mediators that trigger the allergy, such as histamine, prostaglandin DS (PGD2), tumour necrosis factor (TNF) and several cytokines like IL (40).

In addition to clinical studies, model biomembranes of both multi and unilamellar vesicles in conjunction with molecular dynamic simulation and imaging studies also revealed a membrane stabilising action of quercetin and its related compounds (196). The simulated images by Sinha *et al*. suggest that quercetin moved from the bilayer centre towards the head group region where it forms a large network of intermolecular hydrogen bonds with the head groups. The substituents in the flavonoid structure that actively involved in the hydrogen bond formation were stated as 4`- OH and 3`-OH groups in the ring B along with 7-OH in the

ring A. The authors also observed the contribution of 3-OH and 5-OH groups. The observed localisation with the polar head group region did not change during the entire simulation, and such localisation of quercetin at the interfacial region was proposed to introduce a stabilising action which was also confirmed by the transmission electron microscope (TEM) images (196).

4.2.6 Visualisation of lipid monolayer via BAM

BAM was applied for the topographical characterization of monolayer surface. The images were taken in every ten seconds from the beginning of the compression all the way beyond the collapse pressure. The surface was further characterised an hour after reaching the collapse pressure.

Visualisation of DOPC monolayer surface at different surface pressure values is given in **Figure 4.8**, note that the interferences on these images are always present even when there is no monolayer. In agreement with previous studies (183, 197), pure DOPC monolayers formed the features of the interference fringes as well as 2D foam-like structures with circular shapes and small domains within their interior at very low surface pressures. All these structures disappeared during monolayer compression, and no visible features were seen up to the collapse point (~π = 46), evidencing the existence of homogeneous liquid expanded phase only (111). A few small bright features were formed and flickered at the collapse point. Such formations were assumed to be an indication of multilayer formation (198).

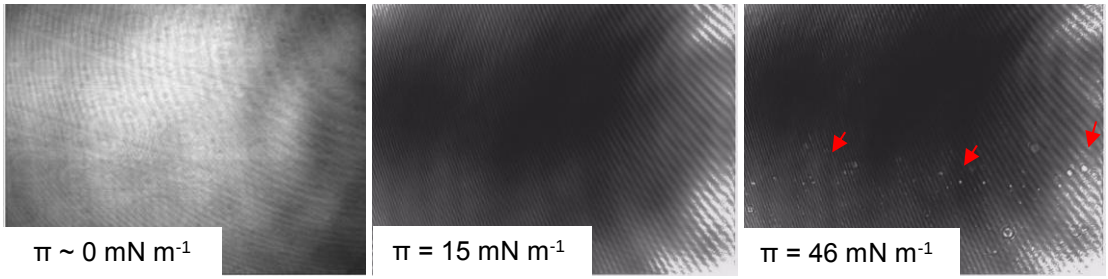

Figure 4.8 Visualisation of pure DOPC all along the compression and at monolayer collapse.

BAM images of DOPC monolayer-flavonoid systems at LE phase (π = 28) are given in **Figure 4.9**. Unlike pure DOPC, low density of bright crystallites were observed with quercetin **Figure 4.9(a)** and tiliroside throughout the compression **Figure 4.9(b)**, rutin, however, did not alter the morphology of the DOPC monolayer and the film preserved its original homogeneous liquid expanded phase **Figure 4.9(c)**.

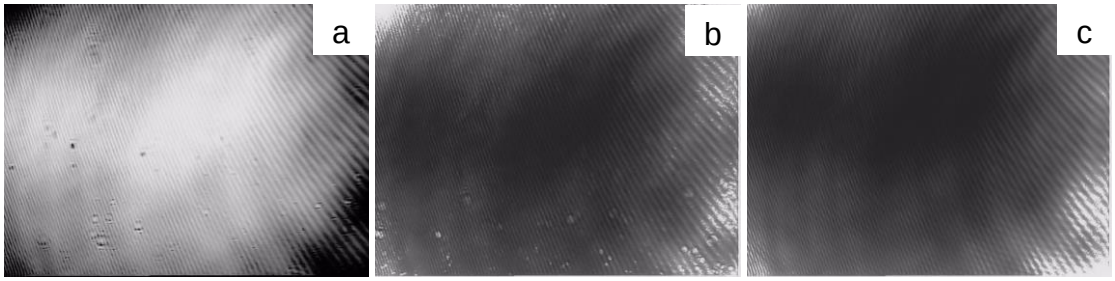

Figure 4.9 Visualization of DOPC flavonoid systems at the LE regime (π = ~ 28 mN m^{-1}) with (a) quercetin, (b) tiliroside and (c) rutin.

The images in **Figure 4.10** illustrate the monolayer structure after the monolayer had been fully compressed to the collapse pressure. **Figure 4.10(a)** shows the formation of large lipid domains with pure DOPC. Although kinetics behind the monolayer collapse are not yet fully understood, it is well known that compressing monolayers beyond the collapse pressure causes 2D to 3D transitions by the formation of the lipid aggregates (199, 200). Such lipid domains were observed move over to the water surface in the absence of flavonoids.

However, these aggregates, which appear as small, moving islands, were completely stabilised and immobilised in the presence of quercetin and tiliroside **(Figure 4.10b, 4.10c)** and the monolayer appearance was still unaltered even after several hours (data not shown). In the presence of rutin **(Figure 4.10d)**, the monolayer structure was completely disrupted and all typical DOPC domain structures disappeared. In other words, introduction of rutin rendered the monolayer appearance entirely smooth and devoid of lipid islands. This suggests the existence of rutin in the monolayer system. Although rutin somehow created an effect, it was not possible to identify neither based on π -A isotherm nor the film stability.

The smooth appearance of the DOPC monolayer with rutin might give an impression that such behaviour might arise from the surface adsorption of this flavonoid. However, if this was the case, a different trend would have also been observed via RCV. RCV characterises the surface adsorption by the suppression of the peaks such as in the case of silica nanoparticles. Hence, surface adsorption does not stand as a valid reason. Such behaviour could be more likely due to the modification of the lipid organisation (111).

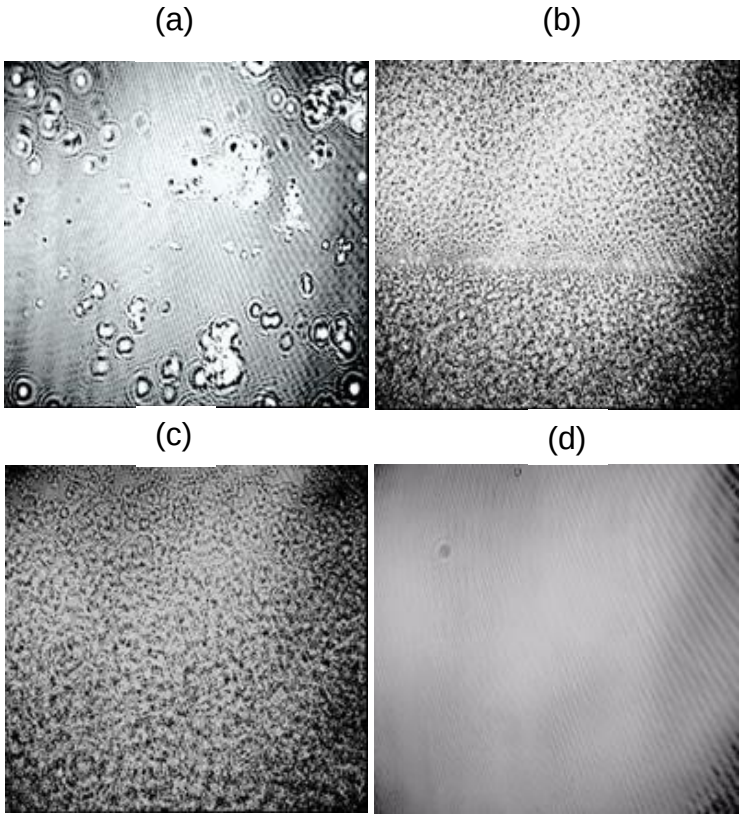

Figure 4.10 BAM images of DOPC monolayers after an hour monolayer collapse (a) pure DOPC monolayer and in the presence of 10 μmol dm^{-3} (b) quercetin (c) tiliroside and (d) rutin in the subphase. (Please note that the line in the image (b) is due to the optical interference).

4.3 Conclusions

In a complementary line of study, free-standing Langmuir monolayers of DOPC at the A-W interface were used to compare the interactions observed with the supported membrane model. The key findings with follow-up flavonoids quercetin, tiliroside and rutin were as follows:

(i) Surface pressure-area isotherms in the presence of quercetin and tiliroside suggested that these flavonoids interacted to varying degrees with free-standing Langmuir monolayers of DOPC at the A-W interface.

(ii) This study is the first reporting the effect of the flavonoids on Langmuir monolayer of DOPC. A particularly exciting finding is that two of the flavonoids; quercetin and tiliroside stabilised the phospholipid film and inhibited film loss. Such information regarding membrane-stabilising action is important in investigating the potential therapeutic mechanisms of flavonoids.

(iii) Interestingly, rutin exhibited a different molecular mechanism of action, rendering the surface completely smooth and devoid of islands.

(iv) The results from Langmuir monolayer study correlated well with the previous monolayer technique using RCV. Both techniques revealed a rank order of interactions as quercetin > tiliroside > rutin.

Chapter 5 Structural characterisation of DOPC MLVs with flavonoids using X-ray Scattering

5.1 Introduction

Until now, the previous work in this thesis has discussed the flavonoid interactions with monolayer model systems to build a structure-activity relationship through supported monolayers on Pt/Hg electrode, and observe the film stability through free-standing monolayers at an A-W interface. However, in a complementary line of the study, this chapter will report the quantitative analysis of the interactions between flavonoids and phospholipid vesicles, a step-up in complexity from monolayers.

Small-angle X-ray Scattering (SAXS) was employed using DOPC multilamellar vesicles (MLVs) to gain more insight into the effect of flavonoids on model biomembranes. Application of SAXS allowed us to access detailed information on both bilayer structural changes; membrane thickness and water layer thickness, and mechanical properties; fluidity and undulations. Moreover, the effective molecular volume and area calculations estimated from SAXS results helped obtain an indirect information concerning the flavonoid location within phospholipid membrane. Thus, we definitely have complementing information to the data obtained in previous monolayer work.

Structural changes in phospholipid vesicles were recorded as a function of flavonoid content and temperature. To add further credence to SAXS observations, flavonoid-DOPC systems were visualised via confocal laser scanning microscope (CLSM). Also, the vesicle size distribution was recorded via static light scattering.

Overall, gaining an understanding regarding the bilayer structural alterations with flavonoids is of great importance to elucidate membrane-associated therapeutic potentials of flavonoids and their anticipated applications in drug and food delivery systems.

5.2 Results and discussion

Initially, the effective molecular area and volume calculations will be estimated for both DOPC MLVs alone and DOPC-flavonoid systems. It is important to have an idea on these estimates for a reliable data interpretation and discussion. Following sections will concentrate on the structural bilayer changes as a function of temperature and flavonoid content.

5.2.1 Volume/Area calculations

The lateral area per molecule calculations for fully hydrated MLVs has been outlined by Hodzic *et al*. (201). As a first step, the molecular volume for each flavonoid was obtained from,

$$V_{flav} = \frac{M_w \left(\frac{g}{mol}\right)}{\rho\left(\frac{g}{cm^3}\right) 0.6022} \left(Å^3\right) \qquad \textbf{(5.1)}$$

Where M_w is the molecular weight and ρ is the density of flavonoid of interest in the solid state. The calculated molecular volumes for all three flavonoids studied are given in **Table 5.1**.

Table 5.1 M_w (g/mol), ρ (g/cm^3), and calculated V_{flav} (Å^3) of three flavonoids studied.

	Quercetin	Tiliroside	Rutin
M_w (g/mol)	302.236	594.52	664.56
ρ (g/cm^3)	1.8[202]	1.68[203]	1.82[204]
V_{flav} (Å^3)	278.8	587.6	606

Next, effective molecular volume in DOPC/flavonoid systems was estimated using the following equation,

$$V_{eff}(x) = xV_{flav} + (1-x)V_{DOPC} \quad \textbf{(5.2)}$$

Where *x* represents the flavonoid concentration incorporated within the vesicle and V_{DOPC} represents the molecular volume of DOPC. Nagle *et al*. published the absolute specific volume of fully hydrated DOPC MLVs; V_{DOPC} = 1303.0 Å^3 at 30 °C (205). Afterwards, Pan *et al*. reported the temperature dependence of V_{DOPC} (see **Table 5.2**) (206). From literature values, we have estimated V_{DOPC} at 25 °C as 1298 Å^3. Concentration-dependent effective volume estimates for flavonoids incorporated into DOPC MLVs at 25 °C were listed in **Table 5.3**.

Table 5.2 Reported V_{DOPC} values for different temperatures (206).

Temperature (°C)	Volume/molecule (Å^3) (literature values)
15	1288
30	1303
45	1318

Table 5.3 Concentration-dependent effective volume estimates for flavonoids incorporated into DOPC MLVs at 25 °C. Veff for DOPC was taken from reference (206).

Concentration (mol %)	$V_{eff\_tiliroside}$ (Å^3)	$V_{eff\_quercetin}$ (Å^3)	V_{eff_rutin} (Å^3)
0	1298	1298	1298
1	1291 ± 20	1288 ± 20	1291 ± 20
2	1284 ± 20	1278 ± 20	1284 ± 20
6	1255 ± 20	1237 ± 20	1256 ± 20
12	-	1175 ± 20	-

The effective lateral area per molecule for bilayers consisting of more than one kind of molecule can be determined using the **equation 5.3** (201),

$$A(x) = \frac{2V(x)}{d_{HH}(x)} \quad \textbf{(5.3)}$$

in which d_{HH} is the membrane thickness and V(x) follows from **equation 5.2**. (Note that, d_{HH} values were directly obtained by the fits which will be described in detail in the following subsection (**section 5.2.3**)). In brief, as shown in **Figure 5.1**, it is possible to extrapolate the specific areas of the flavonoids by applying a linear regression to the data of A(x) as a function of flavonoid load (see **Table 5.4**). Note, the linear decencies of A(x) and V(x) assume that molecular interactions between flavonoids and phospholipids can be neglected. This is the case for relatively low concentrations, but above 6 mol% of tiliroside and rutin, and, 12 mol % of quercetin, phase separation of the membrane into flavonoid-rich and flavonoid-poor domains is likely to occur (this will be discussed in detail later in this chapter). Therefore, the effective molecular volume and hence area calculations were estimated up to the concentrations where no phase separation was observed. The estimated effective area for DOPC/flavonoid systems is given in **Table 5.4**.

Table 5.4 Estimated effective areas for flavonoid - DOPC systems.

Flavonoid concentration (mol%)	A_{eff} for DOPC/tiliroside (Å^2)	A_{eff} for DOPC/quercetin (Å^2)	A_{eff} for DOPC/rutin (Å^2)
0 (pure DOPC)	72.1 ± 2	72.1 ± 2	72.1 ± 2
1	71.7 ± 2	72.1 ± 2	71.6 ± 2
2	71.7 ± 2	72.2 ± 2	71.2 ± 2
6	71.9 ± 2	70.1 ± 2	70.7 ± 2
12	-	68 ± 2	-
100	64 ±10	26±8	51±9

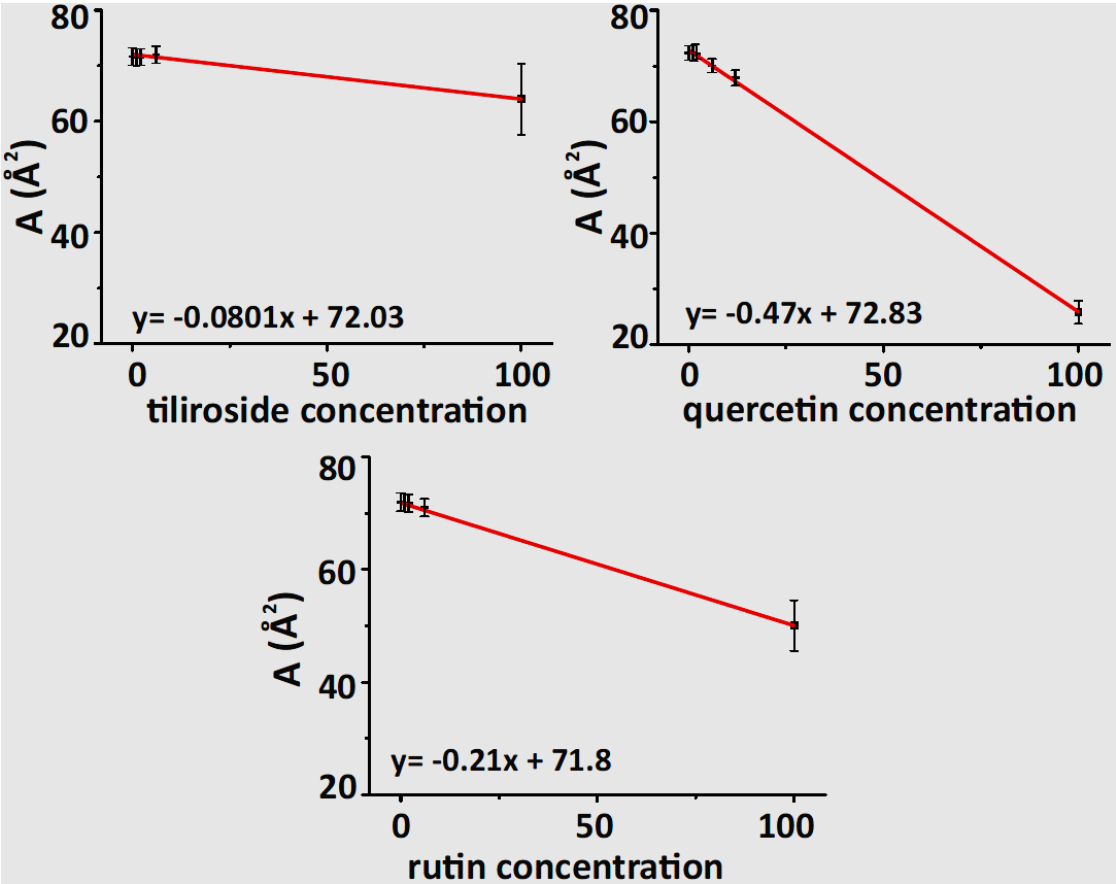

Figure 5.1 Effective area as a function of flavonoid concentration.

As also given in **Table 5.4**, the areas for tiliroside, quercetin and rutin were estimated as 64 Å^2, 26 Å^2 and 51 Å^2, respectively. In comparison, Edholm *et al*. calculated the partitioned areas for cholesterol from the mixtures of cholesterol and DPPC bilayer and they determined the area for cholesterol as 27 Å^2 (207). We will discuss these findings in more detail later in this chapter and attempt to analyse their relevance to the flavonoid localisation within the biomimetic membrane.

5.2.2 The temperature dependence of DOPC MLVs

5.2.2.1 Temperature dependence of membrane fluctuations (η)

Structural features of fully hydrated DOPC MLVs (10 wt%) were studied in the temperature range T=15-65 ^{o}C, and the typical scattering patterns for DOPC were recorded as shown in **Figure 5.2**. All SAXS patterns were globally fitted allowing the extraction of structural parameters (136, 137).

Increasing temperature leads to an increase in molecular motion. As a result, membrane fluidity enhances and individual molecules in the bilayer diffuse more easily (76). High-temperature results in smearing out of the third-order Bragg peak. As presented in **Figure 5.2**, the effect of high temperature and increased fluctuations can be clearly observed from the loss of quasi-long-range order in the scattering patterns**.**

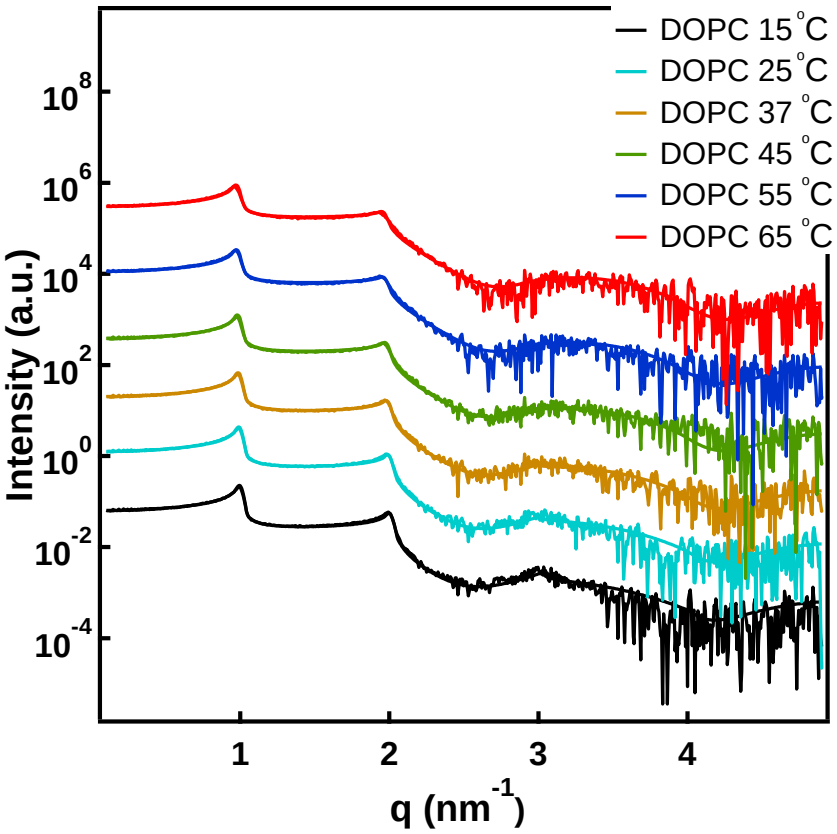

Figure 5.2 Background subtracted SAXS data and corresponding fitted curves (solid lines) for DOPC MLVs at different temperatures.

As detailed in Chapter 2, the term membrane fluctuations is a combination of both stacking disorder and bending undulations, and the best characterization of fluid phase bilayers has been described by Caillé theory. The Caillé parameter, η, translates into the root mean square fluctuations (σ) in the water spacing (aqueous region) between bilayers, by the relation

$$\boldsymbol{\sigma = \sqrt{\eta}\frac{d}{\pi}} \qquad \textbf{(5.4)}$$

The plot in **Figure 5.3** shows the mean fluctuation of intermembrane distances (σ) for pure DOPC MLVs as a function of temperature (15–65 °C). The quantitative values for σ were also listed in **Table 5.5.** As seen, these fluctuations monotonously increase with temperature from σ= 5.24 Å at 15 °C, to σ= 7.11 Å at 65 °C.

Increased bilayer fluctuations with temperature have also been reported for other fully hydrated vesicles comprising 1,2-Dimyristoyl-sn-glycero-3-phosphorylcholine (DMPC) (208), and 1-palmitoyl-2-oleoyl-sn-glycero-3-phosphocholine (POPC) (209, 210). It has been stated that an increase in bilayer fluctuations is mainly governed by a progressive decrease of the bilayer bending rigidity modulus, *K*c (206, 210). These reports suggested that the bending rigidity modulus, *K*c, for DOPC decreased with an increase in temperature.

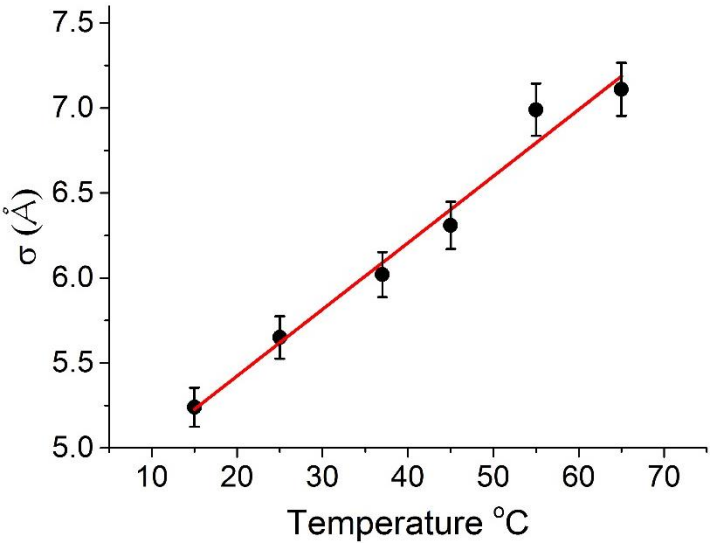

Figure 5.3 Mean fluctuation of inter-membrane distance, σ, in the 15°-65 °C temperature range.

5.2.2.2 Temperature dependence of membrane thickness (d_{HH})

Figure 5.4 shows the resulting electron density profiles (EDPs) of DOPC MLVs as a function of temperature. The distance between the head group peaks as reflected in the electron density profile decreases as the temperature increases, i.e. the DOPC bilayer becomes thinner. The reduction in the membrane thickness on heating is also consistent with other phospholipid studies (144). Such trend is readily understood as more and more *trans-to-gauche* conformations are induced to the system as the temperature rises, which in turn leads to a shortening of the lipid chains (211).

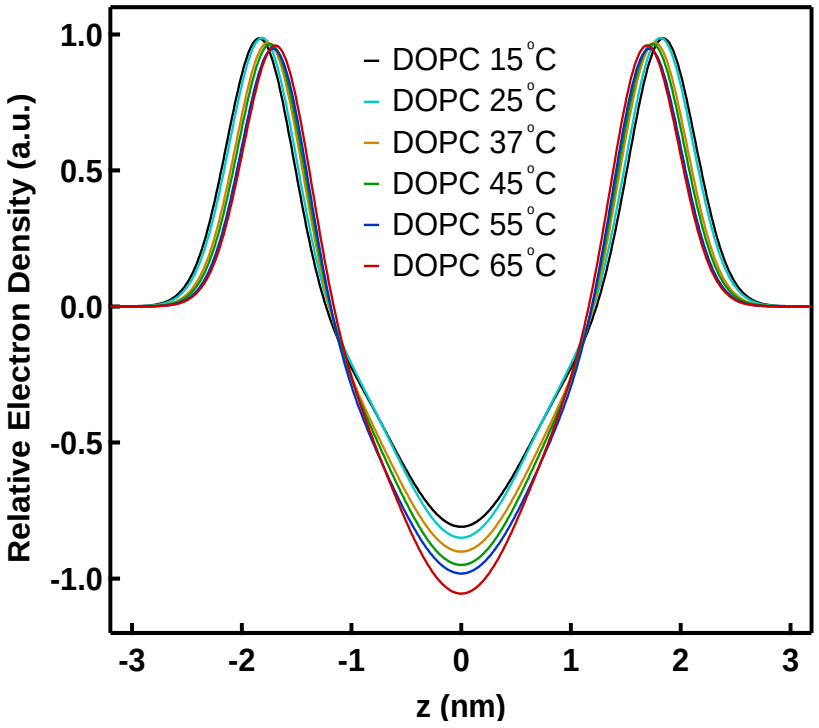

Figure 5.4 Electron density profiles of DOPC MLVs as a function of temperature.

Membrane thickness alterations along with other structural parameters as a function of temperature are demonstrated in **Figure 5.5**. As seen, an almost linear decrease in membrane thickness is observed upon heating.

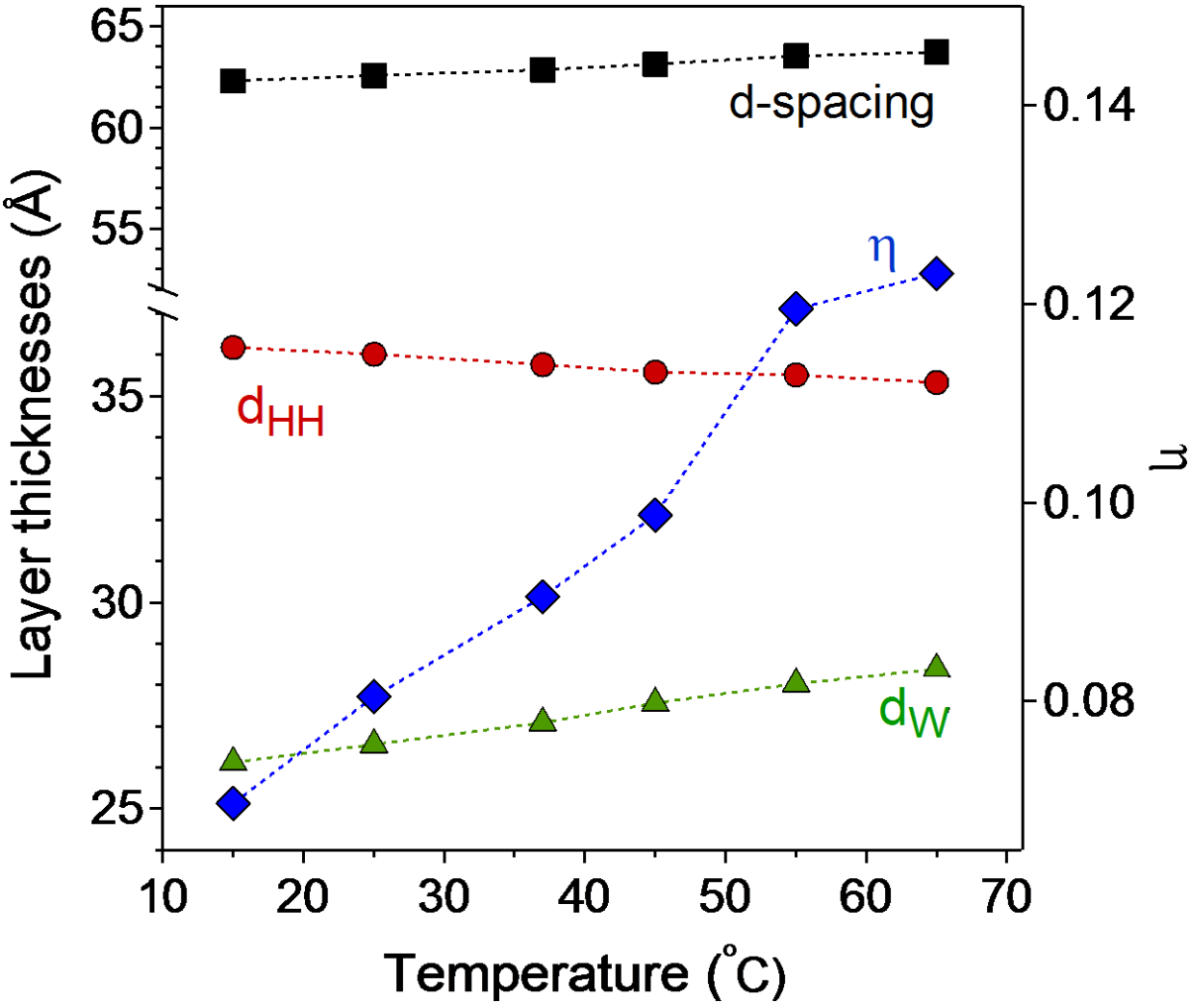

Figure 5.5 Membrane parameters, *d*-spacing (black dotted line), d_{HH} (head-to head group distance) (red dotted line), d_W (water layer thickness) (green dottet line), and η (bending fluctuation) (blue dottet line) as a function of temperature in PBS, at pH 7.0 (Note, that $d = d_{HH} + d_W$, without headgroup extension, d_H).

Along with the reduction of membrane thickness, a progressive increase in temperature leads to an increase in the volume occupied by the acyl chains due to their augmenting conformational disorder. Consequently also the lateral area per lipid increases. For example, Pan *et al*. reported the area for DOPC as 69.1 Å^2 and 75.5 Å^2, at the temperatures of 15 °C and

45 ^{o}C, respectively (206). A schematic description of the bilayer and water layer thicknesses upon heating and cooling is given in **Figure 5.6**.

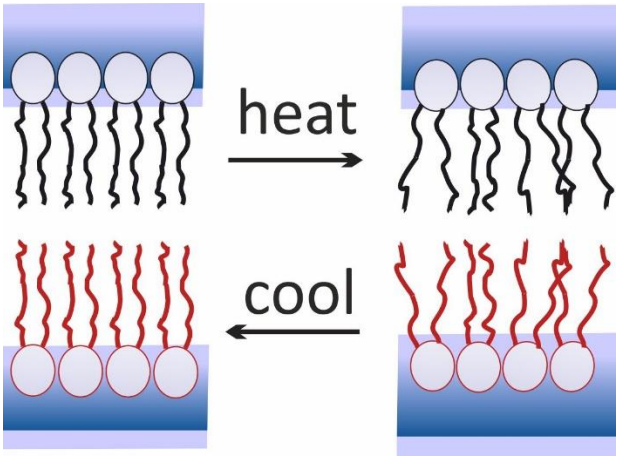

Figure 5.6 Schematic description of bilayer and water layer thicknesses upon heating and cooling.

In summary, temperature increase results in more flexible membrane due to the more trans-to-gauche conformations induced that means whole membrane becomes thinner and more flexible (76).

5.2.2.3 Lamellar repeat unit (d-spacing) and water layer thickness (d_W)

The lamellar repeat spacing of a multi-bilayer system, *d,* and its alterations is always a combined effect of the changes in membrane thickness and inter-bilayer water layer thickness. As shown previously in **Figure 5.5**, the *d*-spacing increases almost linearly as the temperature rises. This increase, despite a continuous decrease in membrane thickness, is explained by the dominating effect with the uptake of water (212). Undulating bilayers experience an effective entropic force (213), causing the bilayers to repel each other, resulting in the uptake of water and an increase in *d*-spacing.

Temperature dependence of bilayer interactions in DOPC MLVs has been well-documented (206, 208, 214). The only long-range inter-bilayer interactions are described as the attractive

van der Waals forces and steric repulsive forces arising from thermal fluctuations. As described previously, the bending modulus, *Kc*, decreases as the temperature increases, which leads to an increase in overall membrane fluctuations. The increased fluctuations, in turn, give rise to the repulsive forces between adjacent bilayers to be more dominant forces than the attractive van der Waals forces. This results consequently in an increase in the inter-bilayer water spacing between bilayers.

The alterations in *d*-spacing have also been reported for other phospholipid vesicles. In the same temperature range (15-65 ^{o}C), the phospholipid POPC displays a dip in *d*-spacing at lower temperatures, followed by an increase on further heating (132). The different behaviour between DOPC and POPC can be explained due to the significant differences in the main transition temperature (T_m) of both phospholipids. Unlike POPC ($T_{m\ POPC}$ = -2 ^{o}C), DOPC in the 15^{o} - 65 ^{o}C temperature range is already way above the main transition temperature which is near -17 ^{o}C. ($T_{m\ DOPC}$ = -17 ^{o}C).

Table 5.5 Structural data of fully hydrated lipid bilayers of DOPC.

Temperature	15 ^{o}C	25 ^{o}C	37 ^{o}C	45 ^{o}C	55 ^{o}C	65 ^{o}C
d (Å)	62.3	62.6	62.9	63.2	63.5	63.7
d_{HH} (Å)	36.2	36	35.8	35.6	35.2	34.8
d_w (Å)	26.1	26.6	27.1	27.6	28.9	28.9
η	0.07	0.08	0.09	0.098	0.12	0.12
σ (Å)	5.2	5.6	6	6.3	7.0	7.1

5.2.3 Interactions of DOPC MLVs with flavonoids

The influence of quercetin, rutin, and tiliroside on the structural properties of DOPC vesicles, such as membrane thickness, water layer thickness, and membrane fluctuations have been recorded via SAXS as a function of temperature and flavonoid concentration. To help the

clarity of the presentation, membrane behaviour of each flavonoid will be presented in separate subsections.

5.2.3.1 Behaviour of DOPC-quercetin vesicles

Figure 5.7 presents the scattering curves of DOPC MLVs in the absence (black colour) and the presence of quercetin (coloured lines) at different concentrations. Best fits to the data are given by solid lines.

DOPC MLVs were loaded with a broad range of quercetin concentration: from 1 mol% up to 24 mol%. As seen in **Figure 5.7**, the typical scattering pattern of DOPC was preserved with quercetin up to 12 mol%. Upon increasing the quercetin content up to 24 mol%, an additional scattering contribution at low q values is observed. This scattering contribution most probably accounts for an exceeded solubility of quercetin, since insolubilised quercetin crystals would scatter at low q. In order to exclude any misinterpretations due to this solubility limit, the structural analysis of quercetin by SAXS will be restricted to 12 mol% concentration.

Figure 5.8 displays the EDPs of DOPC MLVs with and without quercetin and **Figure 5.9** demonstrates the influence of quercetin on the structural parameters, extracted from EDPs by global analysis fits. The effect of quercetin on each structural parameter intensified as a function of increased concentration and temperature. The behaviour of quercetin is quite straightforward to explain. In general, the lattice spacing, *d*, fluctuates and it does not change significantly by the addition of quercetin (less than 1% variation). However, a closer look at the membrane thickness, $d_{HH,}$ reveals that quercetin leads to a membrane thinning effect in a concentration and temperature dependent manner (**Figure 5.9**, third panel from top). As in the case of quercetin, a decrease in membrane thickness is usually accompanied by an increase in the water layer thickness, *d*w, and a concomitant increase also in the fluctuation

parameter, σ (215). **Table 5.6** gives the quantitative values for quercetin concentration dependence of the membrane thickness, d_{HH}, water layer thickness d_W, lamellar repeat, d, membrane fluidity, η, and fluctuation parameter, σ.

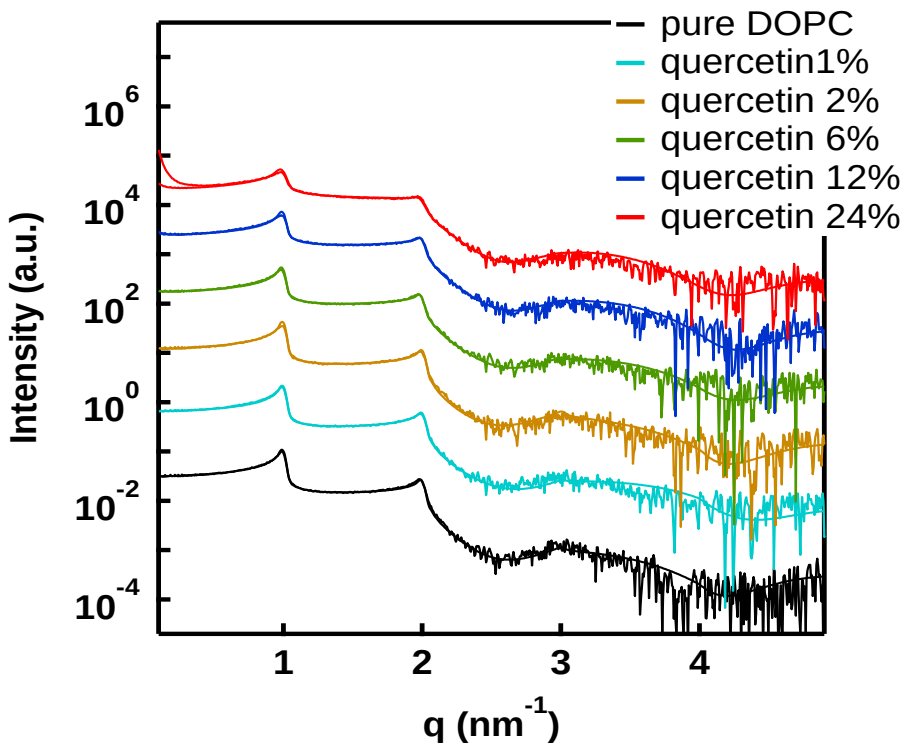

Figure 5.7 Background subtracted SAXS data, and corresponding fitted curves (solid lines) for pure DOPC MLVs (black line) and quercetin-loaded MLVs at different concentrations (coloured lines), recorded at 25 °C in PBS (pH 7.0).

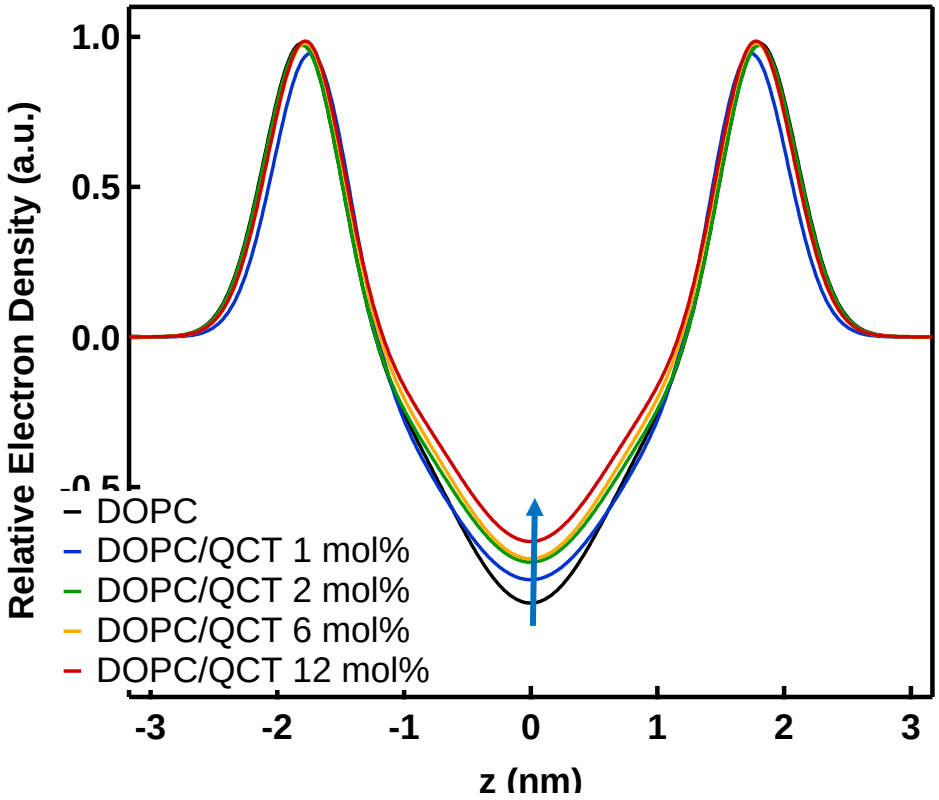

Figure 5.8 Electron density profiles of pure DOPC MLVs (black line), DOPC with 1 mol% of quercetin (blue line), DOPC with 2 mol% (green line), DOPC with 6 mol% (yellow line) and DOPC with 12 mol% (red line), recorded at 25 ^{o}C in PBS at pH 7.0.

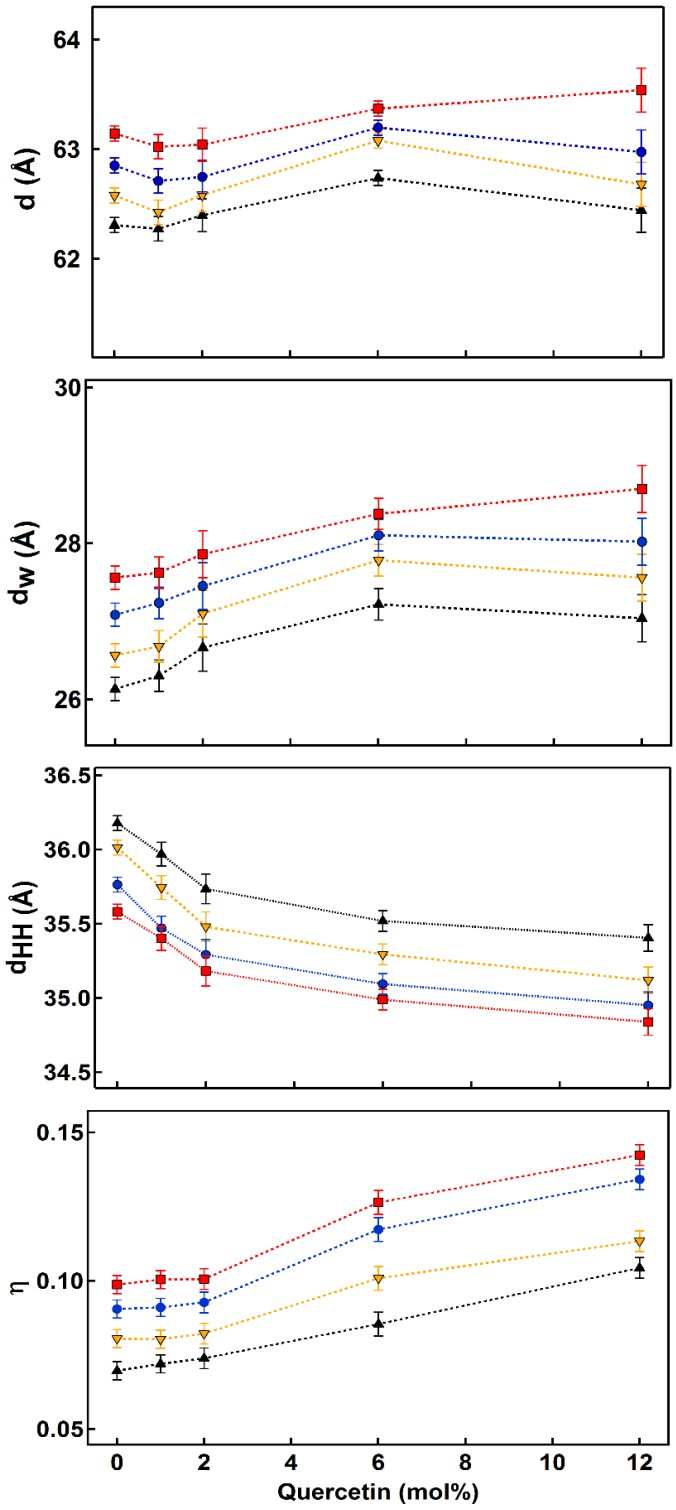

Figure 5.9 Membrane parameters, d, d_{HH}, d_W and η as a function of temperature and quercetin concentration. Black, yellow, blue and red lines are temperature lines at 15, 25, 37 and 45 ^{o}C, respectively.

Table 5.6 Structural parameters of DOPC MLVs in the presence of quercetin at 25 ^{o}C mention in the context

	DOPC_25 ^{O}C	DOPC_1mol% Quercetin	DOPC_2mol% Quercetin	DOPC_6mol% Quercetin	DOPC_12mol% Quercetin
d (Å)	62.6 ± 0.1	62.4 ± 0.1	62.4 ± 0.1	62.8 ± 0.1	62.7 ± 0.1
d_{HH} (Å)	36 ± 0.7	35.7 ± 0.7	35.4 ± 0.7	35.3 ± 0.7	34.6 ± 0.7
d_w (Å)	26.5 ± 0.7	26.7 ± 0.7	27.1 ± 0.7	27.5 ± 0.7	28.1 ± 0.7
η	0.08 ± 0.1	0.08 ± 0.1	0.085 ± 0.1	0.1 ± 0.1	0.11 ± 0.1
σ (Å)	5.6 ± 0.9	5.6 ± 0.9	5.7 ± 0.9	6.3 ± 0.9	6.7 ± 0.9

5.2.3.2 Behaviour of DOPC-rutin vesicles

Figure 5.10 presents the scattering curves of both pure DOPC (black colour) and rutin loaded DOPC MLVs (coloured lines) at varying concentrations. Best fits to the data are given by solid lines.

As seen in **Figure 5.10**, perfect incorporation of rutin within DOPC MLVs is observed up to 6 mol%. Further increase of the rutin content up to 12 and 24 mol% displays additional scattering contributions at low q, which is similar to the influence exerted by quercetin on the scattering pattern at 24 mol%. As mentioned previously in explaining the quercetin results, such additional, diffuse scattering strongly suggest that rutin has reached to its solubility limit. Therefore, in order to prevent any misinterpretations that might arise from coexisting rutin crystals, the effect of rutin on the structural parameters will be discussed only up to 6 mol%.

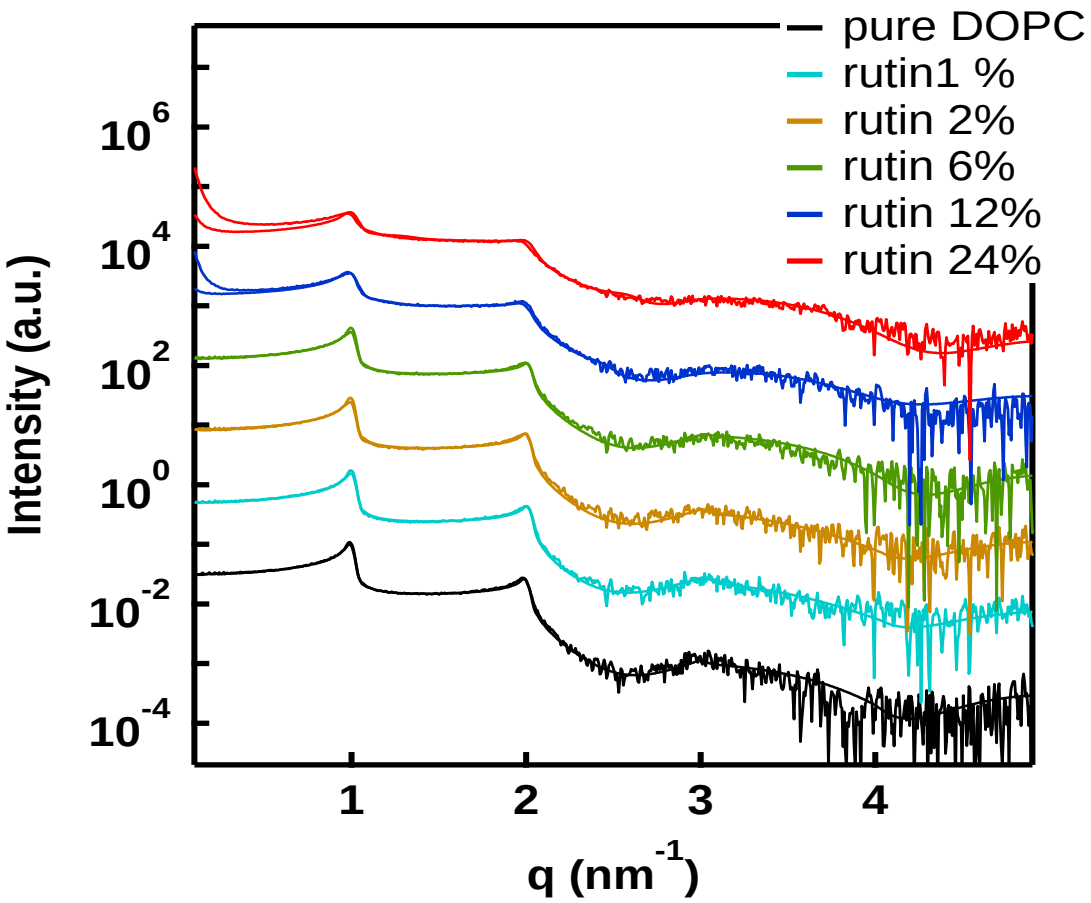

Figure 5.10 Background subtracted SAXS data and corresponding fitted curves (solid lines). Black line is for pure DOPC, cyan line is DOPC with 1 mol% of rutin, brown line is DOPC with 2 mol% of rutin, green line is DOPC with 6 mol% of rutin, blue line is DOPC with 12 mol% of rutin, and red line is DOPC with 24 mol% of rutin recorded at 25 ^{o}C in PBS at pH 7.0.

Structural parameters of pure and rutin-loaded vesicles are displayed in **Figure 5.11.** Rutin did not create significant alterations on the structural parameters even at the concentration of 6 mol%. Although at first sight, the presence of 1 mol% rutin seems to very slightly rigidify the membrane, followed by an opposite fluidising effect at increased concentrations, rutin-induced alterations are very weak compared to quercetin, i.e. typically less than 1 Å, in general.

When looking at the overall membrane behaviour under the influence of rutin, it can be concluded that rutin leads to only a small decrease in membrane thickness accompanied by and a slight enhancement in membrane fluctuations.

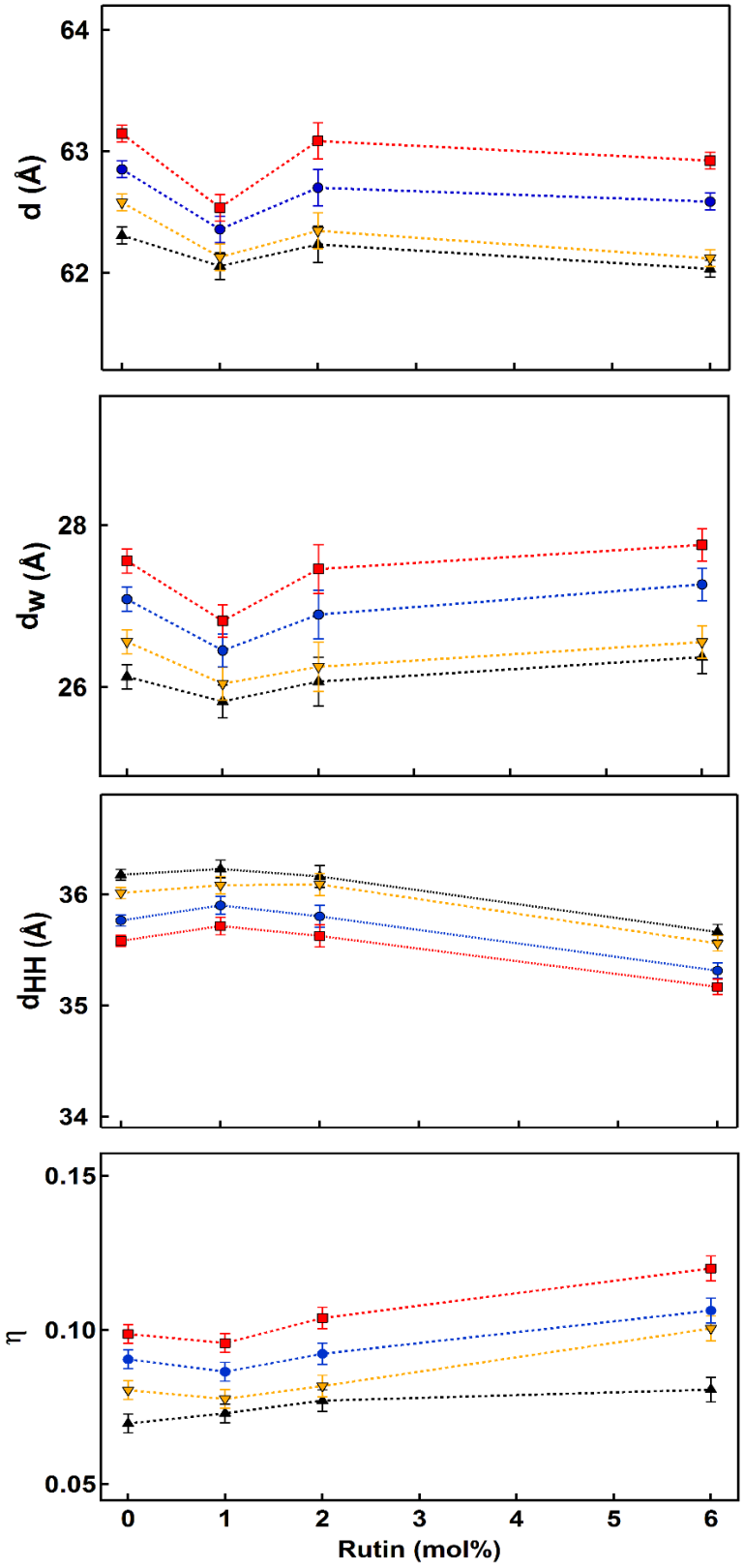

Figure 5.11 Membrane parameters, d, d_{HH}, d_W, and η as a function of temperature and rutin concentration. Black, yellow, blue and red lines are temperature lines at 15, 25, 37 and 45 ^{o}C, respectively.

5.2.3.3 Behaviour of DOPC-tiliroside vesicles

Figure 5.12 presents the scattering curves of DOPC MLVs in the absence (black colour) and the presence of tiliroside (coloured lines) at varying concentrations. Best fits to the data are given by solid lines.

Similar to rutin, tiliroside was also able to incorporate within DOPC MLVs up to 6 mol %. Further increase of tiliroside content within vesicles resulted in additional peaks to occur that can be clearly seen in **Figure 5.12**, from the scattering curve at 24 mol%. At this concentration, besides an enhanced scattering observed at low q, an additional diffraction peak (circled in pink) appeared at q = 4.3 nm^{-1}. Although this additional peak is not clearly visible with 12 mol%, tiliroside still exhibited a complex behaviour at this concentration which will be discussed further in this chapter. Unlike quercetin and rutin, we have investigated tiliroside behaviour in a broader range of concentrations, but for the clarity of the discussion, the analysed data up to and above 6 mol% will be presented separately.

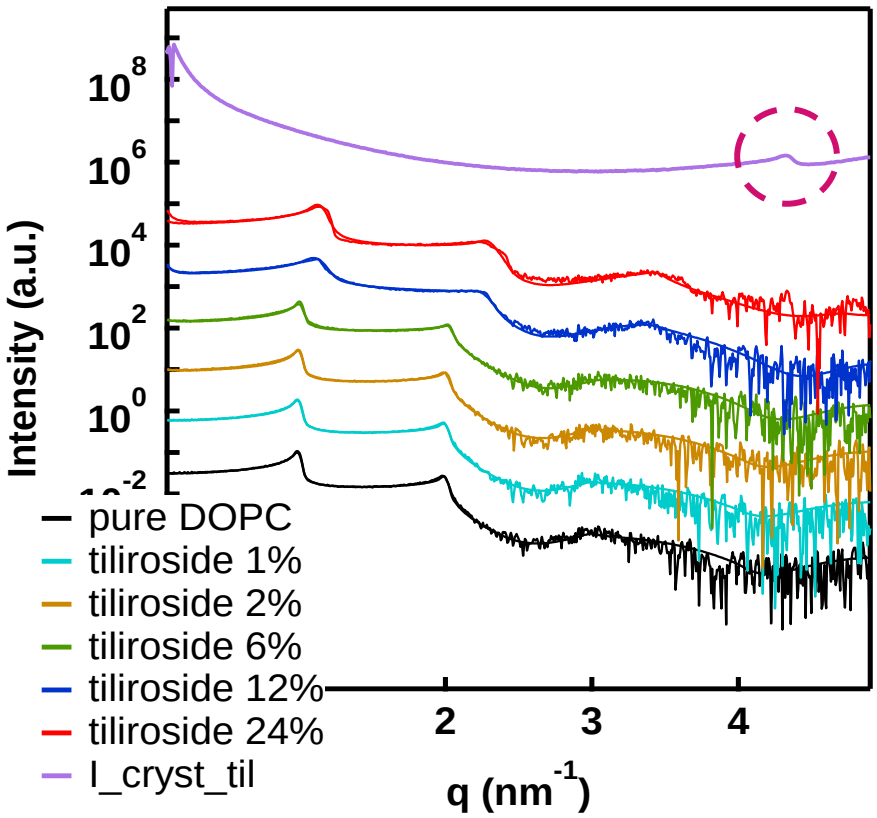

Figure 5.12 Background subtracted SAXS data and corresponding fitted curves (solid lines). Pure DOPC (black), DOPC with 1 mol% of tiliroside (cyan), DOPC with 2 mol% of tiliroside brown), DOPC with 6 mol% of tiliroside (green), DOPC with 12 mol% of tiliroside (blue) and DOPC with 24 mol% of tiliroside (red) were recorded at 25 °C in PBS buffer at pH 7.0. The scattering pattern of pure tiliroside crystal powder is presented on top.

The influence of tiliroside (up to 6 mol %) on the structural properties of DOPC was demonstrated as a function of temperature in **Figure 5.13.** It can be clearly seen that tiliroside`s incorporation into DOPC vesicles exhibits a similar trend to that of quercetin and rutin with a decrease in membrane thickness along with an increase in membrane fluctuations.

Here it should also be mentioned that tiliroside at 6 mol% exerts a more pronounced response than the other flavonoids studied. For example, tiliroside fluidised the membrane most at this

concentration with an increase in the bending fluctuation to ~ 0.11 compared to pure DOPC (~ 0.08), and DOPC-quercetin system (~ 0.1) at 25 °C. Similarly, the overall membrane thinning with tiliroside was slightly more pronounced than quercetin. d_{HH} values of pure DOPC, DOPC-tiliroside, DOPC- quercetin and DOPC-rutin are as follows: 36.01 Å, 34.95 Å, 35.3 Å, and, 35.6, respectively.

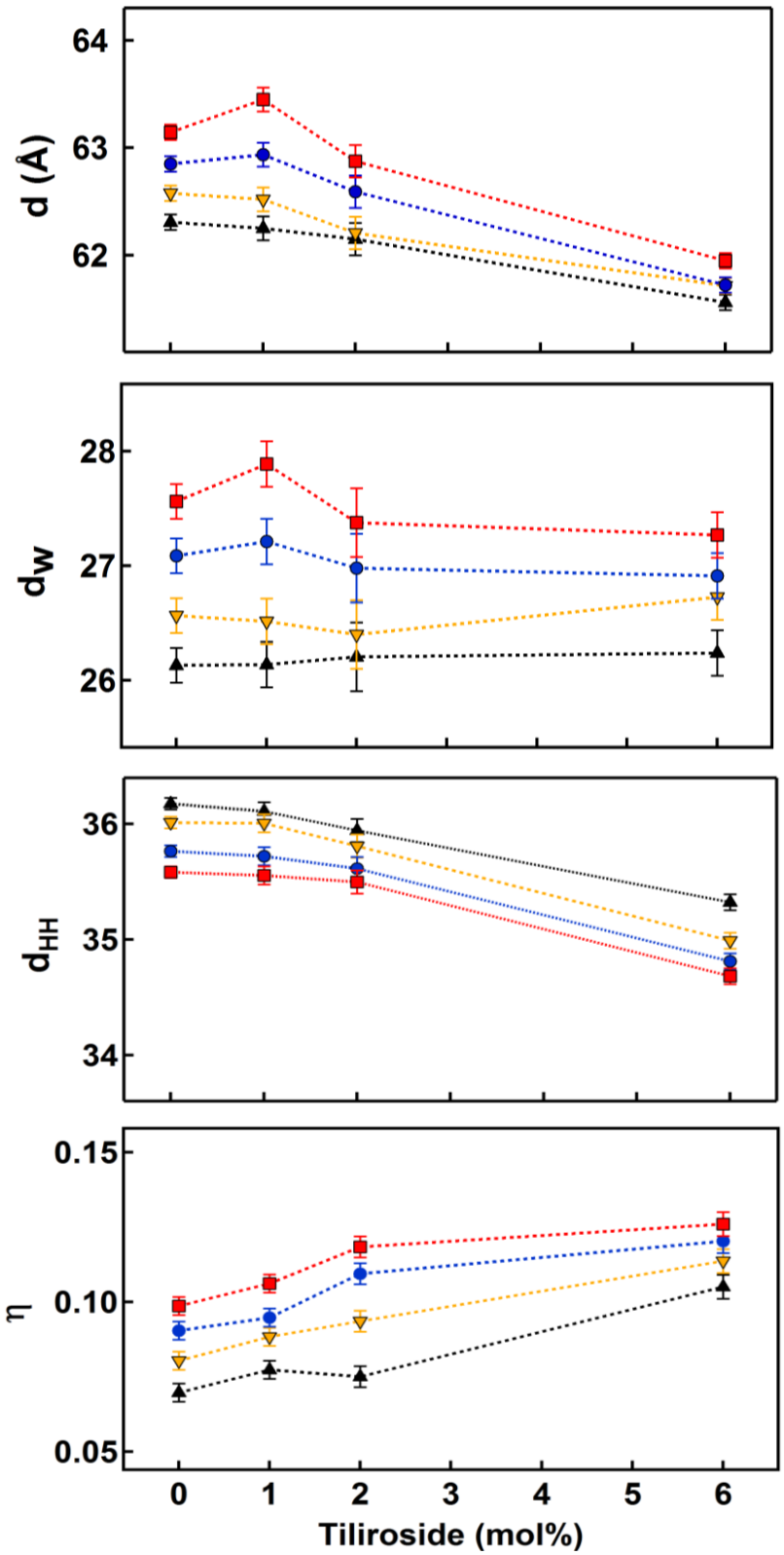

Figure 5.13 Membrane parameters, d, d_{HH}, d_W, and η as a function of temperature and tiliroside concentration. Black, yellow, blue and red lines refer to different experiments conducted at 15, 25, 37 and 45 ^{o}C, respectively.

At higher concentrations (> 6 mol%) two sets of diffraction peaks with lamellar repeat were observed, meaning that a phase separation has taken place. It also means that each of the separated lamellar phases is in the registry in the radial direction of the multilamellar vesicles. It is tempting to explain this phase separation by the formation of tiliroside rich and tiliroside poor regions. Furthermore, as stated beforehand, even a third phase was observed at the highest tiliroside concentration, i.e. a single diffraction peak at q = 4.3 nm^{-1} that stems from pure tiliroside crystals (see for comparison the scattering of pure tiliroside powder in the top of **Figure 5.12**).

A detailed data analysis has been conducted to understand the phase separation where a high concentration of tiliroside may in extreme cases lead to its crystallisation. Therefore, we decided that it was worth looking at the data obtained from the 24 mol% concentration**.** **Figure 5.14** presents the effect created by tiliroside (24 mol%) on the structural parameters of DOPC vesicles. As seen in this figure, the lamellar repeat distance decreases in both phases, with a more pronounced decrease in phase II. Also, water layer thickness decreases despite a continues, extreme thinning of the membrane thickness, d_{HH}, from 36.0 Å to 29.4 Å at 25 ^{o}C. At first instance, this trend seemed unusual since water layer thickness is usually expected to increase accompanied by a decrease in membrane thickness such as in the case of quercetin and rutin. Such behaviour might be explained by induced partial interdigitation. Importantly, this membrane thinning does not necessarily mean that the membrane becomes more fluid (an increase of chain disorder), but on the contrary partial interdigitation may lead to a reduction in chain disorder (due to increased inter-chain van der Waals interaction) (216); and hence become more rigid instead. That would go hand in hand with an even lower water layer thickness (d_W) caused by a reduction in membrane undulations (reduction of repulsive forces).

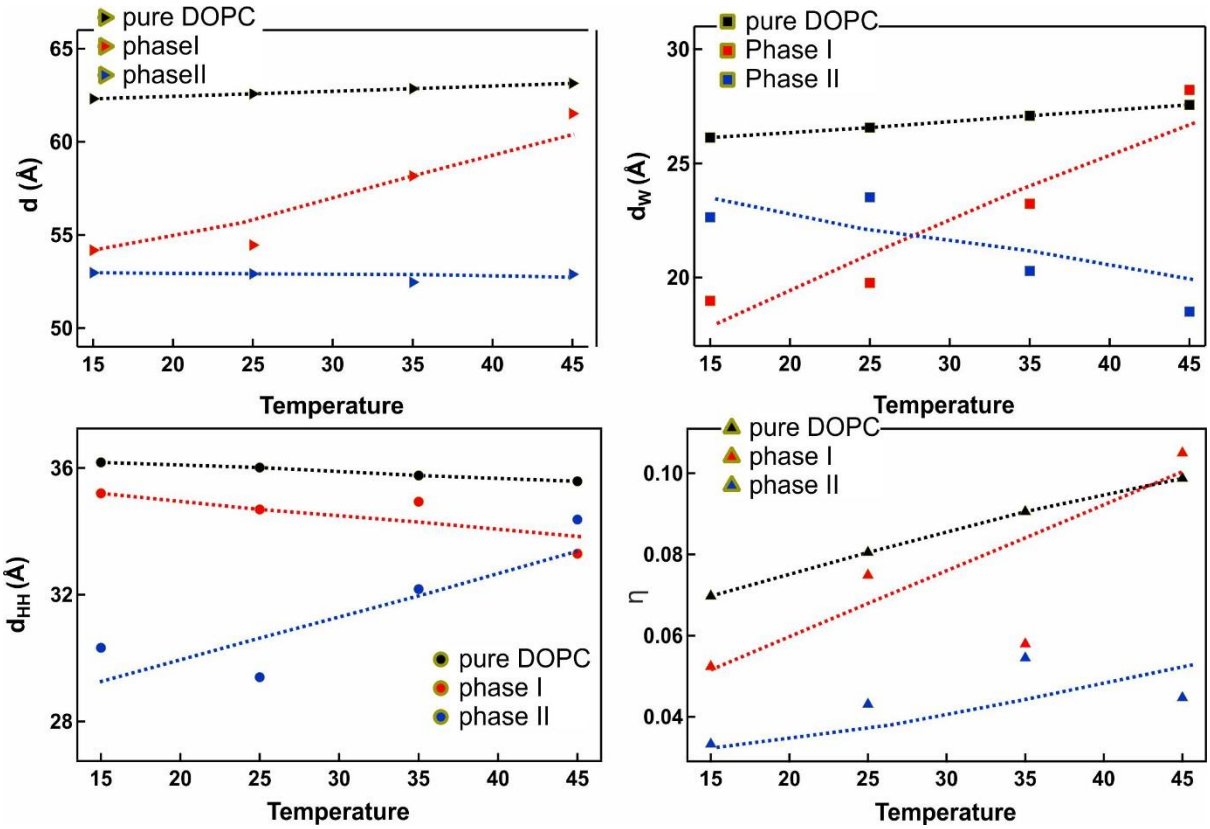

Figure 5.14 Membrane phase separation with tiliroside at the concentration of 24 mol %, phase I and phase II indicate tiliroside poor and tiliroside rich regions, respectively. Note, the dashed lines are inserted to guide the eye.

A thorough scan of the existing literature has been done to understand the partial interdigitation of DOPC bilayer with tiliroside, where the flavonoid content is high enough to cause phase separation. Partial interdigitation of lipid bilayers was studied in great detail by Mavromoustakos and co-workers (217, 218). The authors argued that such effect can occur in the fluid phase. Moreover, they classified the characteristic properties of bioactive molecules that possibly cause such interdigitation upon their incorporation into lipid bilayers. Their findings indicate that the molecules that are (i) amphiphilic; (ii) preferably bulky (occupying similar lateral areas as the membrane lipids); (iii) interface active and (iv) not very long are likely to cause the greatest effect in partial interdigitation when incorporated into

bilayer vesicles. Remarkably, tiliroside meets all these characteristics reported in the literature to trigger partial interdigitation. Furthermore, molecules that cause such effect were reported to prefer to localise at the apolar/polar interface region of the membranes, such as in the case of vinca alkaloids: vinblastine and vincristine (219). The reason for partial interdigitation is in turn believed to arise from the shorter molecular length of the membrane interacting molecules – as compared to the length of the lipids – leading to void-like formations in their monolayer leaflet that are then subsequently occupied by lipids of the opposite leaflet (see **Figure 5.15**). These conclusions were further supported by comparative studies using anaesthetic steroids that mainly influenced the alkyl chain region of the membrane without causing any interdigitation effect in the bilayers (220).

A realistic membrane model for tiliroside induced partial interdigitation is proposed in **Figure 5.15**. As seen, the interdigitation effect is expected to be biggest, if the partial lateral areas of tiliroside are comparable to those of DOPC. Based on the estimated molecular areas for DOPC and tiliroside (A_{DOPC} = 72.1 Å^2 and $A_{tiliroside}$ = 64 Å^2) reported in **section 5.2.1**, it can be seen that the area for DOPC and tiliroside are quite close to each other. Hence, a nearly perfect area match is likely to occur between the phospholipid DOPC and tiliroside.

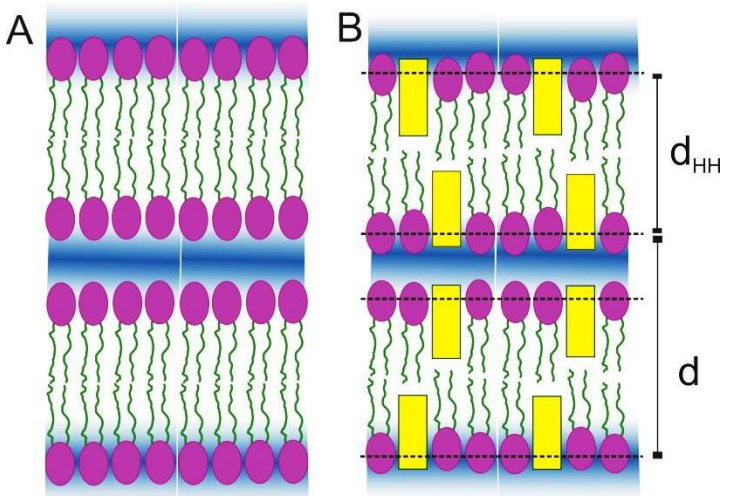

Figure 5.15 Schematic illustration of DOPC bilayer structure alterations induced by tiliroside. Pure DOPC bilayers at 25 °C **(A)**. The incorporation of 24 mol% tiliroside (yellow rectangles) induces the formation of tiliroside-rich domains (phase II) with chain interdigitation **(B)**. For values of d and d_{HH} please see Figure 5.14.

Another indicator for partial interdigitation could be the parameter σ_C (standard deviation of the methyl trough region) (218). As mentioned in **chapter 2**, σ_C describes the width of the hydrophobic region of the lipid bilayers, and it shows how pronounced the central trough region for the methyl terminals is (214). Indeed, partial interdigitation is expected to reduce the sharpness of the methyl trough region in the EDP (increase in σ_C), since the methyl groups are not clearly separated anymore by the two opposite monolayer leaflets. The quantitative σ_C values for pure DOPC together with phase I and phase II at 25 °C are given in **Figure 5.16**, respectively. Note that, the phase separation, in general, was found to be favoured by an increase in the temperature.

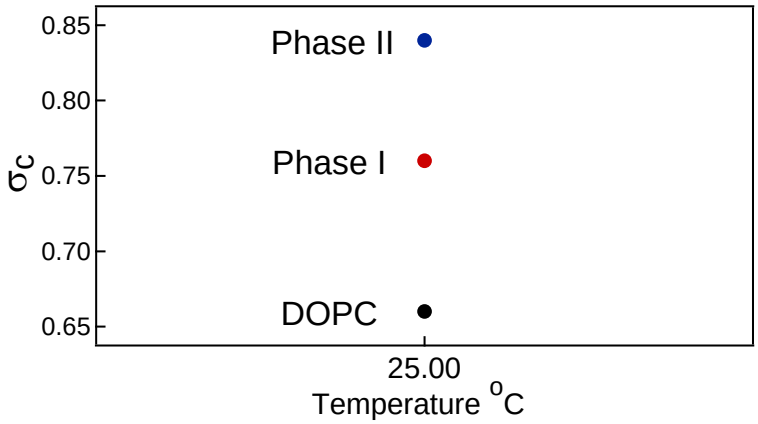

Figure 5.16 Methyl trough region alterations with flavonoids (for details see main text).

All these findings presented above can be discussed in the concept of (i) membrane thickness, and (ii) membrane fluidity alterations with flavonoids, and (iii) their localisation within the membrane.

To start with membrane thickness alterations; numerous experiments with model biomembranes confirm that flavonoid insertion into a lipid bilayer modifies membrane thickness (33, 156, 221). To the best of our knowledge, Raghunathan and co-workers, for the first time, used SAXS technique to record the changes in membrane thickness with two isoflavonoids; genistein and daidzein (45). Both flavonoids reduced the membrane thickness which is also in very good agreement with the current findings using different flavonoids.

Another work – a molecular dynamic simulation study- reported surface deformations in the DOPC bilayers induced by quercetin (33). Such deformations on the membrane surface caused the creation of small cavities with water molecules where quercetin molecules were positioned. The formation of these cavities was linked to a decrease in the membrane thickness (33).

A membrane thinning effect by the different group of flavonoids - green tea catechins - was also reported (222, 223). Sun *et al*. conducted an extensive study to understand the effect of catechin (-)- Epigallocatechin gallate (EGCg) on giant unilamellar vesicles (GUVs) using three different lipids; DOPC, POPC and Egg lecithin (EggPC) (222). Membrane thickness alterations were measured via X-ray diffraction as a function of EGCg/lipid content, and EGCg was found to thin the membrane for each model system studied. The same group also reported a similar membrane-thinning effect of DOPC bilayer with curcumin, a type of polyphenol (see the **Figure 5.17** for its chemical structure) using (46).

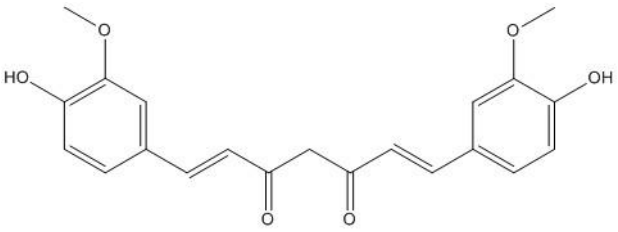

Figure 5.17 The structure of curcumin.

The membrane thickness alterations indicated above were associated with the ion channel activity, i.e. both theoretical and experimental studies showed that gramicidin lifetime might be sensitive to the lipid bilayer thickness (46, 224, 225). A possible mechanism underlying this relationship was explained with hydrophobic matching between the gramicidin channel and the lipid bilayer (225). Harroun *et al*. stated that when a protein is embedded within a lipid membrane, hydrocarbon thickness of the membrane surrounding the protein is adjusted to match the length of the hydrophobic surface of the protein. In the case of a hydrophobic mismatch between the channel and the surrounding membrane at unperturbed state, local deformations occur in the membrane according to the elasticity theory because membranes are reported to be 400 times more deformable than proteins (225).

Due to the possible association between the ion channel activity and membrane thickness, it might be therefore speculated that the molecules that can alter membrane thickness, might also influence the ion channel activity. Raghunathan *et al*. tested this hypothesis with the flavonoids daidzein and genistein and demonstrated an increase in the lifetime of gramicidin A (gA) channel (45). The authors proposed two possible mechanisms to describe the increased gA channel lifetimes induced by flavonoids. The first mechanism was linked to the ability of flavonoids to reduce the energy of hydrophobic mismatch between the gA channel and the lipid bilayer by reducing the bending modulus, *K*c. This, in turn, indicates a softer and hence more easily deformable bilayer. The second mechanism was explained with reduced bilayer thickness with flavonoids. Both daidzein and genistein thinned the bilayer, and this helped to increase the attractive interactions between gA dimers and the flavonoids which resulted in more stable interactions between gA dimers and the flavonoids and hence less likely breakage into gA monomers. This, in turn, increases the lifetimes of the channel (45).

Curcumin has also been proposed to be an ion channel modifier because of its ability to alter the lipid membrane and hence modify the lipid membrane environment that surrounds the channel (226). This molecule was considerably shown to increase the single-channel lifetime of gramicidin in DOPC bilayers without changing its single-channel conductance (226). Since there was no change in the single-channel conductance, the authors strongly suggested there was no direct interaction between curcumin and gramicidin. This study was later on pursued by a different group, Hung *et al*. under the same experimental conditions i.e. the same curcumin solution and the phospholipid, (DOPC) to gain a better understanding of the curcumin-induced ion channel mechanism (46). The authors reported a concentration-dependent, nonlinear membrane thinning along with a reduced elasticity moduli of the bilayers. These findings implied that the consequences of membrane thinning and bilayer

softening might both play a role in increased lifetime of the gramicidin channel (46). They also noted that when a membrane gets thicker, the bilayer is locally deformed which causes a pulling force. This then facilitates the channel dissociation, resulting in a shortened channel lifetime (46).

Although existing reports about the flavonoid effect on membrane thickness are limited, there is an accumulating information concerning the membrane fluidity changes with flavonoids. **Table 5.6** summarises the effect of a variety of flavonoids on the fluidity of membranes with different lipid compositions.

As can be seen from the table, the most widely used technique in studying membrane fluidity has been Electron Paramagnetic Resonance (EPR). Apart from EPR, the other techniques to probe the membrane fluidity were differential scanning calorimetry, fluorescence polarisation spectroscopy, and structural analysis techniques such as X-ray scattering.

The **Table 5.6** clearly presents that the findings in this context remain controversial. Some groups reported a rigidifying effect of membranes of fluid phase (Lα phase) with flavonoids. Arora`s study is one of the first studies that can be shown as an example finding a rigidifying of membranes with flavonoids (227). In that study, the influence of a number of flavonoids, including rutin and naringenin on the fluidity of membranes composed of 1-stearoyl-2-linoleoyl-sn-glycero-3-phosphocholine (SLPC) was measured via anisotropic fluorescent microscopy. Apart from a membrane rigidifying effect, the authors suggested a localisation of the flavonoids in the apolar core of the membranes (227). Similarly, following studies by Tedeschi *et al*. induced rigidification of GUVs made of DOPC with quercetin, rutin, naringenin and naringin at 20 mol% (108).

In contrast, some flavonoid studies reported an opposite effect -fluidising membranes - as in agreement with our findings. For instance, Raghunathan *et al*. revealed a softening effect with genistein and daidzein on DOPC bilayers using a combination of X-ray scattering and molecular dynamic simulations studies (45). Additionally, a flavanone aglycone naringenin has been shown to enhance near-surface erythrocyte membrane fluidity which was proposed as a favourable activity in the adjustment of hemodynamics in cardiovascular diseases (44).

Here it should be noted that some studies also reported a concentration-dependent biphasic effect with flavonoids (228, 229). (for a review see (230)). By literature findings, it can be seen that existing studies are not often conclusive yet, and sometimes even contradicting. The diverse findings and disagreements may originate from the different techniques employed, membrane composition used, and different flavonoid concentration used in the studies. For example, most of the DPPC based membrane models exhibit an increased fluidity upon introducing flavonoids, whereas a vast majority of DOPC based systems undergo higher rigidity. Here, it should also be noted that the same flavonoids behave differently at a different range of concentration as seen from **Table 5.16**. The information extracted from the table clearly shows that depend on lipid membrane composition, a general trend of flavonoids is to enhance membrane fluidity up to a certain flavonoid content, which is followed by a membrane rigidifying effect at higher concentration ranges (230).

The biphasic effect created with flavonoids can be compared to the influence of cholesterol on membrane lipids. Dose-response studies with cholesterol in the presence of an unsaturated phospholipid, POPC demonstrated that at low cholesterol concentrations of 1-5 mol % membrane fluidisation was induced (76). Whereas higher cholesterol content, i.e. greater 10 mol% is sufficient to induce a membrane rigidification, i.e. an additional liquid

ordered phase (Lo) forms (231). Similarly, it may turn out to be justified to think along the same lines also for the effect of flavonoids on membrane fluidity (230). Hence, flavonoids may have some sort of “regulatory role” on membrane fluidity just as cholesterol does (230). Depending on their concentration, flavonoids can either rigidify fluid-like membranes or fluidise membranes with more ordered structures. Current experiments at high flavonoid (tiliroside) content, have also demonstrated the formation of rigid domains with distinct structural properties evidencing the co-existence of flavonoid-rich and flavonoid-poor phases upon incorporation into DOPC vesicles. At high concentrations, the separation into larger, growing domains of flavonoid-rich and flavonoid-poor phases is likely to be driven by a reduction in the free energy of the system. As argued above, the hydrophobic mismatch between phase I and phase II has an energetic cost, i.e. the membranes in the boundary region of phase I and II have to deform in order to conserve the integrity of the membrane (hydrophobic moieties need to be screened from water).

Modification of membrane fluidity by flavonoids is particularly important because the changes in membrane fluidity - accompanied by a variation in membrane thickness and changes in the lateral pressure profile (76) – have been reported to accompany a number of disease processes. The mechanism of several therapeutic activities of flavonoids, for example, their antimicrobial activity is associated with membrane fluidity changes (232, 233). Literature studies report a considerably low fluidity of erythrocyte membrane in patients with essential hypertension compared to healthy controls have (44). It was proposed that elastic deformation of the erythrocyte membrane and, furthermore, hemodynamics are of crucial importance in cardiovascular risks. Ajdžanović *et al*. used naringenin to test the ability of this flavonoid to enhance the near surface fluidity of the erythrocyte membrane. The results showed that naringenin, at all the concentrations applied (0.1 and 1 μg/ml) enhanced the

near surface fluidity. The authors, therefore suggested that naringenin could be used as a potential therapeutic agent in treatment for hypertension and atherosclerosis diseases (44).

Finally, the results will be discussed in the concept of flavonoid localisation within the biomimetic membranes. Concerning the localisation of quercetin and tiliroside, we do have clear evidence for their membrane incorporation from both monolayer and SAXS experiments. Moreover, from the observed induction of increased membrane fluidity, we do know that these flavonoids at least partially reside in the lipid chain region.

Additional to volume/area estimations as explained previously, we further calculated the projected surface area of flavonoids using the software ACD/ChemSketch to propose a relatively realistic orientation of flavonoids within the membrane. For this, the area of flavonoids was calculated based on their three-dimensional (3D) structures at various orientations. The most likely and realistic orientations of three flavonoids within the membrane were selected and displayed in **Figure 5.19**. The surface area at the given orientations for quercetin (**Figure 5.19 (A)**), rutin (**Figure 5.19 (B)**), and tiliroside (**Figure 5.19 (C)**) were calculated as 32 $Å^2$ ± 6, 59 $Å^2$ ± 9 and 70 $Å^2$ ± 10 respectively. These software values match well with the estimated partial, lateral area of flavonoids as reported in the **section 5.2.1**. Based on these calculations, quercetin has an area of 32 $Å^2$ ± 6. However, Langmuir monolayer study by Ferreira *et al*. determined the area per quercetin molecule as A_{flav} = 89 $Å^2$ at π = 20 mN m^{-1} (192). (this study was discussed in detail in **section 4.2.4**). Although the two values seem to be contradicting to each other, this difference might arise from the orientation of quercetin molecule at two different interfaces: At A/W interface, the spread quercetin molecules might preferentially align in a way with the rings oriented perpendicular or parallel to the water surface. A parallel oriented quercetin molecule would have the largest

projected area. However, when incorporated into the membrane, occupied surface area by quercetin with respect to the plane of the interface might be different.

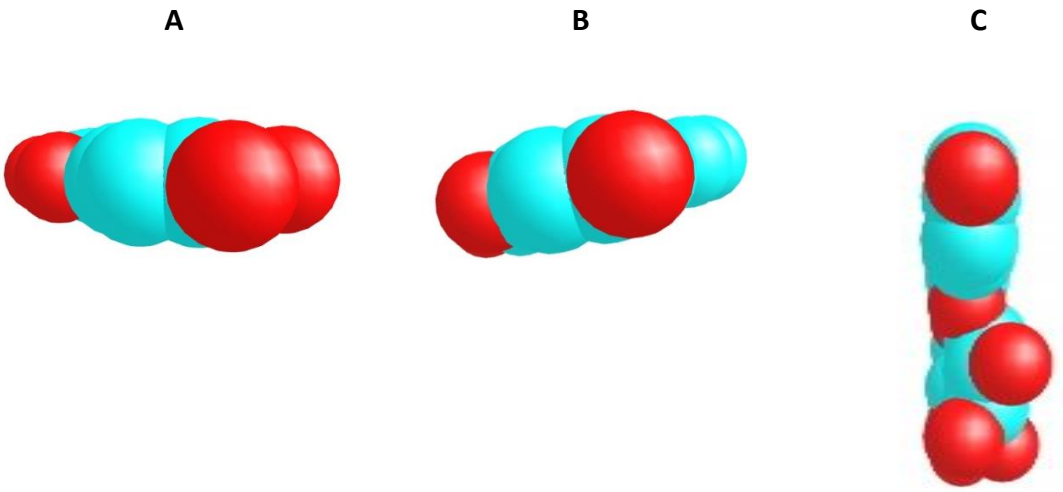

Figure 5.18 Proposed orientations of quercetin (A), rutin (B) and, tiliroside (C) when incorporated into DOPC bilayer.

Based on the orientations given in **Figure 5.18**, the proposed localisation of flavonoids within a single leaflet of DOPC bilayers can be seen in **Figure 5.19**. Note that the scheme bases on our data interpretation being in agreement with all observations made.

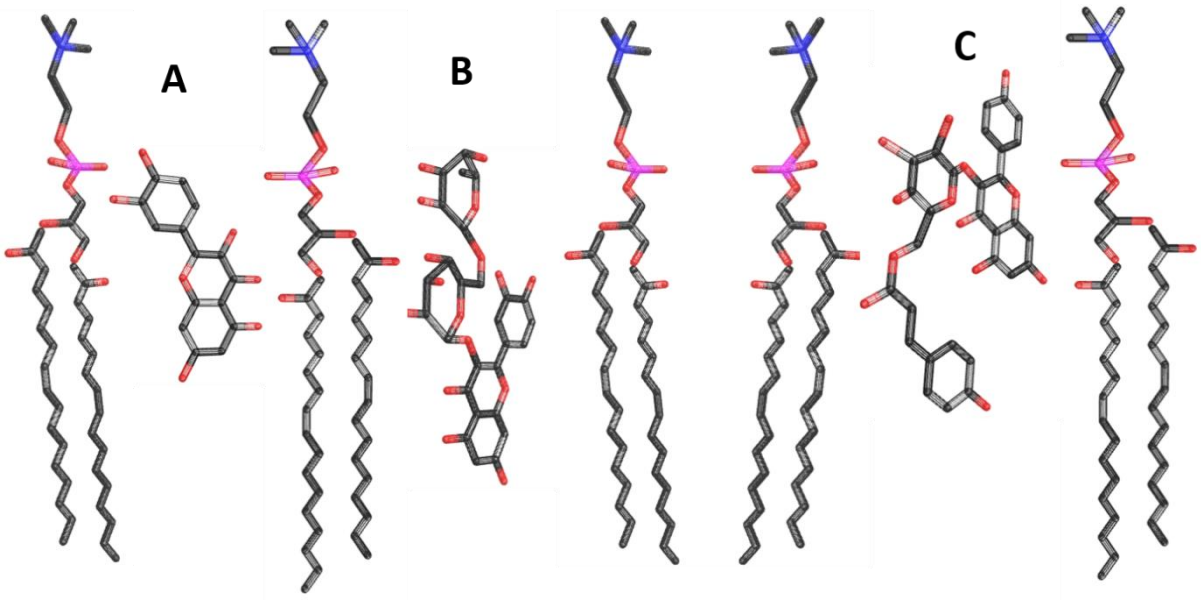

Figure 5.19 A model for the orientation of quercetin (A), rutin (B), and tiliroside (C) within a single leaflet of DOPC bilayers.

The current view for the localisation of the three flavonoids within the biomimetic membrane correlates well with most other existing studies, which suggest localisation of flavonoids between the phospholipid/water interface and the upper half of the hydrocarbon chain region (109, 113, 201, 234, 235). Notwithstanding this view, some studies suggest that the flavonoids partition into the hydrophobic region of the membrane (108, 227).

An extensive NMR study using POPC MLVs as model system proposed flavonoid localisation at the lipid/water interface with the hydroxyl groups have a tendency to hydrogen bond to the polar headgroup zone (109). Movileanu *et al*. proposed a pH-dependent insertion of quercetin within membranes. Quercetin molecules inserted between the polar head groups at alkaline pH, with a deeper location at acidic pH, due to intercalation of quercetin molecules between the acyl chains (234). Rutin–membrane interactions have also been studied via

infrared (IR) spectroscopy. The frequency shift of hydroxyl and keto groups indicated rutin associated with the polar end of the phospholipids (236).

Košinová and co-workers used molecular dynamic (MD) simulations to probe the positioning of quercetin and its derivatives in DOPC lipid bilayer. (33). The authors proposed that flavonoids and their metabolites are preferentially localised at the bilayer/water interface. Moreover, with quercetin, they reported that location of the free-radical-scavenger active OH groups of quercetin (3-OH, 3`- and 4`-OH) was around 1.5 ± 0.2 nm from the membrane centre. Such localisation was related to the ability of flavonoids to inhibit the lipid peroxidation by scavenging the free radicals i.e. (*OH) that flow across the membrane. In contrast to these findings, Arora *et al*. proposed flavonoids and isoflavonoids tended to insert into the hydrophobic core of membranes, as evidenced by a significant decrease in membrane fluidity.

Table 5.7 The influence of flavonoids on membrane fluidity studied by different methods at various concentrations

Flavonoids	Membrane composition Vesicle	Concentrations	Characterization method	Membrane effect	References
Quercetin	DPPC MLVs	Between 1.5-9 mol. %	DSC	Increase the fluidity	(156)
	DOPC MLVs	20 mol. %	EPR	Decrease the fluidity	(108)
	PC:SM and DPPC SUVs	~15 mol. %	Fluorescence Spectroscopy, EPR	Decrease the fluidity	(171)
	DPPC MLVs	5 mol%	EPR with spin labels of n-SASL	No direct effect on the fluidity	(221)
	Liposomes of Chol : PC (1:4 & 1:2.5) PC composition: DPPC:POPC (18:1/16:0) ratio of 0.5	Between 0.5 to 10 µM	Fluorescence polarization	Increase the fluidity below 2.5 µM and Decrease the fluidity above 5 µM	(228)
	DOPC MLVs	6 mol%	SAXS	Increase the fluidity	(111)
Kaempferol	PC:SM and DPPC SUVs	~15 mol. %	Fluorescence Spectroscopy, EPR	Decrease the fluidity	(171)

	MLV and eUV liposomes which consisted of POPC/POPE/POPS/ CH in molar ratios of 4:2:1:3.6	4.5 mM (up to 0.3 Molar ratio)	EPR	Decrease the fluidity below 0.1 molar ratio Increase the fluidity above 0.1 molar ratio	(229)
Myricetin	Phosphatidylcholine (PC) liposomes	5 µM	Fluorescence polarisation assays 6AS-16AP	Decrease the fluidity	(237)
Galangin	Rat liver mitochondria membrane	1-50 µmol/L	Mitochondrial membrane potential and LPO assays	Possible decrease in mitochondrial membrane fluidity	(238)
	DPPC MLVs	From 5 to 50 mol.%	DSC	Increase the fluidity	(112)
Morin	POPC:DPPC liposomes (7:3)	95 µM	Fluorescence spectroscopy	Increase the fluidity (Below T_m)	(110)
	Erythrocyte membranes	95 µM	Fluorescence spectroscopy	Increase the fluidity (Below T_m)	(110)
Fisetin	DPPC MLVs	Dual effect on membranes From 5 to 50 mol. %	DSC	Increase the fluidity (up to 20 mol.%) Decrease the fluidity (above 20 mol. %)	(112)

Apigenin	Liposomes of Chol : PC (1:4 & 1:2.5) PC composition: DPPC:POPC (18:1/16:0) ratio of 0.5	Between 0.5 and 10 µM	Fluorescence polarization	Decrease the fluidity	(228)
Luteloin	POPC:POPE:SOPS:Chol (48: 24: 8: 20, mol%)	10 µM	Fluorescence polarization	Decrease the fluidity	(239)
Naringenin	DPPC multilamellar liposomes	Between 1.5-9 mol. %	DSC	Increase the fluidity	(156)
	DOPC multilamellar liposomes	20 mol. %	EPR	Decrease the fluidity	(108)
	SLPC large unilamellar vesicles	Flavonoid molar ratio to SLPC : 0, 0.2, 0.4, 0.6, 0.8 and 1	FA with 6-AS, 12-AS and 16-AP	Decrease the fluidity	(227)
	Human erythrocyte membranes	0.1 and 1 µg/ml	EPR with 5-DS and 7-DS	Increase the fluidity	(44)
Hesperetin	DPPC multilamellar liposomes	Between 1.5-9 mol. %	DSC	Increase the fluidity	(156)
(+) – catechin	SUVs of phosphatidylcholine (PC) plus sphingomyelin (SM) (2.4:1)	0-4 mol.%	EPR	Slightly decrease the fluidity	(240)

(-) – epicatechin	SUVs of phosphatidylcholine (PC) plus sphingomyelin (SM) (2.4:1)	0-4 mol.%	EPR	Slightly decrease the fluidity	(240)
(-) - epigallocatechin (EGC)	SUVs of phosphatidylcholine (PC) plus sphingomyelin (SM) (2.4:1)	0-4 mol.%	EPR	Slightly decrease the fluidity	(240)
(-) - epigallocatechin-3-gallate (EGCG)	SUVs of phosphatidylcholine (PC) plus sphingomyelin (SM) (2.4:1)	0-4 mol.%	EPR	Slightly decrease the fluidity	(240)
Rutin	DPPC multilamellar liposomes	Between 1.5-9 mol. %	DSC	Increase the fluidity	(156)
	DOPC multilamellar liposomes	20 mol. %	EPR	Decrease the fluidity	(108)
	SLPC large unilamellar vesicles	Flavonoid molar ratio to SLPC : 0, 0.2, 0.4, 0.6, 0.8 and 1	FA with 6-AS, 12-AS and 16-AP	Decrease the fluidity	(227)
	DOPC MLVs	6 mol%	SAXS	Increase the fluidity	(111)
Tiliroside	DOPC MLVs	6 mol%	SAXS	Increase the fluidity	(111)
kaempferol-3-glucoside (KG),	MLV and eUV liposomes which consisted of POPC/POPE/POPS/	4.5 mM (up to 0.3 Molar ratio)	EPR	Decrease the fluidity	(229)

	CH in molar ratios of 4:2:1:3.6				
Naringin	DOPC multilamellar liposomes	20 mol. %	EPR	Decrease the fluidity	(108)
Genistein	SLPC large unilamellar vesicles	Flavonoid molar ratio to SLPC : 0, 0.2, 0.4, 0.6, 0.8 and 1	FA with 6-AS, 12-AS and 16-AP	Decrease the fluidity	(227)
	DOPC MLVs	Up to 20 mol.%	X-ray scattering	Increase the fluidity	(45)
	Diphytanoyl PC (DPhyPC)	Up to 20 mol.%	Molecular dynamic simulations	Increase the fluidity	(45)
	Erythrocyte membrane	0.1 mg/mL	EPR with 5-DS and 12-DS spin probes	Decrease the fluidity	(241)
Daidzein	DOPC MLVs	Up to 14 mol.%	X-ray scattering	Increase the fluidity	(45)
	Diphytanoyl PC (DPhyPC)	Up to 12 mol.%	Molecular dynamic simulations	Increase the fluidity	(45)
	Erythrocyte membrane	0.1 mg/mL	EPR with 5-DS and 12-DS spin probes	Increase the fluidity	(241)
Procyanidins	Phosphatidylcholine (PC) liposomes	5 µM	Fluorescence polarisation assays 6AS-16AP	Decrease the fluidity	(237)

	PC:PS liposomes	0.05 to 1 µg/ml	Jurkat T cell culture studies and molecular probes such as CF: 5(6)-carboxyfluorescein	Increase the fluidity	(242)

5.3 Vesicle size distribution

The mean volume diameters of pure DOPC MLVs and flavonoid treated MLVs obtained via Mastersizer 3000, Malvern Instruments are presented in **Figure 5.20**. The measurements were assessed upon addition of increasing amounts of flavonoids up to 12 mol%. As seen from the volume-weighted size distribution, the introduction of flavonoids resulted in a slight decrease in vesicle size. This decrease was concentration dependent and 12 mol % tiliroside resulted in a decrease in average size from 7.14 µm for pure DOPC MLVs to 3.65 µm.

The data available in the literature regarding the reduced vesicle sizes upon incorporation of bioactive materials is limited. Tefas *et al*. characterised the size distribution of DPPC: CHOL liposomes in the presence of quercetin and reported a slight decrease in mean diameter of vesicles which is more pronounced at higher quercetin content. The authors explained this size reduction by a possible replacement of quercetin molecules with phospholipid molecules incorporated into liposomes (243).

A detailed look on parameters extracted from SAXS measurements showed that the decrease in vesicle size does not scale with the lamellar repeat. However, it goes in parallel with a decrease in the number of lamellar, *N*mean. For example, the average size decrease (in percentage) with 12 mol% quercetin and tiliroside with respect to DOPC, are 38.8% and 48.9%, respectively. On the other hand, *N*mean values extracted from the fits are $N_{\text{DOPC}} = 20$, $N_{DOPC\text{-}Q\text{uercetin}} = 16$ and $N_{\text{DOPC-Tiliroside}} = 6$.

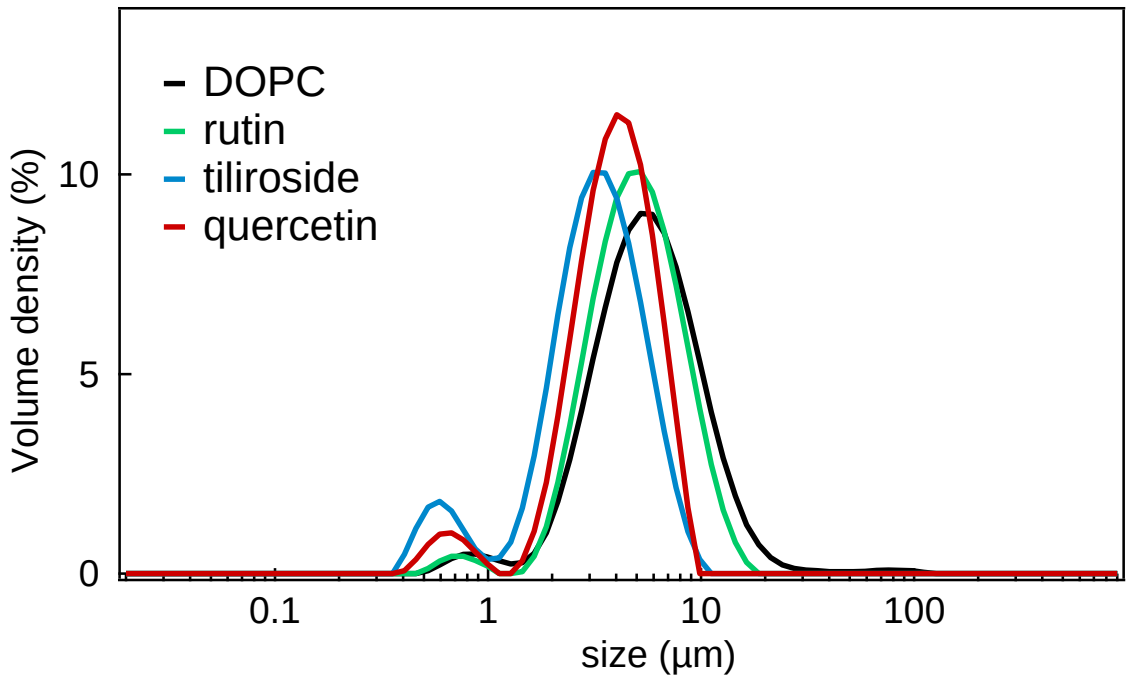

Figure 5.20 Size distribution of pure and flavonoid loaded (12mol%) DOPC vesicles**.**

5.4 Confocal microscopy of pure DOPC bilayers

Complementary to the X-ray scattering measurements, a Leica TCS SP2 confocal laser scanning microscope (operated in fluorescence mode) was used to visualise both pure and flavonoid loaded DOPC vesicles. **Figure 5.21** are representative images of pure DOPC vesicles labelled with a fluorescent dye of Rhodamine B at different magnifications.

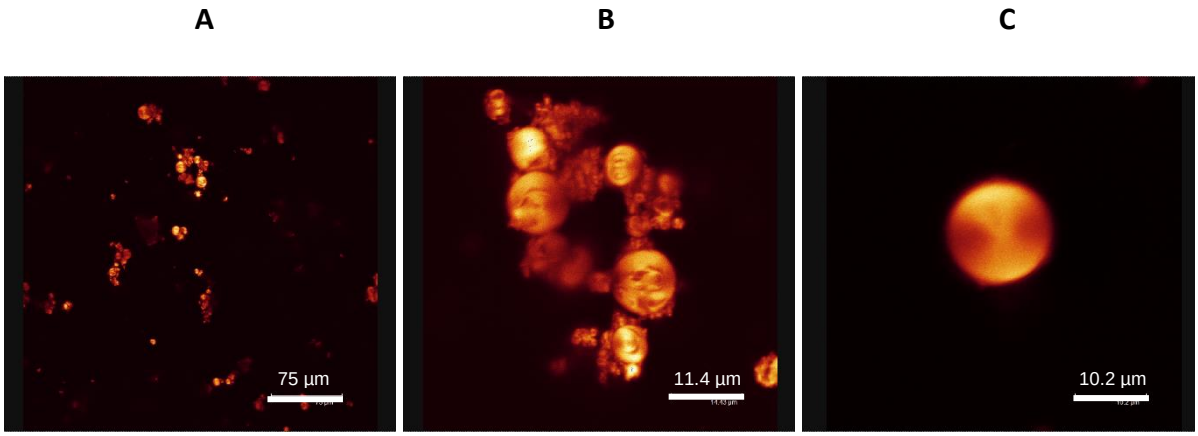

Figure 5.21 Visualisation of pure DOPC vesicles.

DOPC vesicles appear as bright dots at low magnification as seen in **Figure 5.21 (A)**. A closer look at the images (**Figure 5.21 (B&C**)) shows that the vesicles are mostly aggregated clumps of material.

Changes in the vesicle morphology were also investigated due to the presence of flavonoids at different concentrations. **Figure 5.22,** for example**,** shows representative images of quercetin-loaded DOPC vesicles at 1, 6 and 24 mol%. Here, it should be noted that flavonoids are naturally fluorescent at λexc = 476 nm and the fluorescence (brightness) visible in the left-hand set of images is due to flavonoid itself. In the right-hand set of images, the brightness is due to Rhodamine B solubilised in the vesicles.

The images obtained with 1, 6 and also 12 mol% quercetin (12 mol% data are not shown here) exhibited a similar morphology, suggesting effective incorporation of quercetin into the vesicles up to 12 mol % without too much disturbance of the vesicle structure. However, as seen, quercetin also seems to be clustered outside the vesicles in these images. Further increase of quercetin content up to 24 mol% resulted in the appearance of crystal-like structures as shown in **Figure 5.22 (D&E)**. In order to decide, if such features resulted from pure quercetin crystals, a suspension of pure quercetin was also visualised via CLSM at the same concentration, and indeed needle-like crystals were observed. The morphology of quercetin crystals has also been described as needle-like from TEM studies (244).

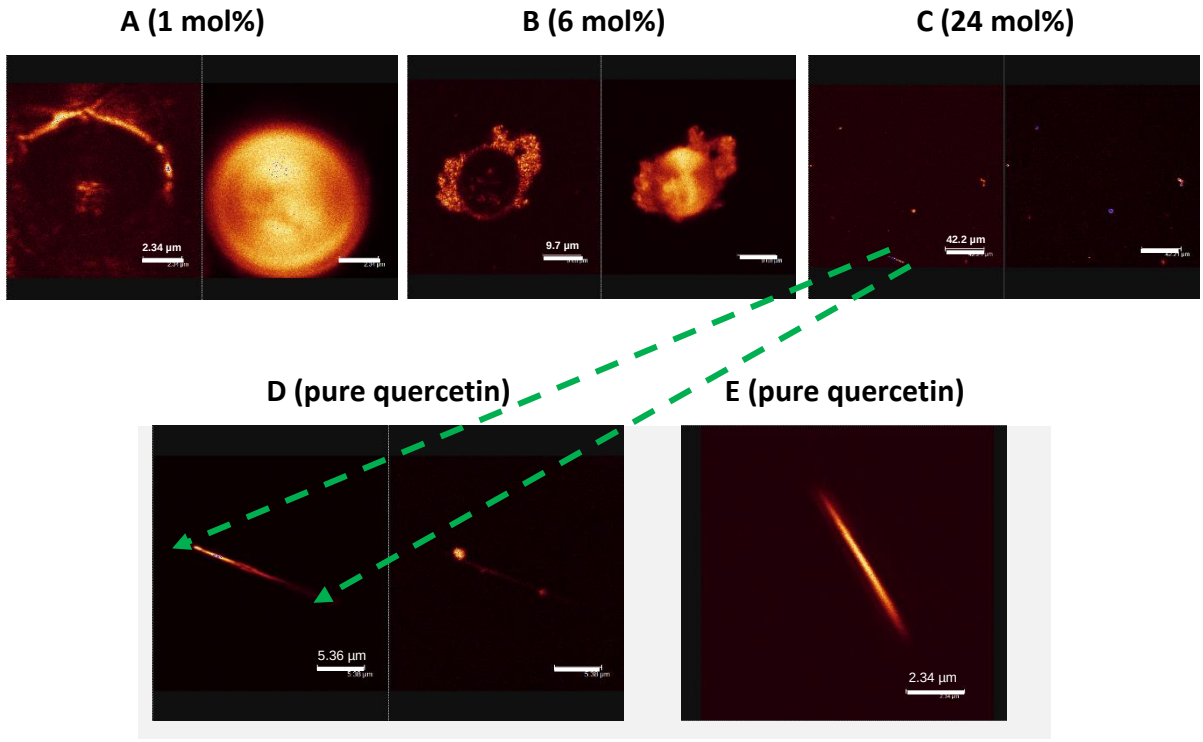

Figure 5.22 Visualisation of quercetin loaded DOPC vesicles (A & B & C) and quercetin alone (D&E).

CLSM images of tiliroside-loaded DOPC vesicles are shown in **Figure 5.23 (A, B&C).** Similar morphologies to that of quercetin-loaded vesicles were observed at concentrations of 1 and 6 mol%, suggesting that tiliroside mostly clusters at the periphery of the vesicles. Increasing the content to 12 mol% resulted in a small population of rod-like crystals outside the vesicles. **Figure 5.23 (D&E)** show the CLSM images of dispersion of pure tiliroside at 1 and 6 mol %, respectively. Rod-like crystals were the dominant crystal population with tiliroside (1 mol%), however, when tiliroside dispersions were visualised at 6 mol%, leaf-like crystal shapes were also visible, although these may have been the same crystals presenting a different orientation. However, SEM images of a tiliroside dispersion were also taken as shown in **Figure 5.24** which give clear evidence of two different crystal morphologies: one rod-like shaped, and another leaf-shaped.

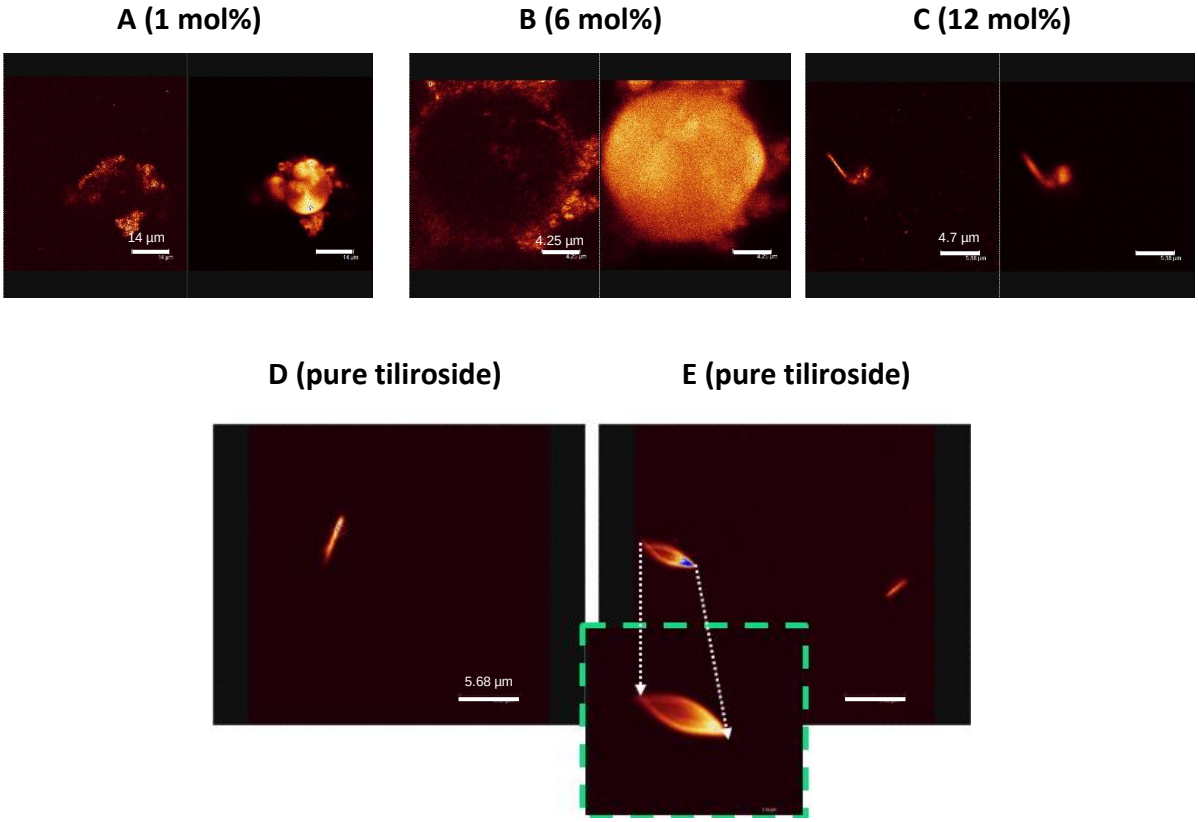

Figure 5.23 Visualisation of tiliroside loaded DOPC vesicles (A,B&C) and tiliroside alone (D&E).

Pure tiliroside

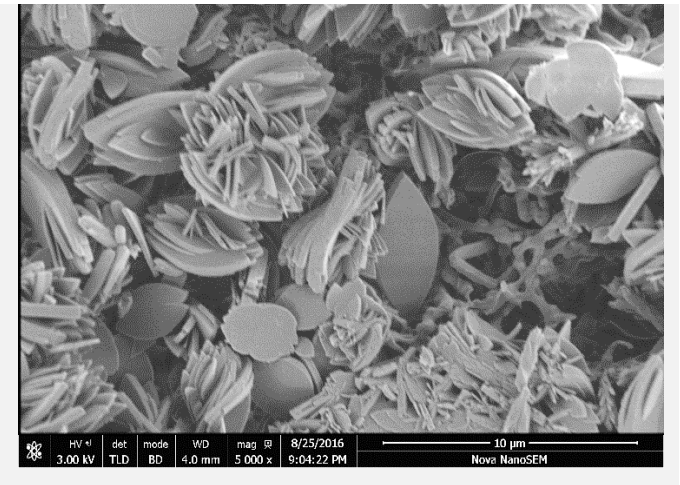

Figure 5.24 SEM image of pure tiliroside (6 mol%). The image courtesy of Dr Alexander Kulak.

Finally, rutin loaded DOPC vesicles were visualised via CLSM as shown in **Figure 5.25 (A, B&C)**. No rutin crystals were visible outside the DOPC vesicles up to 6 mol%. The presence of a few free rutin crystals appeared at 12 mol%, and the morphology of rutin crystals was similar to that of quercetin. A dispersion of pure rutin crystals visualised at 6 mol% are also given in **Figure 5.25 (E)**.

It should be noted that although DOPC vesicles maintained an undisturbed morphology with quercetin and tiliroside, rutin loaded vesicles somehow exhibited a different morphology, showing folded-like spherical structures.

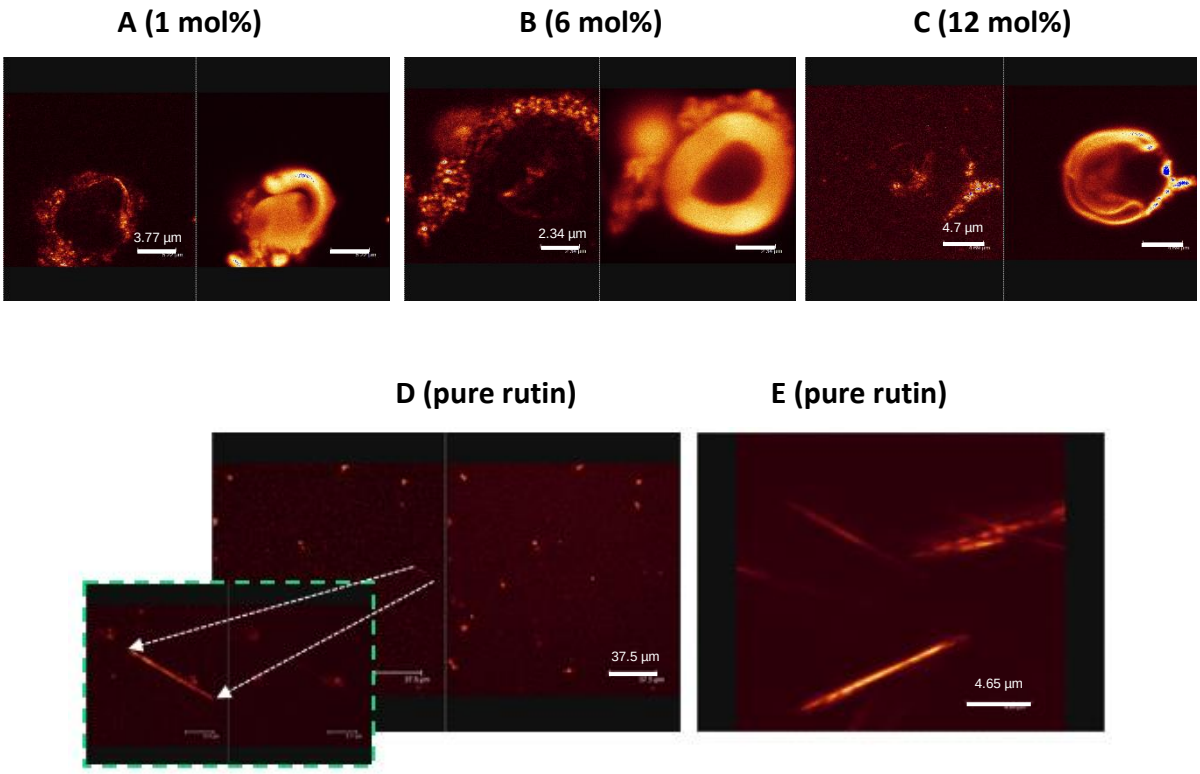

Figure 5.25 Visualisation of rutin loaded DOPC vesicles (A,B&C) and pure rutin (D&E).

Chapter 6 General conclusions and discussion

This chapter summarises the main findings and general conclusions obtained by comparing different membrane models with regard to the flavonoid-biomembrane interactions. Each model employed in cross-platform techniques provided a separate vision and insight into a particular facet of the interactions and hence a better understanding of the nuances that contribute to the flavonoid mechanism of action. Systematic screening of eight flavonoids of varying structure on phospholipid monolayers through an electrochemical membrane model - Hg-supported DOPC monolayer via RCV - revealed that:

(i) The ranking order of the interactions is as follows: quercetin > kaempferol > naringenin > hesperetin > catechin for flavonoid aglycones, and tiliroside > rutin > naringin for flavonoid glycosides.

(ii) The ranking is related to the structural properties of the molecules. Flavonoid aglycones with two coplanar rings i.e. quercetin and kaempferol were more interactive than other aglycones that are non-planar in configuration i.e. naringenin, hesperetin and catechin.

(iii) The presence of sugar group moiety in the flavonoid structure affected the extent of interactions. Because sugar moieties counteract the hydrophobicity and render the molecules larger in size, rutin and naringin with two linked glycoside moieties interacted with DOPC less. Exceptionally, another glycoside, tiliroside with one sugar group moiety interacted much strongly with DOPC. Tiliroside's effect on DOPC monolayer was even comparable with quercetin and kaempferol at increased concentrations. Tiliroside only has one sugar group instead of two, and this is probably a factor behind its stronger response. Another reason

contributing to the high activity of tiliroside on the monolayer might be because of its relatively high $\log_{10}P$ value (2.7).

It should be noted that these structural features were more predominant in determining interactions than the other parameters such as the octanol-water partition coefficients of flavonoids.

In a complementary line of the study, characterisation of the interactions of quercetin, rutin and tiliroside with free-standing Langmuir monolayers by the π-A isotherms and the monolayer stabilising action suggested that:

(1) Quercetin shifted the isotherm towards a larger molecular area at surface pressures above (8 mN m^{-1}) whereas tiliroside caused a very distinct increase in the molecular area of the DOPC monolayer at low surface pressures (between 0 and 12 mN m^{-1}) only. On the other hand, rutin did not cause any changes on the isotherm.

(2) The interactions measured by monolayer stabilisation via Langmuir monolayers and BAM images revealed that quercetin suggests a complete stabilising action on DOPC monolayer. This is followed by tiliroside, which significantly improved the monolayer stability, whereas there was no change in the film stability with rutin.

(3) Langmuir monolayer results were in great agreement with the previous RCV data. For both techniques, the monolayer interaction was strongest with quercetin and ranked in the order quercetin> tiliroside> rutin.

Finally, the interactions measured by the alterations in the bilayer fluidity and thickness via SAXS showed that:

(a) At 1 and 2 mol% of flavonoids; quercetin fluidised the DOPC membrane most and the rank order of membrane fluidity (quercetin > tiliroside > rutin) correlated with previous monolayer studies. However, there is a deviation between the membrane response of quercetin and tiliroside at and above 6 mol% content. Tiliroside fluidised the membrane most at this concentration with an increase in the bending fluctuation to ~ 0.11 compared to pure DOPC vesicles (~ 0.08) at 25 °C.

(b) All flavonoids studied decreased bilayer thickness with the same rank order of quercetin > tiliroside > rutin at 1 and 2 mol% concentrations. The overall membrane thinning was not significant with rutin (less than 1 Å). Increasing the flavonoid content up to 6 mol% resulted in a deviation in the membrane response which is similar to the deviation created in membrane fluidity. Tiliroside thinned the membrane slightly more than quercetin i.e. DOPC bilayer thickness (36.01 Å) was reduced to 34.95 Å and 35.3 Å in the presence of tiliroside and quercetin, respectively.

(c) SAXS study reports a concentration-dependent biphasic effect of tiliroside on DOPC membrane fluidity so that tiliroside initially enhanced the fluidity, up to 6 mol%, followed by a decrease in the fluidity at a higher concentration of 24 mol%. Therefore, it is tempting to suggest that, tiliroside might display a 'regulatory role' on membrane fluidity similar to the effect of cholesterol. Partial interdigitation of DOPC bilayer with tiliroside (24 mol%) caused a phase separation of the membrane into tiliroside rich and tiliroside poor regions.

(d) Quercetin, rutin and tiliroside were able to effectively incorporate within DOPC vesicles up to 12 mol%, 6 mol%, and 6 mol% concentrations. However, above the given concentrations, the solubility limit was exceeded, and free flavonoid crystals were present

outside the vesicles. Both diffraction pattern and confocal images implied the presence of free crystals above the mentioned flavonoid content.

(e) SAXS study proposed an overall location of flavonoids near the apolar/polar interface deduced from the increased membrane fluidity and further supported by volume/area estimations and projected area calculations.

Overall, application of RCV indicated that the ranking for interactions is related to structural properties of flavonoids and this method successfully elucidated the fundamental structural criteria driving flavonoid-monolayer interactions. The other technique - Langmuir monolayers - measured the interactions by monolayer-stabilisation action. Finally, interactions measured by the alterations in the bilayer fluidity and thickness via SAXS showed a clear membrane thinning effect along with an increase in membrane undulations. Both monolayer and bilayer techniques were in great agreement with each other and ranked the interactions in the order of quercetin> tiliroside> rutin, except for tiliroside, where the high concentration (at and above 6 mol%) of tiliroside intensified the interactions on DOPC bilayer as revealed via SAXS.

LIMITATIONS & DIRECTIONS FOR FUTURE RESEARCH

The current study can be performed on following lines depending on the available opportunities:

Effect of flavonoids on different lipid mixture

A considerable amount of today's on-going membrane biophysics' research is in the direction to create artificial membranes to mimic the complex cell behaviour. In this study, we have restricted ourselves to the modelling of a system consisting of one phospholipid type, DOPC only. Because the existing reports on flavonoid-biomembrane interactions, using different

lipid types or their mixtures are not conclusive yet, and sometimes even disagree with each other. In order to elucidate and clarify the role of one of the benchmark lipid, DOPC, involved flavonoid-membrane interactions, we simplified the complex membranes. Therefore, we intentionally excluded other lipid types such as cholesterol to avoid the influence of an additional component that can play a role in the interactions. However, future research based on this study could design more complex and sophisticated model membrane systems to achieve a greater in-depth information about the effects of flavonoids on membrane behaviour.

A strategy for this could be to include cholesterol and different phospholipids and proteins in membrane formulation to screen the flavonoids for their SAR and SAXS-analysis. With this approach, we could achieve a more profound idea about the lipid behaviour with/without cholesterol and protein.

Flavonoids Interacting With Curved Membranes

Cubosomes, which are liquid crystalline nanostructures derived from the cubic phase of lipids, have been widely used as advanced drug delivery systems and nanocarriers (245) due to their specific characteristics. Furthermore, their application as templates for encapsulation and delivery of polyphenols is also emerging (230). However, the influence of flavonoids on cubosomes' structures and functions remains unknown. Investigating the flavonoid interactions with curved membranes can be specifically important to understand their biological functions i.e. absorption of bioactive compounds. Future studies, therefore, can focus on exploring the structural alterations of flavonoid loaded mesosomes to reveal new insights and understandings into the application and formulation of novel mesosome based

functional materials**.** This is of great importance for the anticipated applications of flavonoids in drug and food delivery systems.

References

1. Corradini, E. et al. Flavonoids: chemical properties and analytical methodologies of identification and quantitation in foods and plants. *Natural product research.* 2011, **25**(5), pp.469-495.
2. Rice-Evans, C. and Packer, L. *Flavonoids in health and disease.* 2nd. ed. New York: Marcel Dekker, 2003.
3. Kumar, S. and Pandey, A.K. Chemistry and biological activities of flavonoids: an overview. *The Scientific World Journal.* 2013, **2013**.
4. Halbwirth, H. The creation and physiological relevance of divergent hydroxylation patterns in the flavonoid pathway. *International journal of molecular sciences.* 2010, **11**(2), pp.595-621.
5. Narayana, K.R. et al. Bioflavonoids classification, pharmacological, biochemical effects and therapeutic potential. *Indian journal of pharmacology.* 2001, **33**(1), pp.2-16.
6. Veitch, N.C. and Grayer, R.J. Flavonoids and their glycosides, including anthocyanins. *Natural product reports.* 2008, **25**(3), pp.555-611.
7. Tsao, R. Chemistry and Biochemistry of Dietary Polyphenols. *Nutrients.* 2010, **2**(12), p.1231.
8. Andersen, O.M. and Markham, K.R. *Flavonoids : Chemistry, Biochemistry and Applications.* New ed. Boca Raton, Fla. ; London: CRC, 2006.
9. Kang, J.-T. et al. Effect of antioxidant flavonoids (quercetin and taxifolin) on in vitro maturation of porcine oocytes. *Asian-Australasian journal of animal sciences.* 2016, **29**(3), p.352.
10. Saklani, A. and Kutty, S.K. Plant-derived compounds in clinical trials. *Drug Discovery Today.* 2008, **13**(3), pp.161-171.
11. Cragg, G.M. Paclitaxel (Taxol®): a success story with valuable lessons for natural product drug discovery and development. *Medicinal research reviews.* 1998, **18**(5), pp.315-331.
12. Cassidy, A. and Minihane, A.-M. The role of metabolism (and the microbiome) in defining the clinical efficacy of dietary flavonoids. *Am J Clin Nutr.* 2017, **105**(1), pp.10-22.
13. Bentsath, A. et al. Vitamin nature of flavones. *Nature.* 1936, **138**, pp.798-798.
14. Bohm, B.A. *Introduction to flavonoids.* Amsterdam: Harwood Academic, 1998.
15. Joshipura, K.J. et al. The effect of fruit and vegetable intake on risk for coronary heart disease. *Annals of Internal Medicine.* 2001, **134**(12), pp.1106-1114.
16. Cui, L. et al. Flavonoids, flavonoid subclasses, and esophageal cancer risk: a meta-analysis of epidemiologic studies. *Nutrients.* 2016, **8**(6), p.350.
17. Joshipura, K.J. et al. The Effect of Fruit and Vegetable Intake on Risk for Coronary Heart Disease. *Annals of Internal Medicine.* 2001, **134**(12), pp.1106-1114.
18. Saver, J.L. Number needed to treat estimates incorporating effects over the entire range of clinical outcomes: Novel derivation method and application to thrombolytic therapy for acute stroke. *Archives of Neurology.* 2004, **61**(7), pp.1066-1070.
19. Connor, S. Glaxo chief: Our drugs do not work on most patients. *The Independent.* 2003, **8**.
20. Groopman, J. Hartzband P. Obama's $80 billion exaggeration. *Wall Street J.* 2009.

21. Hansell, S. Your Medical Mind: How to Decide What Is Right for You. In: *Oncology Nursing Forum*, 2012, p.415.
22. Percival, M. Antioxidants. *Clinical Nutrition Insights.* 1998, **31**, pp.1-4.
23. Rahman, K. Studies on free radicals, antioxidants, and co-factors. *Clin Interv Aging.* 2007, **2**(2), pp.219-36.
24. Anand, P. et al. Cancer is a Preventable Disease that Requires Major Lifestyle Changes. *Pharmaceutical Research.* 2008, **25**(9), pp.2097-2116.
25. Devasagayam, T.P. et al. Free radicals and antioxidants in human health: current status and future prospects. *J Assoc Physicians India.* 2004, **52**, pp.794-804.
26. Lugasi, A. Natural Antioxidants Chemistry, Health Effects, and Applications. Edited by F. Shahidi. VIII and 432 pages, numerous figures and tables. AOCS Press, Champaign, Illinois, 1997. Price: 105.00 U$. *Food / Nahrung.* 1997, **41**(5), pp.321-321.
27. Bouayed, J. and Bohn, T. Exogenous antioxidants - Double-edged swords in cellular redox state: Health beneficial effects at physiologic doses versus deleterious effects at high doses. *Oxid Med Cell Longev.* 2010, **3**(4), pp.228-237.
28. Rahman, K. Studies on free radicals, antioxidants, and co-factors. *Clin Interv Aging.* 2007, **2**(2), p.219.
29. Zhang, M. et al. Antioxidant properties of quercetin. In: *Oxygen Transport to Tissue XXXII*. Springer, 2011, pp.283-289.
30. Magalingam, K.B. et al. Protective effects of quercetin glycosides, rutin, and isoquercetrin against 6-hydroxydopamine (6-OHDA)-induced neurotoxicity in rat pheochromocytoma (PC-12) cells. *International journal of immunopathology and pharmacology.* 2016, **29**(1), pp.30-39.
31. Rengarajan, T. and Yaacob, N.S. The flavonoid fisetin as an anticancer agent targeting the growth signaling pathways. *Eur J Pharmacol.* 2016, **789**, pp.8-16.
32. Sangeetha, K.S.S. et al. FLAVONOIDS: THERAPEUTIC POTENTIAL OF NATURAL PHARMACOLOGICAL AGENTS. *International Journal of Pharmaceutical Sciences and Research.* 2016, **7**(10), pp.3924-3930.
33. Košinová, P.n. et al. Positioning of antioxidant quercetin and its metabolites in lipid bilayer membranes: implication for their lipid-peroxidation inhibition. *The Journal of Physical Chemistry B.* 2012, **116**(4), pp.1309-1318.
34. Rice-Evans, C.A. et al. Structure-antioxidant activity relationships of flavonoids and phenolic acids. *Free Radical Biology and Medicine.* 1996, **20**(7), pp.933-956.
35. Patil, C.S. et al. Protective effect of flavonoids against aging-and lipopolysaccharide-induced cognitive impairment in mice. *Pharmacology.* 2003, **69**(2), pp.59-67.
36. Zhang, R. et al. Increase of rutin antioxidant activity by generating Maillard reaction products with lysine. *Bioorganic & medicinal chemistry letters.* 2016, **26**(11), pp.2680-2684.
37. Chicaro, P. et al. Flavonoids from Lychnophora passerina (Asteraceae): potential antioxidants and UV-protectants. *Biochemical systematics and ecology.* 2004, **32**(3), pp.239-243.
38. Velagapudi, R. et al. Tiliroside, a dietary glycosidic flavonoid, inhibits TRAF-6/NF-κB/p38-mediated neuroinflammation in activated BV2 microglia. *Biochimica et Biophysica Acta (BBA)-General Subjects.* 2014, **1840**(12), pp.3311-3319.
39. Okamoto, T. Safety of quercetin for clinical application (Review). *International journal of molecular medicine.* 2005, **16**(2), pp.275-278.

40. Weng, Z. et al. Quercetin is more effective than cromolyn in blocking human mast cell cytokine release and inhibits contact dermatitis and photosensitivity in humans. *Plos One.* 2012, **7**(3), p.e33805.
41. Horcajada, M.-N. et al. Oleuropein or rutin consumption decreases the spontaneous development of osteoarthritis in the Hartley guinea pig. *Osteoarthritis and Cartilage.* 2015, **23**(1), pp.94-102.
42. Reygaert, W.C. The antimicrobial possibilities of green tea. *Frontiers in microbiology.* 2014, **5**, p.434.
43. Sharma, A. et al. Green tea extract: possible mechanism and antibacterial activity on skin pathogens. *Food Chemistry.* 2012, **135**(2), pp.672-675.
44. Ajdžanović, V. et al. Positive effects of naringenin on near-surface membrane fluidity in human erythrocytes. *Acta Physiologica Hungarica.* 2015, **102**(2), pp.131-136.
45. Raghunathan, M. et al. Structure and elasticity of lipid membranes with genistein and daidzein bioflavinoids using X-ray scattering and MD simulations. *The Journal of Physical Chemistry B.* 2012, **116**(13), pp.3918-3927.
46. Hung, W.-C. et al. Membrane-thinning effect of curcumin. *Biophysical Journal.* 2008, **94**(11), pp.4331-4338.
47. Bai, W. et al. Intakes of total and individual flavonoids by US adults. *International journal of food sciences and nutrition.* 2014, **65**(1), pp.9-20.
48. Vogiatzoglou, A. et al. Flavonoid intake in European adults (18 to 64 years). *Plos One.* 2015, **10**(5), p.e0128132.
49. Suzuki, T. et al. Kaempferol enhances intestinal barrier function through the cytoskeletal association and expression of tight junction proteins in Caco-2 cells. *J Nutr.* 2011, **141**(1), pp.87-94.
50. Jalili, T. et al. Quercetin Reduces Blood Pressure in Hypertensive Subjects. *Circulation.* 2006, **114**(18 Supplement), p.II_890.
51. Perez-Vizcaino, F. and Duarte, J. Flavonols and cardiovascular disease. *Molecular aspects of medicine.* 2010, **31**(6), pp.478-494.
52. M Calderon-Montano, J. et al. A review on the dietary flavonoid kaempferol. *Mini reviews in medicinal chemistry.* 2011, **11**(4), pp.298-344.
53. Goto, T. et al. Tiliroside, a glycosidic flavonoid, ameliorates obesity-induced metabolic disorders via activation of adiponectin signaling followed by enhancement of fatty acid oxidation in liver and skeletal muscle in obese–diabetic mice. *The Journal of nutritional biochemistry.* 2012, **23**(7), pp.768-776.
54. Luo, Z. *Uptake and metabolism of tiliroside in model systems*. thesis, University of Leeds, 2011.
55. Cavia-Saiz, M. et al. Antioxidant properties, radical scavenging activity and biomolecule protection capacity of flavonoid naringenin and its glycoside naringin: a comparative study. *Journal of the Science of Food and Agriculture.* 2010, **90**(7), pp.1238-1244.
56. Kanaze, F. et al. Pharmacokinetics of the citrus flavanone aglycones hesperetin and naringenin after single oral administration in human subjects. *European journal of clinical nutrition.* 2007, **61**(4), pp.472-477.
57. Shimizu, M. et al. Green tea extracts for the prevention of metachronous colorectal adenomas: a pilot study. *Cancer Epidemiology Biomarkers & Prevention.* 2008, **17**(11), pp.3020-3025.

58. Sharangi, A. Medicinal and therapeutic potentialities of tea (Camellia sinensis L.)–A review. *Food Research International.* 2009, **42**(5), pp.529-535.
59. Hollman, P.C. Absorption, bioavailability, and metabolism of flavonoids. *Pharmaceutical Biology.* 2004, **42**(s1), pp.74-83.
60. Walle, T. et al. Flavonoid glucosides are hydrolyzed and thus activated in the oral cavity in humans. *J Nutr.* 2005, **135**(1), pp.48-52.
61. Walle, U.K. et al. Transport of genistein-7-glucoside by human intestinal CACO-2 cells: potential role for MRP2. *Research communications in molecular pathology and pharmacology.* 1999, **103**(1), pp.45-56.
62. Crespy, V. et al. Quercetin, but not its glycosides, is absorbed from the rat stomach. *Journal of Agricultural and Food Chemistry.* 2002, **50**(3), pp.618-621.
63. Rios, L.Y. et al. Cocoa procyanidins are stable during gastric transit in humans. *Am J Clin Nutr.* 2002, **76**(5), pp.1106-1110.
64. Hollman, P.C. et al. Absorption of dietary quercetin glycosides and quercetin in healthy ileostomy volunteers. *Am J Clin Nutr.* 1995, **62**(6), pp.1276-82.
65. Day, A.J. et al. Dietary flavonoid and isoflavone glycosides are hydrolysed by the lactase site of lactase phlorizin hydrolase. *Febs Letters.* 2000, **468**(2-3), pp.166-70.
66. Walle, T. et al. Quercetin glucosides are completely hydrolyzed in ileostomy patients before absorption. *J Nutr.* 2000, **130**(11), pp.2658-2661.
67. Walgren, R.A. et al. Cellular uptake of dietary flavonoid quercetin 4'-β-glucoside by sodium-dependent glucose transporter SGLT1. *Journal of Pharmacology and Experimental Therapeutics.* 2000, **294**(3), pp.837-843.
68. Singer, S.J. and Nicolson, G.L. The fluid mosaic model of the structure of cell membranes. *Science.* 1972, **175**(4023), pp.720-731.
69. Simons, K. and Ikonen, E. Functional rafts in cell membranes. *Nature.* 1997, **387**(6633), pp.569-572.
70. Brown, D. and London, E. Functions of lipid rafts in biological membranes. *Annual review of cell and developmental biology.* 1998, **14**(1), pp.111-136.
71. Dopico, A. *Methods in membrane lipids.* Springer Science & Business Media, 2007.
72. Van Meer, G. et al. Membrane lipids: where they are and how they behave. *Nature reviews molecular cell biology.* 2008, **9**(2), pp.112-124.
73. Snape, A. et al. *Biochemistry and Molecular Biology.* Oxford University Press, 2014.
74. Puligundla, P. et al. Emerging Trends in Modification of Dietary Oils and Fats, and Health Implications-A Review. *Sains Malaysiana.* 2012, **41**(7), pp.871-877.
75. Buehler, L.K. *Cell Membranes.* New York: Garland Science, Taylor & Francis Group, LLC, 2015.
76. Rappolt, M. et al. Structural, dynamic and mechanical properties of POPC at low cholesterol concentration studied in pressure/temperature space. *European Biophysics Journal.* 2003, **31**(8), pp.575-585.
77. Dufourc, E.J. Sterols and membrane dynamics. *Journal of chemical biology.* 2008, **1**(1-4), pp.63-77.
78. Chan, Y.-H.M. and Boxer, S.G. Model membrane systems and their applications. *Current Opinion in Chemical Biology.* 2007, **11**(6), pp.581-587.
79. Eeman, M. and Deleu, M. From biological membranes to biomimetic model membranes. *Biotechnologie Agronomie Societe Et Environnement.* 2010, **14**(4), pp.719-736.

80. Anderson, T.H. et al. Formation of supported bilayers on silica substrates. *Langmuir.* 2009, **25**(12), pp.6997-7005.
81. McCabe, I.P. and Forstner, M.B. Polymer supported lipid bilayers. 2013.
82. Nelson, A. Electrochemistry of mercury supported phospholipid monolayers and bilayers. *Current Opinion in Colloid & Interface Science.* 2010, **15**(6), pp.455-466.
83. Coldrick, Z. et al. Phospholipid monolayer coated microfabricated electrodes to model the interaction of molecules with biomembranes. *Electrochimica Acta.* 2009, **54**(22), pp.4954-4962.
84. Vakurov, A. et al. Direct characterization of fluid lipid assemblies on mercury in electric fields. *Acs Nano.* 2014, **8**(4), pp.3242-3250.
85. Mandler, D. and Turyan, I. Applications of self-assembled monolayers in electroanalytical chemistry. *Electroanalysis.* 1996, **8**(3), pp.207-213.
86. Cohen-Atiya, M. et al. Characterization of n-alkanethiol self-assembled monolayers on mercury by impedance spectroscopy and potentiometric measurements. *Journal of Electroanalytical Chemistry.* 2006, **593**(1), pp.227-240.
87. Pagano, R.E. and Miller, I.R. Transport of ions across lipid monolayers. IV. Reduction of polarographic currents by spread monolayers. *Journal of Colloid and Interface Science.* 1973, **45**(1), pp.126-137.
88. Lecompte, M.F. and Miller, I.R. Interaction of Prothrombin and Its Fragments with Monolayers Containing Phosphatidylserine .2. Electrochemical Determination of Lipid Layer Perturbation by Interacting Prothrombin and Its Fragments. *Biochemistry.* 1980, **19**(15), pp.3439-3446.
89. Muskal, N. and Mandler, D. Thiol self-assembled monolayers on mercury surfaces: the adsorption and electrochemistry of ω-mercaptoalkanoic acids. *Electrochimica Acta.* 1999, **45**(4), pp.537-548.
90. Brezesinski, G. and Möhwald, H. Langmuir monolayers to study interactions at model membrane surfaces. *Advances in Colloid and Interface Science.* 2003, **100**, pp.563-584.
91. Mareš, T. et al. Role of phospholipid asymmetry in the stability of inverted hexagonal mesoscopic phases. *The Journal of Physical Chemistry B.* 2008, **112**(51), pp.16575-16584.
92. Martin, D. *Nanobiotechnology of biomimetic membranes.* Springer Science & Business Media, 2007.
93. Girard-Egrot, A.P. and Blum, L.J. Langmuir-Blodgett technique for synthesis of biomimetic lipid membranes. In: *Nanobiotechnology of biomimetic membranes*. Springer, 2007, pp.23-74.
94. 3 - Langmuir Monolayers. In: Lyklema, J. ed. *Fundamentals of Interface and Colloid Science*. Academic Press, 2000, pp.3.1-3.247.
95. Lodish, H. and Zipursky, S.L. Molecular cell biology. *Biochemistry and Molecular Biology Education.* 2001, **29**, pp.126-133.
96. Gramse, G. et al. Nanoscale measurement of the dielectric constant of supported lipid bilayers in aqueous solutions with electrostatic force microscopy. *Biophysical Journal.* 2013, **104**(6), pp.1257-1262.
97. Martinsen, O.G. and Grimnes, S. *Bioimpedance and bioelectricity basics.* Academic press, 2011.
98. Gadsby, D.C. Ion channels versus ion pumps: the principal difference, in principle. *Nature reviews molecular cell biology.* 2009, **10**(5), pp.344-352.

99. Bard, A.J. and Faulkner, L.R. *Electrochemical Methods, Student Solutions Manual: Fundamentals and Applications.* Wiley, 2002.
100. Avison, J. *The World of Physics.* Nelson, 1989.
101. Ulander, J. and Haymet, A.D.J. Permeation Across Hydrated DPPC Lipid Bilayers: Simulation of the Titrable Amphiphilic Drug Valproic Acid. *Biophysical Journal.* 2003, **85**(6), pp.3475-3484.
102. Starzak, M.E. *The physical chemistry of membranes.* Academic Press London, UK:, 1984.
103. Bard, A.J. and Faulkner, L.R. *Electrochemical methods: fundamentals and applications.* Wiley New York, 1980.
104. Bard, A.J. *Electrochemical methods : fundamentals and applications / Allen J. Bard, Larry R. Faulkner.* New York: Wiley, 1980.
105. Koester, J. and Siegelbaum, S.A. Membrane potential. *Principles of neural science.* 1991, **4**, pp.125-139.
106. Tsuchiya, H. Membrane Interactions of Phytochemicals as Their Molecular Mechanism Applicable to the Discovery of Drug Leads from Plants. *Molecules.* 2015, **20**(10), pp.18923-18966.
107. Ingólfsson, H.I. et al. Phytochemicals perturb membranes and promiscuously alter protein function. *ACS chemical biology.* 2014, **9**(8), pp.1788-1798.
108. Tedeschi, A. et al. Effect of flavonoids on the Aβ(25-35)-phospholipid bilayers interaction. *European Journal of Medicinal Chemistry.* 2010, **45**(9), pp.3998-4003.
109. Scheidt, H.A. et al. Investigation of the membrane localization and distribution of flavonoids by high-resolution magic angle spinning NMR spectroscopy. *Biochimica et Biophysica Acta (BBA)-Biomembranes.* 2004, **1663**(1), pp.97-107.
110. Günther, G. et al. Flavonoids in Microheterogeneous Media, Relationship between Their Relative Location and Their Reactivity towards Singlet Oxygen. *Plos One.* 2015, **10**(6), p.e0129749.
111. Sanver, D. et al. Experimental Modeling of Flavonoid–Biomembrane Interactions. *Langmuir.* 2016, **32**(49), pp.13234-13243.
112. Sinha, R. et al. In-vitro anti-proliferative and anti-oxidant activity of galangin, fisetin and quercetin: role of localization and intermolecular interaction in model membrane. *European Journal of Medicinal Chemistry.* 2014, **79**, pp.102-109.
113. Ollila, F. et al. Characterization of Flavonoid–Biomembrane Interactions. *Archives of Biochemistry and Biophysics.* 2002, **399**(1), pp.103-108.
114. van Dijk, C. et al. The uncoupling efficiency and affinity of flavonoids for vesicles. *Biochemical Pharmacology.* 2000, **60**(11), pp.1593-1600.
115. Selvaraj, S. et al. Influence of membrane lipid composition on flavonoid–membrane interactions: Implications on their biological activity. *Progress in Lipid Research.* 2015, **58**(0), pp.1-13.
116. Nelson, L.A. and Coldrick, Z. *Biosensor*. Google Patents, 2013.
117. Lojou, E. and Bianco, P. Application of the electrochemical concepts and techniques to amperometric biosensor devices. *Journal of Electroceramics.* 2006, **16**(1), pp.79-91.
118. Vakurov, A. et al. Electrochemical modeling of the silica nanoparticle–biomembrane interaction. *Langmuir.* 2011, **28**(2), pp.1246-1255.

119. Coldrick, Z. et al. High throughput systems for screening biomembrane interactions on fabricated mercury film electrodes. *Journal of applied electrochemistry.* 2011, **41**(8), pp.939-949.
120. Mohamadi, S. *Electrochemical screening of biological membrane active compounds*. thesis, University of Leeds, 2014.
121. Galluzzi, M. et al. Interaction of imidazolium-based room-temperature ionic liquids with DOPC phospholipid monolayers: electrochemical study. *Langmuir.* 2013, **29**(22), pp.6573-6581.
122. Vakurov, A. et al. Electrochemical Modeling of the Silica Nanoparticle-Biomembrane Interaction. *Langmuir.* 2012, **28**(2), pp.1246-1255.
123. Protopapa, E. et al. Interaction of self-assembling β-sheet peptides with phospholipid monolayers: The effect of serine, threonine, glutamine and asparagine amino acid side chains. *Electrochimica Acta.* 2010, **55**(9), pp.3368-3375.
124. Murray, B.S. Equilibrium and dynamic surface pressure-area measurements on protein films at air-water and oil-water interfaces. *Colloids and Surfaces A: Physicochemical and Engineering Aspects.* 1997, **125**(1), pp.73-83.
125. Janmey, P. and Kinnunen, P. Biophysical properties of lipids and dynamic membranes. *Trends in cell biology.* 2006, **16**(10), pp.538-546.
126. Giner-Casares, J. and Brezesinski, G. Brewster Angle Microscopy (BAM) for in situ characterization of ultrathin films at air/liquid interfaces. *Current Microscopy Contributions to Advances in Science and Technology: Formatex.* 2012.
127. Hönig, D. and Möbius, D. Reflectometry at the Brewster angle and Brewster angle microscopy at the air-water interface. *Thin Solid Films.* 1992, **210**, pp.64-68.
128. Garofalakis, G. and Murray, B.S. Surface pressure isotherms, dilatational rheology, and Brewster angle microscopy of insoluble monolayers of sugar monoesters. *Langmuir.* 2002, **18**(12), pp.4765-4774.
129. Valério, J. et al. Temperature effect on the bilayer stacking in multilamellar lipid vesicles. *The Journal of Physical Chemistry B.* 2011, **116**(1), pp.168-178.
130. Kornmueller, K. et al. Peptides at the interface: self-assembly of amphiphilic designer peptides and their membrane interaction propensity. *Biomacromolecules.* 2016.
131. Rappolt, M. The biologically relevant lipid mesophases as “seen” by X-rays. *Advances in planar lipid bilayers and liposomes.* 2006, **5**, pp.253-283.
132. Drasler, B. et al. Fullerene up-take alters bilayer structure and elasticity: A small angle X-ray study. *Chemistry and physics of lipids.* 2015, **188**, pp.46-53.
133. Patil-Sen, Y. et al. Facile preparation of internally self-assembled lipid particles stabilized by carbon nanotubes. *JoVE (Journal of Visualized Experiments).* 2016, (108), pp.e53489-e53489.
134. Pabst, G. et al. Structural information from multilamellar liposomes at full hydration: full q-range fitting with high quality x-ray data. *Physical Review E.* 2000, **62**(3), p.4000.
135. Pabst, G. et al. Structure and interactions in the anomalous swelling regime of phospholipid bilayers. *Langmuir.* 2003, **19**(5), pp.1716-1722.
136. Rappolt, M. and Pabst, G. Flexibility and structure of fluid bilayer interfaces. *Structure and Dynamics of Membranous Interfaces.* 2008, pp.45-81.
137. PABST, G. Global properties of biomimetic membranes: perspectives on molecular features. *Biophysical Reviews and Letters.* 2006, **1**(01), pp.57-84.

138. Rappolt, M. Bilayer thickness estimations with “poor” diffraction data. *Journal of Applied Physics.* 2010, **107**(8), p.084701.
139. Heftberger, P. et al. Global small-angle X-ray scattering data analysis for multilamellar vesicles: the evolution of the scattering density profile model. *Journal of applied crystallography.* 2014, **47**(1), pp.173-180.
140. Brown, F.L. Regulation of protein mobility via thermal membrane undulations. *Biophysical Journal.* 2003, **84**(2), pp.842-853.
141. Lipowsky, R. The morphology of lipid membranes. *Current opinion in structural biology.* 1995, **5**(4), pp.531-540.
142. Pabst, G. et al. X-ray kinematography of temperature-jump relaxation probes the elastic properties of fluid bilayers. *Langmuir.* 2000, **16**(23), pp.8994-9001.
143. McIntosh, T.J. et al. Membrane fusion promoters and inhibitors have contrasting effects on lipid bilayer structure and undulations. *Biophysical Journal.* 1999, **76**(4), pp.2090-2098.
144. Nagle, J.F. and Tristram-Nagle, S. Structure of lipid bilayers. *Biochimica et Biophysica Acta (BBA)-Reviews on Biomembranes.* 2000, **1469**(3), pp.159-195.
145. Denk, W. et al. Two-photon laser scanning fluorescence microscopy. *Science.* 1990, **248**(4951), pp.73-76.
146. Edward, J.T. Molecular volumes and the Stokes-Einstein equation. *J. chem. Educ.* 1970, **47**(4), p.261.
147. Timm, M. et al. Considerations regarding use of solvents in in vitro cell based assays. *Cytotechnology.* 2013, **65**(5), pp.887-894.
148. Gordeliy, V. et al. Lipid membrane structure and interactions in dimethyl sulfoxide/water mixtures. *Biophysical Journal.* 1998, **75**(5), pp.2343-2351.
149. Ferreira, O. and Pinho, S.o.P. Solubility of flavonoids in pure solvents. *Industrial & Engineering Chemistry Research.* 2012, **51**(18), pp.6586-6590.
150. Razmara, R.S. et al. Solubility of quercetin in water+ methanol and water+ ethanol from (292.8 to 333.8) K. *Journal of Chemical & Engineering Data.* 2010, **55**(9), pp.3934-3936.
151. Toppozini, L. et al. Partitioning of ethanol into lipid membranes and its effect on fluidity and permeability as seen by X-ray and neutron scattering. *Soft Matter.* 2012, **8**(47), pp.11839-11849.
152. Vakurov, A. et al. ZnO nanoparticle interactions with phospholipid monolayers. *Journal of Colloid and Interface Science.* 2013, **404**, pp.161-168.
153. Luo, Z. et al. Particle-Stabilizing Effects of Flavonoids at the Oil−Water Interface. *Journal of Agricultural and Food Chemistry.* 2011, **59**(6), pp.2636-2645.
154. Van Acker, S.A. et al. A quantum chemical explanation of the antioxidant activity of flavonoids. *Chemical research in toxicology.* 1996, **9**(8), pp.1305-1312.
155. Chebil, L. et al. Solubility of flavonoids in organic solvents. *Journal of Chemical & Engineering Data.* 2007, **52**(5), pp.1552-1556.
156. Saija, A. et al. Flavonoids as antioxidant agents: Importance of their interaction with biomembranes. *Free Radical Biology and Medicine.* 1995, **19**(4), pp.481-486.
157. Londoño-Londoño, J. et al. Hesperidin and hesperetin membrane interaction: Understanding the role of 7-< i> O</i>-glycoside moiety in flavonoids. *Archives of Biochemistry and Biophysics.* 2010, **499**(1), pp.6-16.

158. Murota, K. et al. Unique uptake and transport of isoflavone aglycones by human intestinal Caco-2 cells: comparison of isoflavonoids and flavonoids. *J Nutr.* 2002, **132**(7), pp.1956-1961.
159. Tammela, P. et al. Permeability characteristics and membrane affinity of flavonoids and alkyl gallates in Caco-2 cells and in phospholipid vesicles. *Archives of Biochemistry and Biophysics.* 2004, **425**(2), pp.193-199.
160. Goodwin, J.T. et al. Physicochemical determinants of passive membrane permeability: role of solute hydrogen-bonding potential and volume. *Journal of medicinal chemistry.* 2001, **44**(22), pp.3721-3729.
161. Izumi, T. et al. Soy isoflavone aglycones are absorbed faster and in higher amounts than their glucosides in humans. *J Nutr.* 2000, **130**(7), pp.1695-1699.
162. Chabane, M.N. et al. Quercetin and naringenin transport across human intestinal Caco-2 cells. *Journal of Pharmacy and Pharmacology.* 2009, **61**(11), pp.1473-1483.
163. Tian, X.-J. et al. Studies of intestinal permeability of 36 flavonoids using Caco-2 cell monolayer model. *International Journal of Pharmaceutics.* 2009, **367**(1–2), pp.58-64.
164. Barrington, R. et al. Absorption, conjugation and efflux of the flavonoids, kaempferol and galangin, using the intestinal CaCo-2/TC7 cell model. *Journal of Functional Foods.* 2009, **1**(1), pp.74-87.
165. Tourniaire, F. et al. Molecular mechanisms of the naringin low uptake by intestinal Caco-2 cells. *Molecular Nutrition & Food Research.* 2005, **49**(10), pp.957-962.
166. Brand, W. et al. Metabolism and transport of the citrus flavonoid hesperetin in Caco-2 cell monolayers. *Drug Metabolism and Disposition.* 2008, **36**(9), pp.1794-1802.
167. Luo, Z. et al. Transport of trans-tiliroside (kaempferol-3-β-D-(6'-p-coumaroyl-glucopyranoside) and related flavonoids across Caco-2 cells, as a model of absorption and metabolism in the small intestine. *Xenobiotica.* 2015, (0), pp.1-9.
168. Lipinski, C.A. Lead- and drug-like compounds: the rule-of-five revolution. *Drug Discovery Today: Technologies.* 2004, **1**(4), pp.337-341.
169. Long, G.L. and Winefordner, J. Limit of detection. A closer look at the IUPAC definition. *Anal. Chem.* 1983, **55**(7).
170. Mohamadi, S. et al. Electrochemical screening of biomembrane-active compounds in water. *Analytica chimica acta.* 2014, **813**, pp.83-89.
171. Ulrih, N.P. et al. Kaempferol and quercetin interactions with model lipid membranes. *Food Research International.* 2015, **71**, pp.146-154.
172. H, T. Effects of red wine flavonoid components on biomembranes and cell proliferation. *International Journal of Wine Research.* 2011.
173. Rothwell, J.A. et al. Experimental determination of octanol-water partition coefficients of quercetin and related flavonoids. *Journal of Agricultural and Food Chemistry.* 2005, **53**(11), pp.4355-4360.
174. Ofer, M. et al. Modulation of drug transport by selected flavonoids: Involvement of P-gp and OCT? *European Journal of Pharmaceutical Sciences.* 2005, **25**(2), pp.263-271.
175. Wishart, D.S. et al. DrugBank: a comprehensive resource for in silico drug discovery and exploration. *Nucleic Acids Research.* 2006, **34**(Database issue), pp.D668-D672.
176. Cooper, D.A. et al. Evaluation of the potential for olestra to affect the availability of dietary phytochemicals. *J Nutr.* 1997, **127**(8), pp.1699S-1709S.
177. Shibusawa, Y. et al. Determination of log Po/w for catechins and their isomers, oligomers, and other organic compounds by stationary phase controlled high-speed

countercurrent chromatography. *Journal of Liquid Chromatography & Related Technologies.* 2005, **28**(17), pp.2819-2837.
178. Zhang, S. et al. The effects of substituent grafting on the interaction of pH-responsive polymers with phospholipid monolayers. *Langmuir.* 2011, **27**(13), pp.8530-8539.
179. Lawrie, G. and Barnes, G. Octadecanol monolayers: The phase diagram. *Journal of Colloid and Interface Science.* 1994, **162**(1), pp.36-44.
180. Bibo, A. et al. A monolayer phase miscibility comparison of long-chain fatty acids and their ethyl esters. *The Journal of Physical Chemistry.* 1991, **95**(14), pp.5591-5599.
181. Steitz, R. et al. A grazing-incidence X-ray diffraction study of octadecanol monolayers at high surface pressures. *Langmuir.* 1998, **14**(25), pp.7245-7249.
182. Gradella Villalva, D. et al. Molecular Packing in Langmuir Monolayers Composed of a Phosphatidylcholine and a Pyrene Lipid. *The Journal of Physical Chemistry B.* 2016, **120**(6), pp.1126-1133.
183. Lucero, A. et al. Effect of hydrocarbon chain and pH on structural and topographical characteristics of phospholipid monolayers. *The Journal of Physical Chemistry B.* 2008, **112**(25), pp.7651-7661.
184. Park, J.-W. and Ahn, D.J. Temperature effect on nanometer-scale physical properties of mixed phospholipid monolayers. *Colloids and Surfaces B: Biointerfaces.* 2008, **62**(1), pp.157-161.
185. Niño, M.R.R. et al. Relaxation phenomena in phospholipid monolayers at the air–water interface. *Colloids and Surfaces A: Physicochemical and Engineering Aspects.* 2008, **320**(1), pp.260-270.
186. Kuroda, O. et al. Liposome Deformation by Imbalance of pH and Ionic Strength Across the Membrane. In: *Trends in Colloid and Interface Science XXIV*. Springer, 2011, pp.49-53.
187. Kunz, W. *Specific ion effects.* World Scientific, 2010.
188. Liljeblad, J.F. et al. Phospholipid monolayers probed by vibrational sum frequency spectroscopy: instability of unsaturated phospholipids. *Biophysical Journal.* 2010, **98**(10), pp.L50-L52.
189. Heikkila, R.E. et al. Solution of fatty acids from monolayers spread at the air-water interface: identification of phase transformations and the estimation of surface charge. *Journal of lipid research.* 1970, **11**(3), pp.195-200.
190. Qiao, L. et al. Oxidative Degradation of the Monolayer of 1-Palmitoyl-2-Oleoyl-sn-Glycero-3-Phosphocholine (POPC) in Low-Level Ozone. *The Journal of Physical Chemistry B.* 2015, **119**(44), pp.14188-14199.
191. Wong-Ekkabut, J. et al. Effect of lipid peroxidation on the properties of lipid bilayers: a molecular dynamics study. *Biophysical Journal.* 2007, **93**(12), pp.4225-4236.
192. Ferrreira, J.V.N. et al. Ultrathin films of lipids to investigate the action of a flavonoid with cell membrane models. *Materials Science and Engineering: C.* 2015, **48**(0), pp.112-117.
193. Schmidt, T.F. et al. Binding of Methylene Blue onto Langmuir Monolayers Representing Cell Membranes May Explain Its Efficiency as Photosensitizer in Photodynamic Therapy. *Langmuir.* 2015, **31**(14), pp.4205-4212.
194. Walker, I. et al. A comparative analysis of phenothiazinium salts for the photosensitisation of murine fibrosarcoma (RIF-1) cells in vitro. *Photochemical & Photobiological Sciences.* 2004, **3**(7), pp.653-659.

195. Kurkin, V. et al. Interaction of milk-thistle-fruit flavanonols with Langmuir monolayers of lecithin and bilayers of liposomes. *Pharmaceutical chemistry journal.* 2009, **43**(2), pp.101-109.
196. Sinha, R. et al. Modifying effect of quercetin on model biomembranes: studied by molecular dynamic simulation, DSC and NMR. *Int J Curr Pharm Res.* 2012, **4**, pp.70-9.
197. Patino, J.M.R. et al. Some implications of nanoscience in food dispersion formulations containing phospholipids as emulsifiers. *Food Chemistry.* 2007, **102**(2), pp.532-541.
198. Saccani, J. et al. Stabilization of phospholipid multilayers at the air-water interface by compression beyond the collapse: a BAM, PM-IRRAS, and molecular dynamics study. *Langmuir.* 2004, **20**(21), pp.9190-9197.
199. Lee, K.Y.C. Collapse mechanisms of Langmuir monolayers. *Annu. Rev. Phys. Chem.* 2008, **59**, pp.771-791.
200. Ybert, C. et al. Collapse of a monolayer by three mechanisms. *The Journal of Physical Chemistry B.* 2002, **106**(8), pp.2004-2008.
201. Hodzic, A. et al. Losartan's affinity to fluid bilayers modulates lipid–cholesterol interactions. *Physical Chemistry Chemical Physics.* 2012, **14**(14), pp.4780-4788.
202. Pool, H. et al. Encapsulation and release of hydrophobic bioactive components in nanoemulsion-based delivery systems: impact of physical form on quercetin bioaccessibility. *Food & function.* 2013, **4**(1), pp.162-174.
203. Chemsrc.com. Tiliroside. 2016.
204. Chemsrc.com. Rutin. 2016.
205. Tristram-Nagle, S. et al. Structure and interactions of fully hydrated dioleoylphosphatidylcholine bilayers. *Biophysical Journal.* 1998, **75**(2), pp.917-925.
206. Pan, J. et al. Temperature dependence of structure, bending rigidity, and bilayer interactions of dioleoylphosphatidylcholine bilayers. *Biophysical Journal.* 2008, **94**(1), pp.117-124.
207. Edholm, O. and Nagle, J.F. Areas of molecules in membranes consisting of mixtures. *Biophysical Journal.* 2005, **89**(3), pp.1827-1832.
208. Nagle, J.F. et al. Multiple mechanisms for critical behavior in the biologically relevant phase of lecithin bilayers. *Physical Review E.* 1998, **58**(6), p.7769.
209. Vogel, M. et al. Thermal unbinding of highly oriented phospholipid membranes. *Physical Review Letters.* 2000, **84**(2), p.390.
210. Pabst, G. et al. Enhancement of steric repulsion with temperature in oriented lipid multilayers. *Physical Review Letters.* 2002, **88**(12), p.128101.
211. Seelig, A. and Seelig, J. Dynamic structure of fatty acyl chains in a phospholipid bilayer measured by deuterium magnetic resonance. *Biochemistry.* 1974, **13**(23), pp.4839-4845.
212. Katsaras, J. Adsorbed to a rigid substrate, dimyristoylphosphatidylcholine multibilayers attain full hydration in all mesophases. *Biophysical Journal.* 1998, **75**(5), pp.2157-2162.
213. Helfrich, W. Steric interaction of fluid membranes in multilayer systems. *Zeitschrift für Naturforschung A.* 1978, **33**(3), pp.305-315.
214. Pabst, G. et al. Structural analysis of weakly ordered membrane stacks. *Applied Crystallography.* 2003, **36**(6), pp.1378-1388.
215. Kobayashi, Y. and Fukada, K. Characterization of swollen lamellar phase of dimyristoylphosphatidylcholine–gramicidin A mixed membranes by DSC, SAXS, and

densimetry. *Biochimica et Biophysica Acta (BBA)-Biomembranes.* 1998, **1371**(2), pp.363-370.
216. Kline, R.J. et al. Critical role of side-chain attachment density on the order and device performance of polythiophenes. *Macromolecules.* 2007, **40**(22), pp.7960-7965.
217. Mavromoustakos, T. et al. Partial interdigitation of lipid bilayers. *International Journal of Quantum Chemistry.* 2011, **111**(6), pp.1172-1183.
218. Potamitis, C. et al. Interactions of the AT1 antagonist valsartan with dipalmitoyl-phosphatidylcholine bilayers. *Biochimica et Biophysica Acta (BBA) - Biomembranes.* 2011, **1808**(6), pp.1753-1763.
219. Koukoulitsa, C. et al. The role of the anticancer drug vinorelbine in lipid bilayers using differential scanning calorimetry and molecular modeling. *Chemistry and physics of lipids.* 2006, **144**(1), pp.85-95.
220. Mavromoustakos, T. et al. Topography of alphaxalone and Δ16-alphaxalone in membrane bilayers containing cholesterol. *Biochimica et Biophysica Acta (BBA) - Biomembranes.* 1994, **1194**(1), pp.69-74.
221. Pawlikowska-Pawlęga, B. et al. Modification of membranes by quercetin, a naturally occurring flavonoid, via its incorporation in the polar head group. *Biochimica et Biophysica Acta (BBA)-Biomembranes.* 2007, **1768**(9), pp.2195-2204.
222. Sun, Y. et al. Interaction of tea catechin (—)-epigallocatechin gallate with lipid bilayers. *Biophysical Journal.* 2009, **96**(3), pp.1026-1035.
223. How, C.W. et al. Effects of a synthetic antitumoral catechin and its tyrosinase-processed product on the structural properties of phosphatidylcholine membranes. *Biochimica et Biophysica Acta (BBA)-Biomembranes.* 2014, **1838**(5), pp.1215-1224.
224. Elliott, J. et al. The effects of bilayer thickness and tension on gramicidin single-channel lifetime. *Biochimica et Biophysica Acta (BBA)-Biomembranes.* 1983, **735**(1), pp.95-103.
225. Harroun, T.A. et al. Experimental evidence for hydrophobic matching and membrane-mediated interactions in lipid bilayers containing gramicidin. *Biophysical Journal.* 1999, **76**(2), pp.937-945.
226. Ingolfsson, H.I. et al. Curcumin is a modulator of bilayer material properties. *Biochemistry.* 2007, **46**(36), pp.10384-10391.
227. Arora, A. et al. Modulation of Liposomal Membrane Fluidity by Flavonoids and Isoflavonoids. *Archives of Biochemistry and Biophysics.* 2000, **373**(1), pp.102-109.
228. Tsuchiya, H. et al. Membrane-rigidifying effects of anti-cancer dietary factors. *Biofactors.* 2002, **16**(3-4), pp.45-56.
229. Poklar Ulrih, N. et al. Flavonoids and cell membrane fluidity. *Food Chemistry.* 2010, **121**(1), pp.78-84.
230. Sadeghpour, A. et al. Chapter Four-Interactions of Flavonoids With Lipidic Mesophases. *Advances in Biomembranes and Lipid Self-Assembly.* 2017, **25**, pp.95-123.
231. Finegold, L.X. *Cholesterol in membrane models.* CRC Press, 1992.
232. Tsuchiya, H. Effects of Green Tea Catechins on Membrane Fluidity. *Pharmacology.* 1999, **59**(1), pp.34-44.
233. Cushnie, T.P.T. and Lamb, A.J. Antimicrobial activity of flavonoids. *International Journal of Antimicrobial Agents.* 2005, **26**(5), pp.343-356.
234. Movileanu, L. et al. Interaction of the antioxidant flavonoid quercetin with planar lipid bilayers. *International Journal of Pharmaceutics.* 2000, **205**(1–2), pp.135-146.

235. Pawlikowska-Pawlęga, B. et al. Characteristics of quercetin interactions with liposomal and vacuolar membranes. *Biochimica et Biophysica Acta (BBA) - Biomembranes.* 2014, **1838**(1, Part B), pp.254-265.
236. Singh, D. et al. Rutin-phospholipid complex: an innovative technique in novel drug delivery system-NDDS. *Current drug delivery.* 2012, **9**(3), pp.305-314.
237. Erlejman, A. et al. The interaction of flavonoids with membranes: potential determinant of flavonoid antioxidant effects. *Free Radic Res.* 2004, **38**(12), pp.1311-1320.
238. Dorta, D.J. et al. Antioxidant activity of flavonoids in isolated mitochondria. *Phytotherapy Research.* 2008, **22**(9), pp.1213-1218.
239. Tsuchiya, H. Structure-dependent membrane interaction of flavonoids associated with their bioactivity. *Food Chemistry.* 2010, **120**(4), pp.1089-1096.
240. Abram, V. et al. Effect of flavonoid structure on the fluidity of model lipid membranes. *Food Chemistry.* 2013, **139**(1–4), pp.804-813.
241. Ajdzanovic, V. et al. Effects of genistein and daidzein on erythrocyte membrane fluidity: an electron paramagnetic resonance study. *Canadian journal of physiology and pharmacology.* 2010, **88**(4), pp.497-500.
242. Verstraeten, S.V. et al. Membrane effects of cocoa procyanidins in liposomes and Jurkat T cells. *Biological research.* 2004, **37**(2), pp.293-300.
243. Tefas, L.R. et al. Quercetin-loaded liposomes: Formulation optimization through a D-optimal experimental design. *FARMACIA.* 2015, **63**(1), pp.26-33.
244. Patel, A.R. et al. Quercetin loaded biopolymeric colloidal particles prepared by simultaneous precipitation of quercetin with hydrophobic protein in aqueous medium. *Food Chemistry.* 2012, **133**(2), pp.423-429.
245. Yaghmur, A. et al. Self-assembly in monoelaidin aqueous dispersions: direct vesicles to cubosomes transition. *Plos One.* 2008, **3**(11), p.e3747.